Self-force calculations with matched expansions and quasinormal mode sums

Marc Casals[*]

CENTRA, Instituto Superior Técnico, Lisbon, Portugal and School of Mathematical Sciences,
Dublin City University, Glasnevin, Dublin 9, Ireland

Sam Dolan,[†] Adrian C. Ottewill,[‡] and Barry Wardell[§]

Complex and Adaptive Systems Laboratory and School of Mathematical Sciences,
University College Dublin, Belfield, Dublin 4, Ireland

Accurate modeling of gravitational wave emission by extreme-mass ratio inspirals is essential for their detection by the LISA mission. A leading perturbative approach involves the calculation of the self-force acting upon the smaller orbital body. In this work, we present the first application of the Poisson-Wiseman-Anderson method of "matched expansions" to compute the self-force acting on a point particle moving in a curved spacetime. The method employs two expansions for the Green function, which are, respectively, valid in the "quasilocal" and "distant past" regimes, and which may be matched together within the normal neighborhood. We perform our calculation in a static region of the spherically symmetric Nariai spacetime ($dS_2 \times \mathbb{S}^2$), in which scalar-field perturbations are governed by a radial equation with a Pöschl-Teller potential (frequently used as an approximation to the Schwarzschild radial potential) whose solutions are known in closed form. The key new ingredients in our study are (i) very high order quasilocal expansions and (ii) expansion of the distant past Green function in quasinormal modes. In combination, these tools enable a detailed study of the properties of the scalar-field Green function. We demonstrate that the Green function is singular whenever x and x' are connected by a null geodesic, and apply asymptotic methods to determine the structure of the Green function near the null wave front. We show that the singular part of the Green function undergoes a transition each time the null wave front passes through a caustic point, following a repeating fourfold sequence $\delta(\sigma)$, $1/\pi\sigma$, $-\delta(\sigma)$, $-1/\pi\sigma$, etc., where σ is Synge's world function. The matched-expansion method provides insight into the nonlocal properties of the self-force. We show that the self-force generated by the segment of the worldline lying outside the normal neighborhood is not negligible. We apply the matched-expansion method to compute the scalar self-force acting on a static particle on the Nariai spacetime, and validate against an alternative method, obtaining agreement to six decimal places. We conclude with a discussion of the implications for wave propagation and self-force calculations. On black hole spacetimes, any expansion of the Green function in quasinormal modes must be augmented by a branch-cut integral. Nevertheless, we expect the Green function in Schwarzschild spacetime to inherit certain key features, such as a fourfold singular structure manifesting itself through the asymptotic behavior of quasinormal modes. In this way, the Nariai spacetime provides a fertile testing ground for developing insight into the nonlocal part of the self-force on black hole spacetimes.

I. INTRODUCTION

The last decade has seen a surge of interest in the nascent field of gravitational wave astronomy. Gravitational waves—propagating ripples in spacetime—are generated by some of the most violent processes in the known universe, such as supernovae, black hole mergers, and galaxy collisions. These powerful processes are hidden from the view of "traditional" electromagnetic-wave telescopes behind shrouds of dust and radiation. On the other hand, gravitational waves are not strongly absorbed or scattered by intervening matter, and they carry information about the dynamics at the heart of such processes. The prospects seem good for direct detection of gravitational waves in the near future. A number of ground-based detectors (such as LIGO [1], VIRGO [2], and GEO600 [3]) are now in the data collection phase.

Gravitational wave astronomy will enter a new era with the launch of the first space-based observatory: the Laser Interferometer Space Antenna (LISA) [4]. It is hoped that this joint NASA/ESA mission, presently in the design and planning phase, will be launched within a decade. It will be preceded by a pathfinder mission, due for launch in 2010 [5].

Black hole binary systems are a key target for gravitational wave observatories worldwide. Data analysis methods such as matched filtering may be applied to separate a

_____

[*]marc.casals@dcu.ie
[†]sam.dolan@ucd.ie
[‡]adrian.ottewill@ucd.ie
[§]barry.wardell@ucd.ie

weak gravitational wave signal from a noisy background [6]. An essential prerequisite for detection via matched filtering is an accurate template for the gravitational wave emission from black hole binaries. Breakthroughs in numerical relativity in the last five years have led to a rapid advance in the modeling of comparable-mass binaries, where the partners are of similar mass. Progress in numerical relativity continues apace.

A key target for the LISA mission is the so-called *extreme mass ratio inspiral*: a compact binary in which one partner (mass M) is significantly more massive than the other (mass m). Mass ratios of $\mu \equiv m/M \gtrsim 10^{-8}$ are possible, for example, for a solar-mass black hole orbiting a supermassive black hole [7]. Mass ratios of up to $m/M \gtrsim 1/10$ have been studied by numerical relativists [8]; smaller ratios are presently beyond the scope of numerical relativity due to the existence of two distinct and dissimilar length scales in the system. Perturbative approaches seem more likely to succeed in the extreme-mass regime.

The smaller compact mass m distorts the curvature of the spacetime in which it is moving. Hence, rather than following a geodesic of the background spacetime generated by the larger mass M, the smaller mass follows a geodesic of the *total* spacetime [9]. However, if the mass ratio is extreme, the deviation of the smaller body's motion from the background geodesic will be (locally) small. The deviation may be interpreted as arising from a *self-force*, created by the smaller mass m interacting with its own gravitational field. To leading order, the self-force acceleration is proportional to m. With knowledge of the leading term in the self-force, one may model the evolution of the orbit and subsequent inspiral of the smaller mass, and compute the gravitational wave emission to high accuracy. However, finding the instantaneous self-force in a curved spacetime is not at all straightforward; it turns out to depend on the *entire past history* of the smaller mass, m.

The idea of a self-force has a long history in physics. In the late 19th century it was well known that a charge undergoing an acceleration in flat spacetime will generate electromagnetic radiation, and will feel a corresponding *radiation reaction*. The self-acceleration of a charged point particle in flat spacetime is given by the well-known Abraham-Lorentz-Dirac formula [10]. Radiation reaction implies that the "classical" model of the atom (a point-particle electron orbiting a compact nucleus) is unstable. The observed stability of the atom remained a puzzle for many years and provided a key motivation for the development of quantum mechanics. In the 1960s, DeWitt and Brehme [11] derived a formula for the self-force acting on an electrically charged point particle in a curved background, and a correction was later provided by Hobbs [12]. The gravitational self-force acting on a point mass was found in 1997 by two groups working concurrently and independently: Mino, Sasaki, and Tanaka [13] and Quinn and Wald [14]. Shortly after, Quinn derived the

self-force acting on a minimally coupled scalar charge [15]. These developments are summarized in 2004/05 reviews by Poisson [16] (where the scalar case was extended to cater for nonminimal coupling) and Detweiler [17]. In the subsequent period, a range of complementary approaches to the self-force problem have been developed [18–22].

The self-force expressions for scalar, electromagnetic, and gravitational cases take similar forms [16]. In this paper, we restrict our attention to the simplest case: a pointlike scalar charge q of mass m coupled to a massless scalar field $\Phi(x)$ moving on a curved background geometry. The scalar field $\Phi(x)$ satisfies the field equation

$$(\Box - \xi R)\Phi(x) = -4\pi\rho(x) \tag{1.1}$$

where $\Box$ is the d'Alembertian on the curved background created by the larger mass M, R is the Ricci scalar, and ξ is the curvature coupling constant. The charge density ρ of the point particle is

$$\rho(x) = \int_\gamma q \frac{\delta^4(x^\mu - z^\mu(\tau))}{\sqrt{-g}} d\tau \tag{1.2}$$

where $z(\tau)$ describes the worldline γ of the particle with proper time τ, $g_{\mu\nu}$ is the background metric, $g = \det(g_{\mu\nu})$, and $\delta^4(\cdot)$ is the four-dimensional Dirac distribution. The field exerts a radiation reaction on the particle, creating a self-force [15]

$$f_\mu^{\text{self}} = q\nabla_\mu \Phi_R \tag{1.3}$$

which leads to the equations of motion for the scalar particle,

$$ma^\mu = (g^{\mu\nu} + u^\mu u^\nu)f_\nu^{\text{self}} = q(g^{\mu\nu} + u^\mu u^\nu)\nabla_\nu \Phi_R \tag{1.4}$$

where u^μ is the particle's four-velocity and Φ_R is the *radiative* part of the field. Identifying the correct radiative field (which is regular at the particle's position) is the essential step in the derivation of the self-force [16]. Note that the projection operator $g^{\mu\nu} + u^\mu u^\nu$ has been applied here to ensure that $u_\mu a^\mu = 0$. The mass m appearing in (1.4) is the "dynamical" (and renormalized) particle's mass, which in the scalar case is not necessarily a constant of motion [15]. Rather, it evolves according to

$$\frac{dm}{d\tau} = -qu^\mu \nabla_\mu \Phi_R. \tag{1.5}$$

In other words, a spinless particle may radiate away its mass through the emission of monopolar waves.

A leading method for computing the derivative of the radiative field, $\nabla_\mu \Phi_R$, and hence the self-force, is based on *mode-sum regularization* (MSR). The MSR approach was developed by Barack, Ori, and collaborators [23–26] and Detweiler and coworkers [17,27,28]. The method has been applied to the Schwarzschild spacetime to compute, for

example, the gravitational self-force for circular orbits [26] and the scalar self-force for eccentric orbits [29]. The application to Kerr is in progress [30,31]. It was recently shown [32] that the gravitational self-force computed in the Lorenz gauge is in agreement with that found in the Regge-Wheeler gauge [17,27]. Further gauge-invariant comparisons and comparison with the predictions of post-Newtonian theory [33,34] are presently under consideration [35].

One drawback of the MSR method is that it gives relatively little geometric insight into the physical origin of the self-force. An alternative approach, based on *matched expansions*, was suggested by Poisson and Wiseman in 1998 [36]. Their idea was to compute the self-force by matching together two independent expansions for the Green function, valid in "quasilocal" and "distant past" regimes. This suggestion was analyzed by Anderson and Wiseman [37], who concluded in 2005 that "this approach remains, in our opinion, in the category of 'promising but possessing some technical challenges'." The present paper represents the first practical implementation of this method.

In the following sections we demonstrate that accurate self-force calculations via matched expansions are indeed feasible. We apply the method to compute the self-force for a scalar charge at a fixed position on the product spacetime $dS_2 \times \mathbb{S}^2$ (i.e. the product of a two-sphere and a two-dimensional de Sitter spacetime) introduced long ago by Nariai [38,39]. We introduce a method for calculating the distant past Green function using an expansion in quasinormal modes (QNMs). The effect of caustics upon wave propagation is examined. This work is intended to lay a foundation for future studies of self-force in black hole spacetimes through matched expansions. The prospects for extending the calculation to the Schwarzschild spacetime appear good, although the work remains to be conducted.

The remainder of this paper is organized as follows. In Sec. II we define the self-force and outline the Poisson-Anderson-Wiseman method of matched expansions. In Sec. III we consider wave propagation on the Schwarzschild spacetime. A radial equation of standard form is obtained via the well-known "trick" of replacing the Schwarzschild potential with a so-called Pöschl-Teller potential. We show that a Pöschl-Teller potential arises more naturally if we consider wave propagation on the Nariai spacetime, whose properties are described in detail.

Section IV is concerned with the scalar Green function on the Nariai spacetime. We begin in Sec. IV A by expressing the Green function as a sum over angular modes and integral over frequency. We show in Sec. IV B that performing the integral over frequency leaves a sum of residues: a so-called "quasinormal mode sum," which may be matched onto a quasilocal Green function, briefly described in Sec. IV C.

In Sec. V we consider the singular structure of the Green function. In Sec. V A we demonstrate that the Green function is singular on the null surface, even beyond the boundary of the normal neighborhood and through caustics. We show that the singular behavior arises from the large-l asymptotics of the quasinormal mode sums. To investigate further, we employ two closely related methods for converting sums into integrals, namely, the Watson transform and Poisson sum (Sec. V B). The form of the Green function close to the null cone is studied in detail in Secs. V D and V E, and asymptotic expressions are derived.

In Sec. VI we take a short breath and rewrite the main equations obtained for the Green function.

Section VII describes the calculation of the self-force for the specific case of the static particle. For the Schwarzschild spacetime, the static case has been well studied. We show in Sec. VII B that the massive-field approach of Rosenthal [40,41] may be adapted to the Nariai spacetime. This provides an independent check on the matched-expansion calculation which is described in Sec. VII C. Relevant numerical methods are outlined in Sec. VII D.

In Sec. VIII we present a selection of significant numerical results. We start in Sec. VIII A by examining the properties of the quasinormal mode Green function. In Sec. VIII B we test the asymptotic expressions describing the singularity structure. In Sec. VIII C we show that the quasilocal and distant past Green functions match in an appropriate regime. In Sec. VIII D we present results for the self-force on a static particle.

We conclude in Sec. IX with a discussion of the implications of this study. Throughout the paper, we employ geometrized units $G = c = 1$, and the metric sign convention $\{- + ++\}$.

II. THE METHOD OF MATCHED EXPANSIONS

Here we briefly outline the Poisson-Wiseman-Anderson method of matched expansions [36,37]. We start with an expression for the covariant derivative of the radiative scalar field [15,16],

$$\nabla_\mu \Phi_R(z(\tau)) = -\frac{1}{12}(1 - 6\xi)qRu_\mu + q(g_{\mu\nu} + u_\mu u_\nu)$$
$$\times \left(\frac{1}{3}\dot{a}^\nu + \frac{1}{6}R^\nu{}_\lambda u^\lambda\right) + \Phi_\mu^{\text{tail}}(z(\tau)). \quad (2.1)$$

Here, $R^\nu{}_\lambda$ is the Ricci tensor of the background metric and $\dot{a}^\nu$ is the derivative with respect to proper time of the four-acceleration $a^\nu = u^\nu{}_{;\mu}u^\mu$. The first two sets of terms are evaluated locally [14–16]. The final term Φ_μ^{tail} is nonlocal; it is the so-called *tail integral*,

$$\Phi_\mu^{\text{tail}}(z(\tau)) = q \lim_{\epsilon \to 0^+} \int_{-\infty}^{\tau - \epsilon} \nabla_\mu G_{\text{ret}}(z(\tau), z(\tau'))d\tau' \quad (2.2)$$

where $G_{\text{ret}}(x, x')$ is the retarded Green function, defined by

$$(\Box_x - \xi R)G_{\text{ret}}(x, x') = -4\pi \frac{\delta^4(x^\mu - x'^\mu)}{\sqrt{-g}} \qquad (2.3)$$

together with appropriate causality conditions (which we describe in Sec. IV A).

Note that the tail integral depends on the entire past history of the particle's motion. Its evaluation is the main obstacle to progress. The tail integral (2.2) may be split into so-called *quasilocal* (QL) and *distant past* (DP) parts, as shown in Fig. 1. That is,

$$\Phi_\mu^{\text{tail}}(z(\tau)) = \Phi_\mu^{(\text{QL})}(z(\tau)) + \Phi_\mu^{(\text{DP})}(z(\tau))$$

$$= q \lim_{\epsilon \to 0^+} \int_{\tau - \Delta\tau}^{\tau - \epsilon} \nabla_\mu G_{\text{ret}}(z(\tau), z(\tau'))d\tau'$$

$$+ q \int_{-\infty}^{\tau - \Delta\tau} \nabla_\mu G_{\text{ret}}(z(\tau), z(\tau'))d\tau' \qquad (2.4)$$

where $\tau - \Delta\tau$ is the *matching time*, with $\Delta\tau$ being a free parameter in the method (see Fig. 1).

The QL and DP parts may be evaluated separately using independent methods. In particular, if we choose $\Delta\tau$ to be sufficiently small that $z(\tau)$ and $z(\tau - \Delta\tau)$ are within a *normal neighborhood*[1] [42], then the QL part may be evaluated by expressing the Green function in the Hadamard parametrix [43]. In other words, if $z(\tau)$ and $z(\tau - \Delta\tau)$ are connected by a unique nonspacelike geodesic, then the QL integral is simply

$$q^{-1}\Phi_\mu^{(\text{QL})}(z(\tau)) = -\lim_{\epsilon \to 0^+} \int_{\tau - \Delta\tau}^{\tau - \epsilon} \nabla_\mu V(z(\tau), z(\tau'))d\tau' \qquad (2.5)$$

where $V(x, x')$ is the smooth symmetric biscalar describing the propagation of radiation within the light cone (see Sec. IV C for full details). The approach ultimately yields a series expansion for the QL self-force in the coordinate separation of the points x and x'. The Hadamard-expansion method is now well advanced for several spacetimes of physical relevance, such as Schwarzschild and Kerr [44–49]. In Sec. IV C we apply this method to determine the quasilocal Green function and self-force in the Nariai spacetime.

Evaluating the contribution to the Green function from the distant past is a greater challenge, and is the main focus of this work. One possibility is to decompose the Green function into a sum over angular modes and an integral over frequency. In a spherically symmetric spacetime the "retarded" Green function may be defined in terms of a

---

[1]More precisely, the Hadamard parametrix requires that $z(\tau)$ and $z(\tau - \Delta\tau)$ lie within a *causal domain*—a *convex normal neighborhood* with a causality condition attached. This effectively requires that $z(\tau)$ and $z(\tau - \Delta\tau)$ be connected by a unique nonspacelike geodesic which stays within the causal domain. However, as we expect the term *normal neighborhood* to be more familiar to the reader, we will use it throughout this paper, with implied assumptions of convexity and a causality condition.
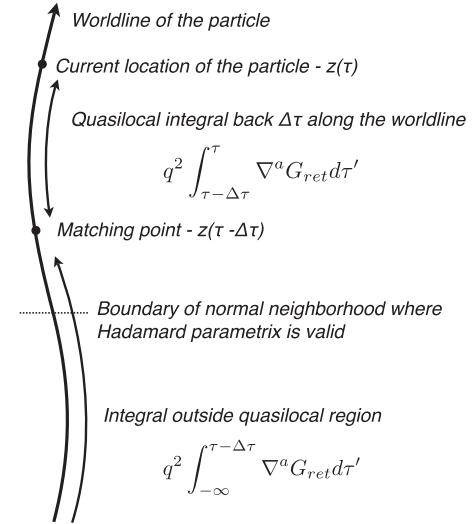

FIG. 1. In the method of matched expansions, the tail integral is split into QL and DP parts.

Laplace integral transform and an angular *l*-mode decomposition as follows,

$$G_{\text{ret}}(x, x') = \frac{1}{2\pi} \int_{-\infty + ic}^{+\infty + ic} d\omega e^{-i\omega(t-t')} \sum_{l=0}^{+\infty}(2l + 1)$$

$$\times P_l(\cos\gamma)\tilde{g}_{l\omega}(r, r'). \qquad (2.6)$$

Here c is a positive constant, t and r are appropriate time and radial coordinates, and $\cos\gamma = \cos\theta\cos\theta' + \sin\theta\sin\theta'\cos(\phi - \phi')$, where γ is the angle between the spacetime points x and x'. The radial Green function $\tilde{g}_{l\omega}(r, r')$ may be constructed from two linearly independent solutions of a radial equation. Since the DP Green function does not need to be extended to coincidence ($\tau' \to \tau$), the mode sum does not require regularization (though it may still be regularized if desired). However, Anderson and Wiseman [37] found the convergence of the mode sum to be poor, noting that going from 10 modes to 100 increased the accuracy by only a factor of 3.

In this paper we explore a new method for evaluating the *distant past* contribution, based on an expansion in so-called *quasinormal modes*. The integral over frequency in Eq. (2.6) may be evaluated by deforming the contour in the complex plane [50,51]. This is shown in Fig. 6 (below). In the Schwarzschild case there arise three distinct contributions to the Green function, from the three sections of the frequency integral in (2.6):

(1) An integral along high-frequency arcs, which leads to a prompt response.
(2) A quasinormal mode sum, arising from the residues of poles in the lower half-plane of complex frequency ω. This contribution leads to a damped ringing, characteristic of the black hole.
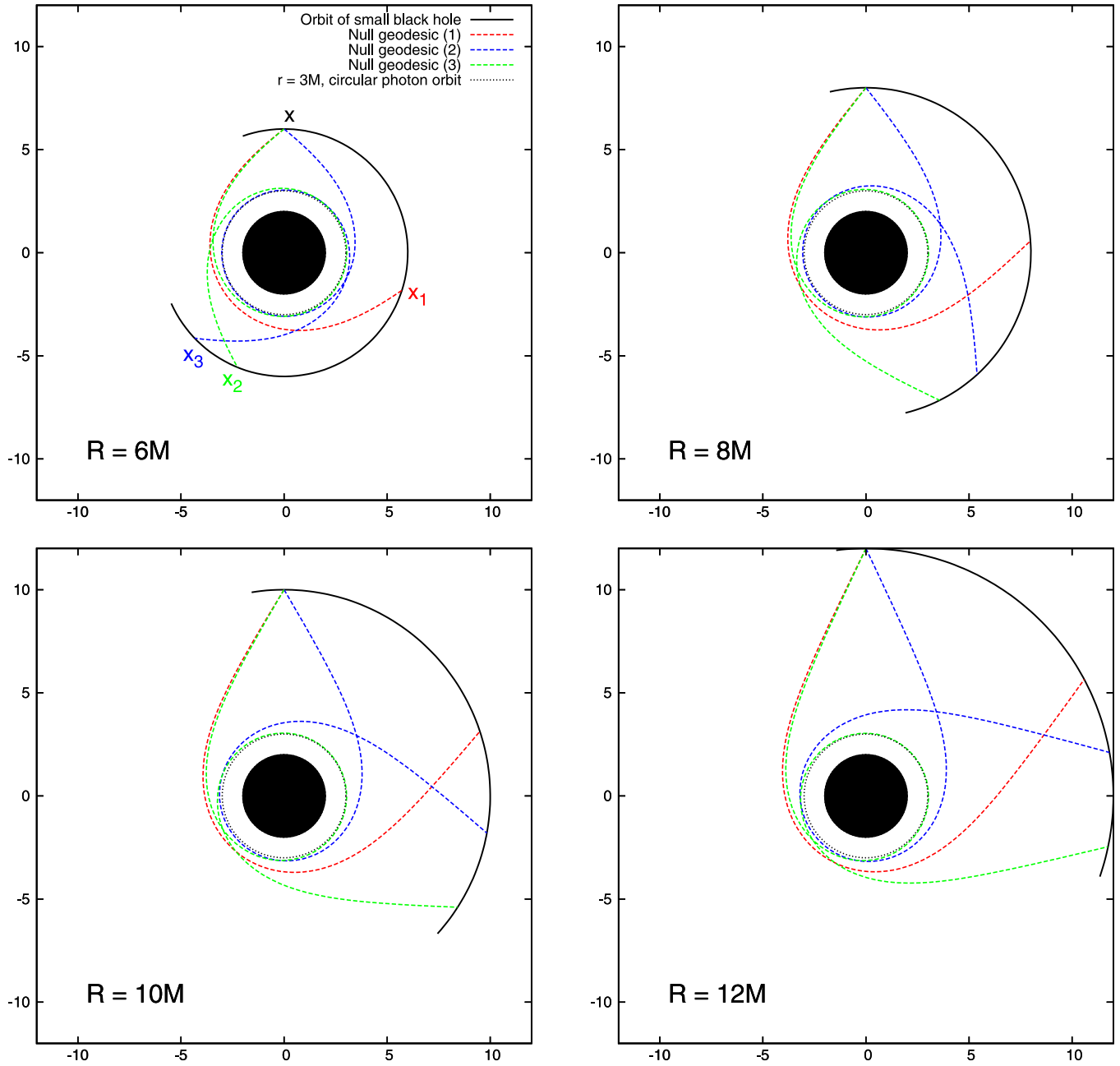(3) An integral along a branch cut, which leads to a power-law tail (among possibly other features).

FIG. 2 (color online). Orbiting null geodesics on the Schwarzschild spacetime that intersect timelike circular orbits of various radii $R = 6M$, $8M$, $10M$, and $12M$. The null geodesics are shown as dotted (colored) lines, and the timelike circular orbit is shown as a solid (black) line. The spacetime point x is connected to x_1, x_2, ... by null geodesics, as well as by the timelike circular geodesic. The Green function is singular when $x' = x_1$, x_2, etc. Note that between $R = 6M$ and $R = 8M$ the ordering of the points x_2 and x_3 becomes reversed.

The three parts (1–3) are commonly supposed to dominate the scattered signal at early, intermediate, and late times, respectively [50,51]. [This may be slightly misleading, however; Leaver [50] notes that, in addition, the branch-cut integral (part 3) "contributes heavily to the initial burst of radiation."] In this work, we investigate an alternative spacetime, introduced by Nariai in 1950 [38,39], in which the power-law tail (part 3) is absent. We demonstrate that, on the Nariai spacetime, at suitably "late times" the distant

past Green function may be written as a sum over quasi-normal modes (defined in Sec. IV B). We use the sum to compute the Green function, the radiative field, and the self-force for a static particle.

The key question addressed in this work is the following: how much of the self-force arises from the quasilocal region, and how much from the distant past? If the Green function falls off fast enough, then only the QL integral would be needed, and, since the QL integral is restricted to

the normal neighborhood, only the Hadamard parametrix is required. Unfortunately, this is not necessarily the case; Anderson and Wiseman [37] note that there are simple situations in which the DP integral in (2.6) gives the dominant contribution to the self-force.

Using the methods presented in this paper, we are able to compute the retarded Green function and the integrand of Eq. (2.2) as a function of time along the past worldline. We show that the DP contribution cannot be neglected. In particular, we find that the Green function and the integrand of Eq. (2.2) are singular whenever the two points $z^\mu(\tau)$ and $z^\mu(\tau')$ are connected by a null geodesic. We show that the singular form of the Green function changes every time a null geodesic passes through a caustic. On a spherically symmetric spacetime, caustics occur at antipodal points.

On Schwarzschild spacetime, the presence of an unstable photon orbit at $r = 3M$ implies that a null geodesic originating on a timelike worldline may later reintersect the timelike worldline, by orbiting around the black hole. Hence the effect of caustics may be significant. For example, Fig. 2 shows orbiting null geodesics on the Schwarzschild spacetime which intersect timelike circular orbits of various radii. We believe that understanding the singular behavior of the integrand of Eq. (2.2) is a crucial step in understanding the origin of the nonlocal part of the self-force. As we shall see, the Nariai spacetime proves a fertile testing ground.

III. SCHWARZSCHILD AND NARIAI SPACETIMES

To evaluate the retarded Green function (2.6) we require solutions to the homogeneous scalar-field equation on the appropriate curved background. In the absence of sources, the scalar-field equation (1.1) is

$$\frac{1}{\sqrt{-g}}\partial_\mu(\sqrt{-g}g^{\mu\nu}\partial_\nu\Phi) - \xi R\Phi = 0. \quad (3.1)$$

For the Schwarzschild spacetime, the line element is

$$ds^2 = -f_S(r)dt_S^2 + f_S^{-1}(r)dr^2 + r^2d\Omega_2^2,$$
$$d\Omega_2^2 = d\theta^2 + \sin^2\theta d\phi^2, \quad (3.2)$$

where $f_S(r) = 1 - 2M/r$ and the label "S" denotes "Schwarzschild." Decomposing the field in the usual way,

$$\Phi(x) = \int_{-\infty}^{\infty} d\omega_S \sum_{l=0}^{+\infty} \sum_{m=-l}^{+l} c_{lm\omega_S}\Phi_{lm\omega_S}(x)$$

where $\Phi_{lm\omega_S}(x) = \frac{u_{l\omega_S}^{(S)}(r)}{r}Y_{lm}(\theta, \phi)e^{-i\omega_S t_S}, \quad (3.3)$

where $Y_{lm}(\theta, \phi)$ are the spherical harmonics, $c_{lm\omega_S}$ are the coefficients in the mode decomposition, and the radial function $u_{l\omega_S}^{(S)}(r)$ satisfies the radial equation

$$\left[\frac{d^2}{dr_*^2} + \omega_S^2 - V_l^{(S)}(r)\right]u_{l\omega_S}^{(S)}(r) = 0 \quad (3.4)$$

with an effective potential

$$V_l^{(S)}(r) = f_S(r)\left(\frac{l(l+1)}{r^2} + \frac{f_S'(r)}{r}\right)$$
$$= \left(1 - \frac{2M}{r}\right)\left(\frac{l(l+1)}{r^2} + \frac{2M}{r^3}\right). \quad (3.5)$$

Here r_* is a tortoise (Regge-Wheeler) coordinate, defined by

$$\frac{dr_*}{dr} = f_S^{-1}(r) \Rightarrow$$
$$r_* = r + 2M\ln(r/2M - 1) - (3M - 2M\ln2). \quad (3.6)$$

The outer region $r \in (2M, +\infty)$ of the Schwarzschild black hole is now covered by $r_* \in (-\infty, +\infty)$. Note that we have chosen the integration constant for our convenience so that, in the high-l limit, the peak of the potential barrier (at $r = 3M$) coincides with $r_* = 0$.

A. Pöschl-Teller potential and Nariai spacetime

Unfortunately, to the best of our knowledge, closed-form solutions to (3.4) with potential (3.5) are not known. However, there is a closely related potential for which exact solutions are available: the so-called Pöschl-Teller potential [52],

$$V_l^{(PT)}(r_*) = \frac{\alpha^2 V_0}{\cosh^2(\alpha(r_* - r_*^{(0)}))} \quad (3.7)$$

where α, V_0, and $r_*^{(0)}$ are constants (V_0 may depend on l). Unlike the Schwarzschild potential, the Pöschl-Teller potential is symmetric about $r_*^{(0)}$, and decays exponentially in the limit $r_* \to \infty$. Yet, like the Schwarzschild potential, it has a single peak, and with an appropriate choice of constants, the Pöschl-Teller potential can be made to fit the Schwarzschild potential in the vicinity of this peak (see Fig. 3). In the Schwarzschild spacetime, the peak of the potential barrier is associated with the unstable photon orbit at $r = 3M$. As mentioned in the previous section (see Fig. 2), the photon orbit may lead to singularities in the distant past Green function, and in the integrand of (2.2). Hence by building a toy model which includes an unstable null orbit, we hope to capture the essential features of the distant past Green function. Authors have found that the Pöschl-Teller potential is a useful model for exploring (some of the) properties of the Schwarzschild solution, for example, the quasinormal mode frequency spectrum [53,54]. In this work, we hope to gain some insight into the distant past integral on the Schwarzschild spacetime by using the exact wave functions for the Pöschl-Teller potential, given later in Sec. IV A 1.

An obvious question follows: is there a spacetime on which the scalar-field equation reduces to a radial wave equation with a Pöschl-Teller potential? The answer turns out to be yes [55,56]. The relevant spacetime was first introduced by Nariai in 1950 [38,39].

To show the correspondence explicitly, let us define the line element

$$ds^2 = -f(\rho)dt_N^2 + f^{-1}(\rho)d\rho^2 + d\Omega_2^2, \qquad (3.8)$$

where $f(\rho) = 1 - \rho^2$ and $\rho \in (-1, +1)$. The line element (3.8) describes the central diamond of the Penrose diagram of the Nariai spacetime (Fig. 4), which is described more fully in Sec. III B. Consider the wave equation (3.1) on this spacetime. We seek separable solutions of the form $\Phi(x) = u_{l\omega_N}^{(N)}(\rho)Y_{lm}(\theta, \phi)e^{-i\omega_N t_N}$, where the label "$N$" denotes "Nariai." The radial function satisfies the equation

$$f(\rho)\frac{d}{d\rho}\left(f(\rho)\frac{du_{l\omega_N}^{(N)}}{d\rho}\right)$$
$$+ (\omega_N^2 - f(\rho)[l(l+1) + \xi R])u_{l\omega_N}^{(N)}(\rho) = 0 \quad (3.9)$$

where ξ is the curvature coupling constant and $R = 4$ is the Ricci scalar. Now let us define a new tortoise coordinate in the usual way,

$$\frac{d\rho_*}{d\rho} = f^{-1}(\rho) \Rightarrow \rho_* = \tanh^{-1}\rho. \qquad (3.10)$$

Note that $f(\rho) = \text{sech}^2(\rho_*)$ and the tortoise coordinate is in the range $\rho_* \in (-\infty, +\infty)$. Hence the radial equation (3.9) may be rewritten in Pöschl-Teller form,

$$\left(\frac{d^2}{d\rho_*^2} + \omega_N^2 - \frac{U_0}{\cosh^2\rho_*}\right)u_{l\omega_N}^{(N)}(\rho_*) = 0 \qquad (3.11)$$

where $U_0 = l(l+1) + 4\xi$. We take the point of view that, as well as being of interest in its own right, the Nariai spacetime can provide insight into the propagation of waves on the Schwarzschild spacetime. The closest analogy between the two spacetimes is found by making the associations

$$\rho_* \rightleftharpoons \alpha r_*, \qquad t_N \rightleftharpoons \alpha t_S,$$
$$\omega_N \rightleftharpoons \omega_S/\alpha \quad \text{where } \alpha = 1/(\sqrt{27}M). \qquad (3.12)$$

Figure 3 shows the corresponding match between the potential barriers $V_l^{(S)}(r_*)$ and $V_l^{(PT)}(\rho_*)$. In the following sections, we drop the label "N," so that $t \equiv t_N$ and $\omega \equiv \omega_N$.

The solutions of Eq. (3.11) are presented in Sec. IV A 1. First, though, we consider the Nariai spacetime in more detail.

B. Nariai spacetime

The Nariai spacetime [38,39] may be constructed from an embedding in a six-dimensional Minkowski space
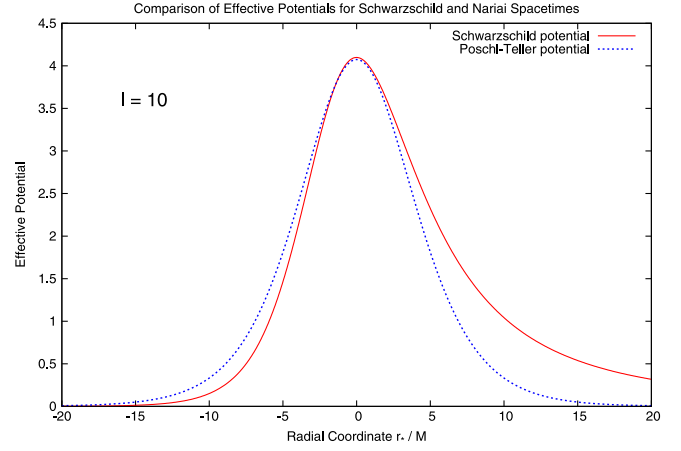

FIG. 3 (color online). Effective potentials for Schwarzschild (3.5) and Pöschl-Teller (3.7) radial wave equations. Note that here the Schwarzschild tortoise coordinate is defined in (3.6) so that the peak is near $r_* = 0$. The constants in (3.7) are $V_0 = l(l+1)$, $r_*^{(0)} = 0$, and $\alpha = 1/(\sqrt{27}M)$.

$$ds^2 = -dZ_0^2 + \sum_{i=1}^{5} dZ_i^2 \qquad (3.13)$$

of a 4-D surface determined by the two constraints

$$-Z_0^2 + Z_1^2 + Z_2^2 = a^2,$$
$$Z_3^2 + Z_4^2 + Z_5^2 = a^2, \quad \text{where } a > 0, \qquad (3.14)$$

corresponding to a hyperboloid and a sphere, respectively. The entire manifold is covered by the coordinates $\{\mathcal{T}, \psi, \theta, \phi\}$ defined via

$$Z_0 = a\sinh\left(\frac{\mathcal{T}}{a}\right), \qquad Z_1 = a\cosh\left(\frac{\mathcal{T}}{a}\right)\cos\psi,$$
$$Z_2 = a\cosh\left(\frac{\mathcal{T}}{a}\right)\sin\psi, \qquad (3.15)$$

$$Z_3 = a\sin\theta\cos\phi, \qquad Z_4 = a\sin\theta\sin\phi,$$
$$Z_5 = a\cos\theta, \qquad (3.16)$$

with $\mathcal{T} \in (-\infty, +\infty)$, $\psi \in [0, 2\pi)$, $\theta \in [0, \pi]$, $\phi \in [0, 2\pi)$. The line element is given by

$$ds^2 = -d\mathcal{T}^2 + a^2\cosh^2\left(\frac{\mathcal{T}}{a}\right)d\psi^2 + a^2 d\Omega_2^2. \qquad (3.17)$$

From this line element one can see that the spacetime has the following features: (1) it has geometry $dS_2 \times \mathbb{S}^2$ and topology $\mathbb{R} \times \mathbb{S}^1 \times \mathbb{S}^2$ (the radius of the one-sphere diminishes with time down to a value a at $\mathcal{T} = 0$ and then increases monotonically with time $\mathcal{T}$, whereas the two-spheres have *constant* radius a), (2) it is symmetric (i.e., $R_{\mu\nu\rho\sigma;\tau} = 0$), with $R_{\mu\nu} = \Lambda g_{\mu\nu}$ and a constant Ricci scalar $R = 4\Lambda$, where $\Lambda = 1/a^2$ is the value of the cosmological constant, (3) it is spherically symmetric (though

not isotropic), homogeneous, and locally (not globally) static, and (4) its conformal structure can be obtained by noting the Kruskal-like coordinates defined via $U = -(1 - \Lambda UV)(Z_0 + Z_1)/2$, $V = -(1 - \Lambda UV)(Z_0 - Z_1)/2$, for which the line element is then

$$ds^2 = -\frac{4 dU dV}{(1 - \Lambda UV)^2} + d\Omega_2^2. \qquad (3.18)$$

Its two-dimensional conformal *Penrose diagram* is shown in Fig. 4 (see, e.g., [57]), where we have defined the conformal time $\zeta \equiv 2 \arctan(\mathcal{T}/a) \in (0, \pi)$. Its Penrose diagram differs from that of de Sitter spacetime in that here each point represents a two-sphere of *constant* radius; note also that the corresponding angular coordinate ψ in de Sitter spacetime has a different range, $\psi \in [0, \pi)$, which corresponds to its $\mathbb{R} \times \mathbb{S}^3$ topology. Past and future timelike infinity $i^{\pm}$ coincide with past and future null infinity $\mathcal{I}^{\pm}$, respectively, and they are all spacelike hypersurfaces. A consequence of the latter fact is the existence of *past/future (cosmological) event horizons* [57–59]: not all events in the spacetime will be influentiable/observable by a geodesic observer; the boundary of the future/past of the worldline of the observer is its past/future (cosmological) event horizon.

In this paper, we consider the *static* region of the Nariai spacetime which is covered by the coordinates $\{t, \rho, \theta, \phi\}$, where $\rho \equiv a \tanh(\rho_*/a) \in (-a, +a)$, $\rho_* \equiv (v - u)/2 \in (-\infty, +\infty)$, $t \equiv (v + u)/2 \in (-\infty, +\infty)$, and the null coordinates $\{u, v\}$ are given via $U = ae^{-u/a}$, $V = -ae^{v/a}$. This coordinate system, $\{t, \rho, \theta, \phi\}$, covers the diamond-shaped region in the Penrose diagram (Fig. 4) around the hypersurface, say, $\psi = \pi$ (because of homogeneity we could choose any other $\psi = $ constant hypersurface). We denote by $\mathcal{H}_{\pm}^-$ the past cosmological event horizon at $\rho = \pm a$ of an observer moving along $\psi = \pi$; similarly, $\mathcal{H}_{\pm}^+$

will denote its future cosmological event horizon at $\rho = \pm a$. Interestingly, Ginsparg and Perry [60] showed that this static region is obtained from the Schwarzschild–de Sitter black hole spacetime as a particular limiting procedure in which the event and cosmological horizons of the Schwarzschild–de Sitter coincide (see also [61–64]).

Note that there are three hypersurfaces $\rho = 0$, only two of which (those corresponding to $\psi = 0$ and 2π) are identified (the one corresponding to $\psi = \pi$ is not). Without loss of generality, we will take $\Lambda = 1 = a$. The line element corresponding to this static coordinate system is given in (3.8).

C. Geodesics on Nariai spacetime

Let us now consider geodesics on the Nariai spacetime. Our chief motivation is to find the orbiting geodesics, the analogous rays to those shown in Fig. 2 for the Schwarzschild spacetime. We wish to find the coordinate times $t - t'$ for which two angularly separated points at the same "radius" ρ (the quotes indicate the fact that the area of the two-spheres does not depend on ρ) may be connected by a null geodesic. We expect the Green function to be singular at these times $t - t'$.

We will assume that particle motion takes place within the central diamond of the Penrose diagram in Fig. 4, that is, the region $-1 < \rho < 1$ (notwithstanding the fact that timelike geodesics may pass through the future horizons $\mathcal{H}_{+}^+$ and $\mathcal{H}_{-}^+$ in finite proper time). Without loss of generality, let us consider motion in the equatorial plane ($\theta = \pi/2$) described by the worldline $z^{\mu}(\lambda) = [t(\lambda), \rho(\lambda), \pi/2, \phi(\lambda)]$ with the tangent vector $u^{\mu} = [\dot{t}, \dot{\rho}, 0, \dot{\phi}]$, where the overdot denotes differentiation with respect to an affine parameter λ. Symmetry implies two constants of motion, $k = f(\rho)\dot{t}$ and $h = \dot{\phi}$. The radial equation is $\dot{\rho} = \pm H(\rho^2 - \rho_0^2)^{1/2}$, where $\rho_0 = \sqrt{1 - k^2/H^2}$ is the closest approach
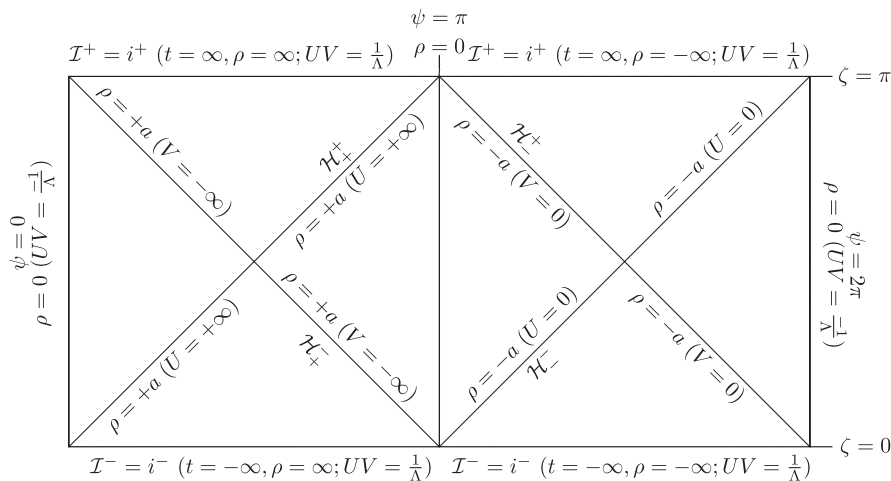

$\psi = \pi$

$\mathcal{I}^+ = i^+ \ (t = \infty, \rho = \infty; UV = \frac{1}{\Lambda})$ $\quad \rho = 0$ $\quad \mathcal{I}^+ = i^+ \ (t = \infty, \rho = -\infty; UV = \frac{1}{\Lambda})$ $\qquad \zeta = \pi$

$\rho = +a \ (V = -\infty)$ $\quad \mathcal{H}_+^+ \ (U = +\infty)$ $\quad \rho = -a \ \mathcal{H}_+^+$ $\quad \rho = -a \ (U = 0)$

$\psi = 0 \ (UV = \frac{-1}{\Lambda})$ $\quad \rho = 0$

$\rho = +a \ (U = +\infty)$ $\quad \mathcal{H}_+^- \ (V = -\infty)$ $\quad \rho = +a \ (V = 0)$ $\quad \rho = -a \ (U = 0)$ $\quad \mathcal{H}_-^- \ \rho = -a \ (V = 0)$

$\rho = 0 \ (UV = \frac{-1}{\Lambda})$ $\qquad\qquad\qquad$ $\psi = 2\pi \ (UV = \frac{-1}{\Lambda})$

$\mathcal{I}^- = i^- \ (t = -\infty, \rho = \infty; UV = \frac{1}{\Lambda})$ $\quad \mathcal{I}^- = i^- \ (t = -\infty, \rho = -\infty; UV = \frac{1}{\Lambda})$ $\qquad \zeta = 0$

FIG. 4. Penrose diagram for the Nariai spacetime in coordinates (ψ, ζ). The hypersurfaces $\psi = 0$ and $\psi = 2\pi$ are identified. Past/future timelike infinity $i^{-/+}$ coincides with past/future null infinity $\mathcal{I}^{-/+}$, and they are all spacelike hypersurfaces. Thus, there exist observer-dependent past and future cosmological event horizons, here marked as $\mathcal{H}_{\pm}^{\pm}$ for an observer along $\psi = \pi$.

point and $H^2 = h^2 + \kappa m_0^2$. Here, m_0 is the scaling of the affine parameter (which is equal to the particle's rest mass in the case of a massive particle following a timelike geodesic) and $\kappa = +1$ for timelike geodesics, $\kappa = 0$ for null geodesics, and $\kappa = -1$ for spacelike geodesics. We still have the freedom to rescale the affine parameter λ by choosing a value for m_0. It is conventional to rescale so that λ corresponds to proper time or distance, that is, set $m_0 = 1$. Instead, we will rescale so that $\lambda = \phi$ [N.B. here ϕ and $\Delta\phi$ are unbounded, $\phi, \Delta\phi \in [0, +\infty)$, as opposed to $\gamma \in [0, \pi]$]; that is, we set $h = 1$.

Let us consider a geodesic that starts at $\rho = \rho_1$, $\phi = 0$ which returns to radius $\rho = \rho_1$ after passing through an angle of $\Delta\phi$. The geodesic distance in this case is $s = -\kappa(H^2 - 1)^{1/2}\Delta\phi$. It is straightforward to show that

$$\rho(\phi) = \rho_1 \frac{\cosh(H\phi - H\Delta\phi/2)}{\cosh(H\Delta\phi/2)}, \quad (3.19)$$

hence the radius of closest approach ρ_0 is

$$\rho_0 = \rho_1 \mathrm{sech}(H\Delta\phi/2). \quad (3.20)$$

The coordinate time Δt_1 it takes to go from $\rho = \rho_1$, $\phi = 0$ to $\rho = \rho_1$, $\phi = \Delta\phi$ is

$$\Delta t_1 = 2\rho_{*_1} + \ln\left(\frac{\rho_1 - \rho_0^2 + \sqrt{(1 - \rho_0^2)(\rho_1^2 - \rho_0^2)}}{\rho_1 + \rho_0^2 - \sqrt{(1 - \rho_0^2)(\rho_1^2 - \rho_0^2)}}\right) \quad (3.21)$$

where $\rho_{*_1} = \tanh^{-1}(\rho_1)$. Substituting (3.20) into (3.21) yields Δt_1 as a function of the angle $\Delta\phi$,

$$\Delta t_1 = 2\rho_{*_1} + \ln\left(\frac{1 - \rho_1\mathrm{sech}^2(H\Delta\phi/2) + \tanh(H\Delta\phi/2)\sqrt{1 - \rho_1^2\mathrm{sech}^2(H\Delta\phi/2)}}{1 + \rho_1\mathrm{sech}^2(H\Delta\phi/2) - \tanh(H\Delta\phi/2)\sqrt{1 - \rho_1^2\mathrm{sech}^2(H\Delta\phi/2)}}\right). \quad (3.22)$$

This takes a particularly simple form as $\rho_1 \to 1$,

$$\Delta t_1 \sim 2\rho_{*_1} + \ln(\sinh^2(H\Delta\phi/2)), \quad \text{for } \rho_1 \to 1. \quad (3.23)$$

As $\Delta\phi \to \infty$, the geodesic coordinate time increases linearly with the orbital angle $\Delta\phi$,

$$\Delta t_1 \sim 2\rho_{*_1} + H\Delta\phi, \quad \text{for } \Delta\phi \to \infty, \ \rho_1 \to 1. \quad (3.24)$$

In other words, for fixed spatial points near $\rho = 1$, the geodesic coordinate times Δt_1 are very nearly periodic, with the period $2\pi H$. Results (3.19), (3.22), (3.23), and (3.24) will prove useful when we come to consider the singularities of the Green function in Secs. V D and V E.

IV. THE SCALAR GREEN FUNCTION

A. Retarded Green function as a mode sum

The retarded Green function for a scalar field on the Nariai spacetime is defined by Eq. (2.3), together with appropriate causality conditions. As described in Sec. II the retarded Green function may be defined through a Laplace integral transform and an angular l-mode sum,

$$G_{\mathrm{ret}}(t, \rho_*; t', \rho'_*; \gamma) = \frac{1}{2\pi}\int_{-\infty+ic}^{+\infty+ic} d\omega \sum_{l=0}^{+\infty} \tilde{g}_{l\omega}(\rho_*, \rho'_*)$$
$$\times (2l+1)P_l(\cos\gamma)e^{-i\omega(t-t')}, \quad (4.1)$$

where ρ_* and t are the "tortoise" and "time" coordinates in the line element (3.8), c is a positive real constant, $t - t'$ is the coordinate time difference, and γ is the spatial angle separating the points. The remaining ingredient in this formulation is the one-dimensional (radial) Green function $\tilde{g}_{l\omega}(\rho_*, \rho'_*)$ which satisfies

$$\left[\frac{d^2}{d\rho_*^2} + \omega^2 - \frac{U_0}{\cosh^2\rho_*}\right]\tilde{g}_{l\omega}(\rho_*, \rho'_*) = -\delta(\rho_* - \rho'_*). \quad (4.2)$$

The radial Green function may be constructed from two linearly independent solutions of the radial equation (3.11). To ensure a *retarded* Green function we apply causal boundary conditions: no flux may emerge from the past horizons $\mathcal{H}^-_-$ and $\mathcal{H}^-_+$ (see Fig. 4). To this end, we will employ a pair of solutions denoted $u^{\mathrm{in}}_{l\omega}$ and $u^{\mathrm{up}}_{l\omega}$, in analogy with the Schwarzschild case. These solutions are defined in the next subsection.

1. Radial solutions

The homogeneous radial equation (3.11) may be rewritten as the Legendre differential equation

$$\frac{d}{d\rho}\left((1 - \rho^2)\frac{du_{l\omega}}{d\rho}\right) + \left(\beta(\beta + 1) - \frac{\mu^2}{1 - \rho^2}\right)u_{l\omega} = 0 \quad (4.3)$$

where

$$\mu = \pm i\omega, \qquad \beta = -1/2 + i\lambda, \quad (4.4)$$

$$\lambda = \pm\sqrt{(l + 1/2)^2 + d}, \qquad d = 4\xi - 1/2. \quad (4.5)$$

We choose $\mu = i\omega$, $\lambda = \sqrt{(l + 1/2)^2 + d}$ and note that the choice of signs will not have a bearing on the result. The value of the constant ξ in the conformally coupled case in a D-dimensional spacetime is $(D - 2)/(4(D - 1))$. Note that for conformal coupling in 4-D ($\xi = 1/6$), the constant is $d = 1/6$, and for minimal coupling ($\xi = 0$) we have $d = -1/2$. For the special value $\xi = 1/8$, we have

$d = 0$. The possible significance of the value $\xi = 1/8$, the conformal-coupling factor in three dimensions, was recently noted in a study of the self-force on wormhole spacetimes [65].

The solutions of Eq. (4.3) are associated Legendre functions of complex order, which are defined in terms of hypergeometric functions as follows [Ref. [66], Eq. (8.771)],

$$P_\beta^\mu(\rho) = \frac{1}{\Gamma(1-\mu)}\left(\frac{1+\rho}{1-\rho}\right)^{\mu/2}$$
$$\times {}_2F_1\left(-\beta, \beta+1; 1-\mu; \frac{1-\rho}{2}\right). \quad (4.6)$$

Note that $P_{-1/2+i\lambda}^\mu(\rho) = P_{-1/2-i\lambda}^\mu(\rho)$, so clearly any results will be independent of the choice of sign for λ in (4.5). In the particular case $\mu = 0$, the solutions belong to the class of conical functions [Ref. [66], Eq. (8.840)]. We define the pair of linearly independent solutions (see Penrose diagram in Fig. 5) to be

$$u_{l\omega}^{(\text{in})}(\rho) = \Gamma(1-\mu)P_\beta^\mu(-\rho), \quad (4.7)$$

$$u_{l\omega}^{(\text{up})}(\rho) = \Gamma(1-\mu)P_\beta^\mu(\rho). \quad (4.8)$$

These solutions are labeled "in" and "up" because they obey analogous boundary conditions to the "ingoing at
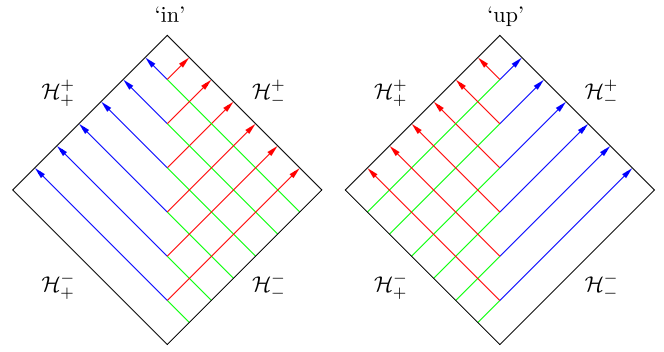

FIG. 5 (color online). Penrose diagrams for "in" and "up" radial solutions.

horizon" and "outgoing at infinity" solutions that are causally appropriate in the Schwarzschild case [51]. It is straightforward to verify that the in and up solutions obey

$$u_{l\omega}^{(\text{in})} \sim e^{-i\omega\rho_*} \quad \text{as } \rho_* \to -\infty, \quad (4.9)$$

$$u_{l\omega}^{(\text{up})} \sim e^{+i\omega\rho_*} \quad \text{as } \rho_* \to +\infty. \quad (4.10)$$

To find the asymptotes of $u_{l\omega}^{(\text{in})}$ near $\rho = 1$, we may employ the series expansion

$$\begin{aligned} {}_2F_1(a, b; c; z) = {} & \frac{\Gamma(c)\Gamma(a+b-c)}{\Gamma(a)\Gamma(b)}(1-z)^{c-a-b}\left[\sum_{k=0}^\infty \frac{(c-a)_k(c-b)_k}{(c+1-a-b)_k}\frac{(1-z)^k}{k!}\right] \\ & + \frac{\Gamma(c)\Gamma(c-a-b)}{\Gamma(c-a)\Gamma(c-b)}\left[\sum_{k=0}^\infty \frac{a_k b_k}{(1+a+b-c)_k}\frac{(1-z)^k}{k!}\right] \end{aligned} \quad (4.11)$$

where $(z)_k \equiv \Gamma(z+k)/\Gamma(z)$ is the Pochhammer symbol. In our case $a = -\beta$, $b = \beta+1$, $c = 1-\mu$, and $1-z = (1-\rho)/2$. It is straightforward to show that

$$u_{l\omega}^{(\text{in})}(\rho_*) \sim \begin{cases} e^{-i\omega\rho_*} & \rho_* \to -\infty \\ A_{l\omega}^{(\text{out})}e^{i\omega\rho_*} + A_{l\omega}^{(\text{in})}e^{-i\omega\rho_*} & \rho_* \to +\infty, \end{cases} \quad (4.12)$$

where

$$A_{l\omega}^{(\text{in})} = \frac{\Gamma(1-i\omega)\Gamma(-i\omega)}{\Gamma(1+\beta-i\omega)\Gamma(-\beta-i\omega)}, \quad (4.13)$$

$$A_{l\omega}^{(\text{out})} = \frac{\Gamma(1-i\omega)\Gamma(i\omega)}{\Gamma(1+\beta)\Gamma(-\beta)}, \quad (4.14)$$

with β as defined in (4.4). The up solution is found from the in solution via spatial inversion $\rho \to -\rho$; hence

$$u_{l\omega}^{(\text{up})}(\rho_*) \sim \begin{cases} A_{l\omega}^{(\text{out})}e^{-i\omega\rho_*} + A_{l\omega}^{(\text{in})}e^{i\omega\rho_*} & \rho_* \to -\infty \\ e^{i\omega\rho_*} & \rho_* \to +\infty. \end{cases} \quad (4.15)$$

The Wronskian W of the two linearly independent solutions $u_{l\omega}^{\text{in}}(\rho_*)$ and $u_{l\omega}^{\text{up}}(\rho_*)$ can be easily obtained:

$$W = u_{l\omega}^{\text{in}}(\rho_*)\frac{du_{l\omega}^{\text{up}}}{d\rho_*} - u_{l\omega}^{\text{up}}(\rho_*)\frac{du_{l\omega}^{\text{in}}}{d\rho_*} = 2i\omega A_{l\omega}^{(\text{in})}. \quad (4.16)$$

The one-dimensional Green function $\tilde{g}_{l\omega}(\rho_*, \rho_*')$ is then given by

$$\begin{aligned} \tilde{g}_{l\omega} & (\rho_*, \rho_*') \\ & = -\frac{1}{W}\begin{cases} u_{l\omega}^{\text{in}}(\rho_*)u_{l\omega}^{\text{up}}(\rho_*') & \rho_* < \rho_*' \\ u_{l\omega}^{\text{up}}(\rho_*)u_{l\omega}^{\text{in}}(\rho_*') & \rho_* > \rho_*' \end{cases} \\ & = \frac{1}{2}\Gamma(1+\beta-\mu)\Gamma(-\beta-\mu)P_\beta^\mu(-\rho_<)P_\beta^\mu(\rho_>), \quad (4.17) \end{aligned}$$

where $\rho_< \equiv \min(\rho, \rho')$ and $\rho_> \equiv \max(\rho, \rho')$. The four-dimensional retarded Green function can thus be written as

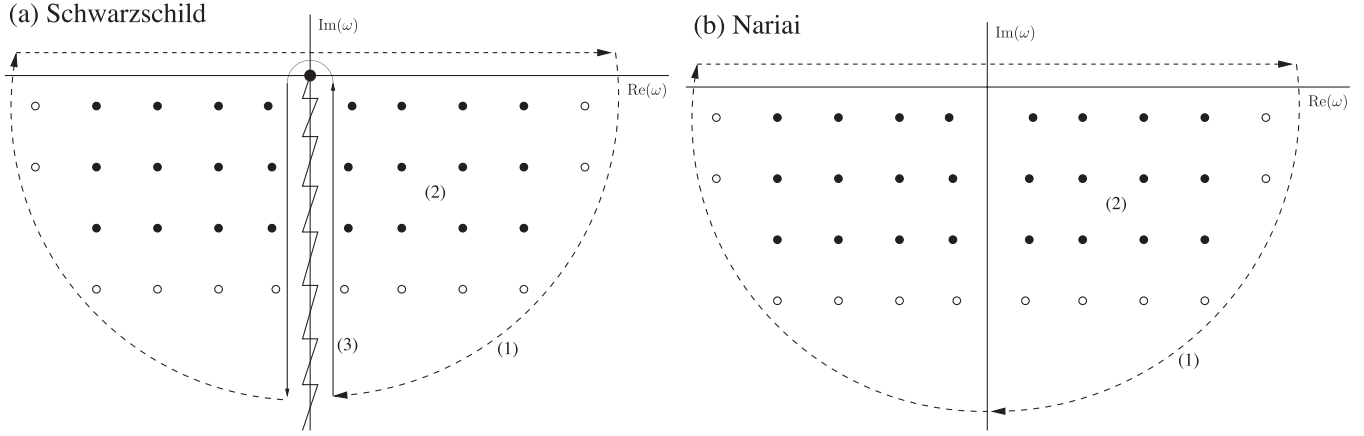(a) Schwarzschild   (b) Nariai

FIG. 6.   Contour integrals. These plots show the deformation of the integral over frequency in the complex plane to include the poles of the Green function (quasinormal modes), for two spacetimes: (a) Schwarzschild (left plot) (including a branch point at $\omega = 0$ and the corresponding branch cut) and (b) Nariai (right plot) (for $\xi > 0$).

$$G_{\rm ret}(x, x') = \frac{1}{4\pi} \sum_{l=0}^{+\infty} (2l + 1) P_l(\cos\gamma) \int_{-\infty+ic}^{+\infty+ic} d\omega\, e^{-i\omega(t-t')} \Gamma\left(\frac{1}{2} + i\lambda - i\omega\right) \Gamma\left(\frac{1}{2} - i\lambda - i\omega\right) P_{-1/2+i\lambda}^{i\omega}(-\rho_<) P_{-1/2+i\lambda}^{i\omega}(\rho_>).$$

(4.18)

Unfortunately, we have not been able to find anywhere in the literature where this retarded Green function has been obtained in closed form. In this paper we will calculate it and extract interesting information about it (such as its singularity structure) by using a combination of analytic and numerical techniques.

B. Distant past Green function: the quasinormal mode sum

As discussed in Sec. II, the integral over frequency in Eq. (4.1) may be evaluated by deforming the contour in the complex plane [50,51]. The deformation is shown in Fig. 6. The left plot (a) shows the Schwarzschild case, and the right plot (b) shows the Nariai case.

On the Schwarzschild spacetime, it is well known that a "power-law tail" arises from the frequency integral along a branch cut along the (negative) imaginary axis [Fig. 6, part (3)]. In the Schwarzschild case, the branch cut is necessary due to a branch point in $\tilde{g}_{l\omega}(r, r')$ at $\omega = 0$ [50,67]. In contrast, for the Nariai case with $\xi > 0$, $\omega = 0$ is a regular point of $\tilde{g}_{l\omega}(r, r')$ [the Wronskian (4.16) is well defined and nonzero in the limit $\omega \to 0$ and the Legendre functions $P_\beta^\mu(\rho)$ are regular for $\rho \in (-1, +1)$]. Interestingly, for minimal coupling ($\xi = 0$), we find that $\omega = 0$ is a simple pole of $\tilde{g}_{l\omega}(r, r')$ when $l = 0$, and yet $A_{l=0,\omega=0}^{(in)} \neq 0$, so this mode does not obey the quasinormal mode boundary conditions (see below); we will not consider the minimal-coupling case in this paper, however. In either case ($\xi > 0$ and $\xi = 0$), $\omega = 0$ is not a branch point and hence power-law decay does not arise on the Nariai spacetime.

The simple poles of the Green function (shown as dots in Fig. 6) occur in the lower half-plane of the complex

frequency plane. Given that the associated Legendre functions $P_\beta^\mu(\rho)$ have no poles for fixed $\rho \in (-1, +1)$, and that the poles of $\Gamma(1 - \mu)$ in Eqs. (4.7) and (4.8) cancel out with those of the Wronskian, the poles of the Green function correspond to the zeros of the Wronskian (4.16). The Wronskian is zero when the in and up solutions are linearly dependent. This occurs at a discrete set of (complex) QNM frequencies ω_q. Beyer [68] has shown that, for the Pöschl-Teller potential, the corresponding QNM radial solutions form a *complete basis* at sufficiently late times ($t > t_c$, to be defined below). Completeness means that *any* wave function obeying the correct boundary conditions at $\rho_* \to \pm\infty$ can be represented as a sum over quasinormal modes, to arbitrary precision. Intuitively, we may expect this to mean that, at sufficiently late times, the Green function itself can be written as a sum over the residues of the poles.

1. Quasinormal modes

QNMs are solutions to the radial wave equation (3.11) which are left-going ($e^{-i\omega\rho_*}$) as $\rho_* \to -\infty$ and right-going ($e^{+i\omega\rho_*}$) as $\rho_* \to +\infty$. QNMs occur at discrete complex frequencies $\omega = \omega_q$ for which $A_{l\omega_q}^{(in)} = 0$ (with the mentioned exception of $\omega = 0$ for modes $l = 0$ in the case $\xi = 0$). At QNM frequencies, the in and up solutions ($u_{l\omega_q}^{in}$ and $u_{l\omega_q}^{up}$) are linearly dependent and the Wronskian (4.16) is zero.

The QNMs of the Schwarzschild black hole have been studied in much detail [69–72]. QNM frequencies are complex, with the real part corresponding to oscillation frequency, and the (negative) imaginary part corresponding to damping rate. QNM frequencies ω_{ln} are labeled by two integers: l, the angular momentum, and $n = 0, 1, \ldots \infty$, the

overtone number. For every multipole l, there are an infinite number of overtones. In the asymptotic limit $l \gg n$, the Schwarzschild QNM frequencies approach [53,73,74]

$$M\omega_{ln}^{(S)} \approx \frac{1}{\sqrt{27}}[\pm(l + 1/2) - i(n + 1/2)]. \quad (4.19)$$

In general, the damping increases with n. The $n = 0$ ("fundamental") modes are the least damped.

The quasinormal modes of the Nariai spacetime are found from the condition $A_{l\omega_{ln}}^{(\mathrm{in})} = 0$. Using (4.13), we find

$$1 + \beta - i\omega_{ln} = -n \quad \mathrm{or} \quad -\beta - i\omega_{ln} = -n \quad (4.20)$$

where n is a non-negative integer. These conditions lead to the QNM frequencies

$$\omega_{ln} = -\lambda - i(n + 1/2), \quad (4.21)$$

where λ is defined in (4.5). (Note we have chosen the sign of the real part of the frequency here for consistency with previous studies [53,54] which use $\sigma = -\omega$ as the frequency variable.)

2. The quasinormal mode sum

The quasinormal mode sum is constructed from (2.6) by taking the sum over the residues of the poles of $\tilde{g}_{l\omega}(\rho, \rho')$ in the complex-ω plane. Applying Leaver's analysis [50] to (2.6), with the radial Green function (4.17), we obtain

$$G_{\mathrm{ret}}^{\mathrm{QNM}}(t, \rho; t', \rho'; \gamma) = 2\,\mathrm{Re}\sum_{n=0}^{+\infty}\sum_{l=0}^{+\infty}(2l + 1)P_l(\cos\gamma)$$

$$\times \mathcal{B}_{ln}\tilde{u}_{ln}(\rho)\tilde{u}_{ln}(\rho')e^{-i\omega_{ln}T}, \quad (4.22)$$

where

$$T \equiv t - t' - \rho_* - \rho'_*, \quad (4.23)$$

and the sum is taken over *either* the third or fourth quadrant of the frequency plane only. Here, ρ and t are the coordinates in line element (3.8), ρ_* is defined in (3.10), ω_{ln} are the QNM frequencies and $\mathcal{B}_{ln}$ are the *excitation factors*, defined as

$$\mathcal{B}_{ln} \equiv \frac{A_{l\omega_{ln}}^{(\mathrm{out})}}{2\omega_{ln}\frac{dA_{l\omega}^{(\mathrm{in})}}{d\omega}|_{\omega_{ln}}}, \quad (4.24)$$

and $\tilde{u}_{ln}(\rho)$ are the QNM radial functions, defined by

$$\tilde{u}_{ln}(\rho_*) = \frac{u_{l\omega_{ln}}^{\mathrm{in}}(\rho_*)}{A_{l\omega_{ln}}^{(\mathrm{out})}e^{i\omega_{ln}\rho_*}}. \quad (4.25)$$

The QNM radial functions are normalized so that $\tilde{u}_{ln}(\rho) \to 1$ as $\rho \to 1$ ($\rho_* \to \infty$). The excitation factors, defined in (4.24), may be shown to be

$$\mathcal{B}_{ln} = \frac{1}{2n!}\frac{\Gamma(n + 1 - 2i\omega_{ln})}{[\Gamma(1 - i\omega_{ln})]^2}$$

$$= \frac{1}{2n!}\frac{\Gamma(-n + 2i\lambda)}{[\Gamma(-n + 1/2 + i\lambda)]^2}. \quad (4.26)$$

The steps in the derivation are given in Appendix A.3 of [54].

The Green function (4.22) now takes the form of a double infinite series, taken over both angular momentum l and overtone number n. Let us briefly consider the convergence properties of these sums.

The infinite series over n taken at fixed l is convergent if $t - t' > t_c$, where $t_c \equiv \rho_* + \rho'_*$ (i.e., at late times $T > 0$), and divergent if $t - t' < t_c$ (i.e., at "early times" $T < 0$). Note that the QNM frequencies have a negative imaginary part. The dominant quantity in the series is the exponential $\exp(-(n + 1/2)T)$, which decays or diverges more powerfully with n than any other factor in the sum (this can be seen from the exact analytic forms shown below for the excitation factors and the radial functions and their large-n asymptotic behavior). More details on the convergence with n in the Schwarzschild case are given in Sec. IIIB of [51], and their arguments follow through to our case. Beyer [68] has shown in the Nariai case that, for late times $T > 0$, QNMs form a *complete basis*. Physically, for the QNM n sum to be appropriate, sufficient coordinate time must elapse for a light ray to propagate inwards from ρ', reflect off the potential barrier near $\rho = 0$, and propagate outwards again to ρ.

The infinite series over l, taken at fixed n, is divergent. For large l, the magnitudes of the factors $(l + 1/2)\mathcal{B}_{ln}$, $P_l(\cos\gamma)$, and $\tilde{u}_{ln}(\rho)$ asymptote as, respectively, $(l + 1/2)^{n+1/2}$, $(l + 1/2)^{-1/2}$ [except at $\gamma = 0, \pi$, where it is equal to $+1$, $(-1)^l$, respectively; see Eq. (C8)] and a bounded term. Therefore, the limit $l = +\infty$ of the summand in (4.22) is not zero and so the l series (for fixed n) is divergent. Despite the series being divergent, we show in Sec. V C by applying a Watson transform that well-defined and meaningful values can be extracted from the series over l. This procedure (the Watson transform) is *not* possible globally, as the series also contains "physical" divergences, associated with the null wave front. We show in Sec. V A that the breakdown in validity of the Watson transform is related to a "coherent phase condition" for terms in the series.

3. Green function near spatial infinity, $\rho, \rho' \to +1$

In the limit that both radial coordinates ρ_* and ρ'_* tend to infinity ($\rho, \rho' \to +1$), the QNM sum (4.22) may be rewritten

$$G_{\mathrm{ret}}^{\mathrm{QNM}}(T, \gamma)$$

$$\sim 2\,\mathrm{Re}\sum_{l=0}^{\infty}(2l + 1)P_l(\cos\gamma)e^{i\lambda T}\sum_{n=0}^{\infty}\mathcal{B}_{ln}e^{-(n+1/2)T},$$

$$\rho_*, \rho'_* \to +\infty, \quad (4.27)$$

where λ was defined in (4.5). Using the expression for the excitation factors (4.26), the sum over n can be evaluated explicitly, as follows,

$$\sum_{n=0}^{\infty} \mathcal{B}_{ln} e^{-(n+1/2)T}$$

$$= \frac{z^{1/2}}{2} \sum_{n=0}^{\infty} \frac{\Gamma(-n + 2i\lambda)}{[\Gamma(-n + 1/2 + i\lambda)]^2} \frac{z^n}{n!}$$

$$= \frac{z^{1/2}}{2} \frac{\Gamma(2i\lambda)}{[\Gamma(1/2 + i\lambda)]^2} \sum_{n=0}^{\infty} \frac{(2i\lambda)_{-n}}{[(1/2 + i\lambda)_{-n}]^2} \frac{z^n}{n!} \quad (4.28)$$

where $z = e^{-T}$ and $(\cdot)_k$ is the Pochhammer symbol. Using the identity $(x)_{-n} = (-1)^n/(1 - x)_n$ and the duplication formula $\Gamma(z)\Gamma(z + 1/2) = 2^{1-2z}\sqrt{\pi}\Gamma(2z)$, we find

$$\sum_{n=0}^{\infty} \mathcal{B}_{ln} e^{-(n+1/2)T}$$

$$= \frac{e^{-T/2}}{4\sqrt{\pi}} \frac{2^{2i\lambda}\Gamma(i\lambda)}{\Gamma(1/2 + i\lambda)} {}_2F_1(-\beta, -\beta; -2\beta; -e^{-T})$$

$$(4.29)$$

where ${}_2F_1$ is the hypergeometric function, and β was defined in (4.4). Hence the Green function near spatial infinity ($\rho, \rho' \to 1$) is

$$G_{\text{ret}}^{\text{QNM}}(T, \gamma) \sim \frac{e^{-T/2}}{\sqrt{\pi}} \text{Re} \sum_{l=0}^{+\infty} \frac{(l + 1/2)\Gamma(i\lambda)}{\Gamma(1/2 + i\lambda)} P_l(\cos\gamma)$$

$$\times e^{i\lambda(T+2\ln 2)} {}_2F_1(-\beta, -\beta; -2\beta; -e^{-T}),$$

$$\rho_*, \rho_*' \to +\infty. \quad (4.30)$$

4. Green function at arbitrary "radii"

Unfortunately, it is not straightforward to perform the sum over n explicitly for general values of ρ and ρ'. Instead we must include the QNM radial functions $\tilde{u}_{ln}(\rho_*)$, defined by (4.7) and (4.25). We note that the Legendre function appearing in (4.7) can be expressed in terms of a hypergeometric function [see Eq. (4.6)], and the hypergeometric function can be written as a power series about $\rho = 1$ [Eq. (4.11)]. At quasinormal mode frequencies, the second term in Eq. (4.11) is zero, and hence the wave function is purely outgoing at infinity, as expected. Combining results (4.6), (4.7), (4.11), and (4.25) we find the normalized wave functions to be

$$\tilde{u}_{ln}(\rho) = \left(\frac{2}{1 + \rho}\right)^{i\omega_{ln}} \mathcal{S}_{ln}(\rho), \quad (4.31)$$

where ρ is the radial coordinate in line element (3.8) and $\mathcal{S}_{ln}$ is a finite series with n terms,

$$\mathcal{S}_{ln}(\rho) = \sum_{k=0}^{n} \frac{1}{k!} \frac{(-n + 2i\lambda)_k(-n)_k}{(-n + 1/2 + i\lambda)_k} \left(\frac{1 - \rho}{2}\right)^k$$

$$= {}_2F_1\left(-n + 2i\lambda, -n; -n + \frac{1}{2} + i\lambda; \frac{1 - \rho}{2}\right),$$

$$(4.32)$$

where we have adopted the sign convention $\omega_{ln} = -\lambda - i(n + 1/2)$ of (4.21). Hence the Green function at arbitrary radii may be written as the double sum

$$G_{\text{ret}}^{\text{QNM}}(x, x') = 2\,\text{Re} \sum_{l=0}^{\infty} (2l + 1) P_l(\cos\gamma) e^{i\lambda[T - \ln(2/(1+\rho)) - \ln(2/(1+\rho'))]} \sum_{n=0}^{\infty} \mathcal{B}_{ln} \left[\frac{4e^{-T}}{(1 + \rho)(1 + \rho')}\right]^{n+1/2} \mathcal{S}_{ln}(\rho)\mathcal{S}_{ln}(\rho'). \quad (4.33)$$

5. Green function approximation from fundamental modes

Expression (4.33) is complicated and difficult to analyze, as it involves a double infinite sum. It would be useful to have a simple approximate expression, with only a single sum, which captures the essence of the physics. At late times, we might expect that the Green function is dominated by the least-damped modes, that is, the $n = 0$ fundamental quasinormal modes. If we discard the higher modes $n > 0$, we are left with an approximation to the Green function which does indeed seem to capture the essential features and singularity structure. However, as we show in Sec. V D, it does not correctly predict the singularity times.

The $n = 0$ approximation to the Green function is

$$G_{\text{ret}}^{(n=0)}(x, x')$$

$$= \left(\frac{e^{-T}}{\pi(1 + \rho)(1 + \rho')}\right)^{1/2} \text{Re} \sum_{l=0}^{+\infty} \frac{(2l + 1)P_l(\cos\gamma)\Gamma(i\lambda)}{\Gamma(1/2 + i\lambda)}$$

$$\times e^{i\lambda[T+\ln(1+\rho)(1+\rho')]}, \quad (4.34)$$

since $\mathcal{S}_{l0}(\rho) \equiv 1$. Note that the sum over l is approximately

periodic in T (exactly periodic in the case $\xi = 1/8$), with period 4π.

C. Quasilocal Green function: Hadamard-WKB expansion

We now consider the Green function in the quasilocal region, which is needed for the calculation of the quasilocal contribution to the scalar self-force $\Phi_\mu^{(\text{QL})}$ given in Eq. (2.4). When spacetime points x and x' are sufficiently close together (within a *normal neighborhood*—see footnote [1]), the retarded Green function may be expressed in the Hadamard parametrix [42,43],

$$G_{\text{ret}}(x, x') = \theta_-(x, x')\{U(x, x')\delta(\sigma(x, x'))$$

$$- V(x, x')\theta(-\sigma(x, x'))\}, \quad (4.35)$$

where $\theta_-(x, x')$ is analogous to the Heaviside step function (unity when x' is in the causal past of x, and zero otherwise), $\delta(\sigma(x, x'))$ is the standard Dirac delta function, $U(x, x')$ and $V(x, x')$ are symmetric bi-scalars having the benefit that they are regular for $x' \to x$, and $\sigma(x, x')$ is the Synge [16,75,76] world function. Clearly, the term involving $U(x, x')$, the "direct" part, will not contribute to the

quasilocal integral in Eq. (2.4) since it has support only on the light cone, while the integral is internal to the light cone. We will therefore only concern ourselves with the calculation of the function $V(x, x')$, the "tail" part, which has support inside the light cone.

The fact that x and x' are close together suggests that an expansion of $V(x, x')$ in powers of the separation of the points may give a good representation of the function within the quasilocal region. In Ref. [77] we use a WKB method (based on that of Refs. [44,78,79]) to derive such a coordinate expansion, and we also give estimates of its range of validity. Referring to the results therein, we have $V(x, x')$ as a power series in $(t - t')$ and $(\cos\gamma - 1)$,

$$V(x, x') = \sum_{i,j=0}^{+\infty} v_{ij}(\rho)(t - t')^{2i}(\cos\gamma - 1)^j, \quad (4.36)$$

where γ is the angular separation of the points. In general, this expression also includes a third index, k, corresponding to the kth power of the radial separation of the points, $(\rho - \rho')^k$. However, for the nonradial motion considered in the present work, we will only need the terms of order $O[(\rho - \rho')^0]$ and $O[(\rho - \rho')^1]$. The $k = 0$ terms, $v_{ij0} = v_{ij}$, are given by Eq. (4.36) and Ref. [77], and the $k = 1$ terms, v_{ij1}, are easily calculated from the $k = 0$ terms using the identity [48]

$$v_{ij1}(\rho) = -\tfrac{1}{2}v_{ij0,\rho}(\rho). \quad (4.37)$$

Equation (4.36) therefore gives the quasilocal contribution to the retarded Green function as required in the present context.

V. SINGULAR STRUCTURE OF THE GREEN FUNCTION

In this section we investigate the singular structure of the Green function. We note that one expects the Green function to be singular when its two argument points are connected by a null geodesic, on account of the "propagation of singularities" theorems of Duistermaat and Hörmander [80,81] and their application to the Hadamard elementary function [which is, except for a constant factor, the imaginary part of the Feynman propagator defined below in Eq. (5.36)] for the Klein-Gordon equation by, e.g., Kay, Radzikowski, and Wald [82]: "if such a distributional bisolution is singular for sufficiently nearby pairs of points on a given null geodesic, then it will necessarily remain singular for all pairs of points on that null geodesic."

We begin in Sec. VA by exploring the large-l asymptotics of the quasinormal mode-sum expressions (4.30), (4.33), and (4.34). The large-l asymptotics of the mode sums are responsible for the singularities in the Green

function. We argue that the Green function is singular whenever a "coherent phase" condition is satisfied. The coherent phase condition is applied to find the times at which the Green function is singular. We show that the "singularity times" are exactly those predicted by the geodesic analysis of Sec. III C. In Sec. V B we introduce two methods for turning the sum over l into an integral. We show in Sec. V C that the Watson transform can be applied to extract meaningful values from the QNM sums, away from singularities. We show in Sec. V D that the Poisson sum formula may be applied to study the behavior of the Green function near the singularities. We show that there is a fourfold repeating pattern in the singular structure of the Green function, and use uniform asymptotics to improve our estimates. In Sec. V E we rederive the same effects by computing the Van Vleck determinant along orbiting geodesics, to find the "direct" part of the Green function arising from the Hadamard form. The two approaches are shown to be consistent.

A. Singularities of the Green function: Large-*l* asymptotics

We expect the Green function $G_{\text{ret}}(x, x')$ to be "singular" if the spacetime points x and x' are connected by a null geodesic. By singular we mean that $G_{\text{ret}}(x, x')$ does not take a finite value, although it may be well defined in a distributional sense. Here we show that the Green function is singular in this sense if the large-l asymptotics of the terms in the sum over l satisfy a *coherent phase condition*.

1. Near spatial infinity ρ, $\rho' \to +1$

Insight into the occurrence of singularities in the Green function may be obtained by examining the large-l asymptotics of the terms in the series (4.30). Let us write

$$G_{\text{ret}}^{\text{QNM}}(x, x') \sim \text{Re} \sum_{l=0}^{\infty} \mathcal{G}_l(T, \gamma), \qquad \rho_*, \rho'_* \to +\infty. \quad (5.1)$$

The asymptotic behavior of the gamma function ratio is straightforward: $\Gamma(i\lambda)/\Gamma(1/2 + i\lambda) \sim \lambda^{-1/2}e^{-i\pi/4}$, $\lambda \to +\infty$. The large-l asymptotics of the hypergeometric function are explored in Appendix A. We find

$$_2F_1(-\beta, -\beta; -2\beta; -e^{-T})$$
$$\sim (1 + e^{-T})^{-1/4} \exp\left(i\lambda\left[\ln\left\{\frac{\sqrt{1 + e^{-T}} + 1}{\sqrt{1 + e^{-T}} - 1}\right\}\right.\right.$$
$$\left.\left. - 2\ln 2 - T\right]\right), \qquad \lambda \to +\infty. \quad (5.2)$$

For simplicity, let us consider the special case of spatial coincidence $\gamma = 0$ (near spatial infinity ρ, $\rho' \to 1$),

$$\mathcal{G}_l(T, \gamma = 0) \sim \frac{e^{-T/2}}{\sqrt{\pi}(1 + e^{-T})^{1/4}} \frac{(l + 1/2)}{\lambda^{1/2}} \exp\left(i\lambda \ln\left[\frac{\sqrt{1 + e^{-T}} + 1}{\sqrt{1 + e^{-T}} - 1}\right] - i\pi/4\right), \qquad \lambda \to \infty. \quad (5.3)$$

Asymptotically, the magnitude of the terms in this series grows with $(l + 1/2)^{1/2}$. Hence the series is divergent. Nevertheless, due to the oscillatory nature of the series, well-defined values can be extracted (see Sec. V C), provided that the *coherent phase condition*

$$\lim_{l \to +\infty} \arg(\mathcal{G}_{l+1}/\mathcal{G}_l) = 2\pi N, \qquad N \in \mathbb{Z}, \qquad (5.4)$$

is *not* satisfied (for a related, but different, coherent phase condition or "resonance" see, for example, [83]). In other words, the Green function is singular in our sense if Eq. (5.4) is satisfied. In this case,

$$\ln\left(\frac{\sqrt{1 + e^{-T}} + 1}{\sqrt{1 + e^{-T}} - 1}\right) = 2\pi N, \qquad N \in \mathbb{Z}. \qquad (5.5)$$

Rearranging, we see that the Green function (4.30) with $\gamma = 0$ is singular when the "QNM time" T is equal to

$$T^{(\rho \sim 1, \gamma = 0)} = t - t' - \rho_* - \rho'_* = \ln[\sinh^2(\pi N)]. \quad (5.6)$$

Note that the coherent phase condition (5.4) implies that the Green function is singular at precisely the null geodesic times (3.23) (with $H = 1$ and $\Delta\phi = 2\pi N$), derived in Sec. V D.

For the more general case where the spacetime points x, x' are separated by an angle γ on the sphere, it is straightforward to use the asymptotics of the Legendre polynomials to show that the Green function (4.30) is singular when the QNM time T is equal to

$$T^{(\rho \sim 1)} = t - t' - \rho_* - \rho'_* = \ln[\sinh^2(\Delta\phi/2)],$$

where $\Delta\phi = 2\pi N \pm \gamma$, $\qquad (5.7)$

again in concordance with (3.23).

2. "Fundamental mode" $n = 0$

In Sec. IV B 5 we suggested that a reasonable approximation to the Green function may be found by neglecting the higher overtones $n > 0$. The fundamental mode series (4.34) also has singularities arising from the coherent phase condition (5.4), but they occur at slightly different times; we find that these times are

$$T^{(n=0)} = \Delta\phi - \ln[(1 + \rho)(1 + \rho')],$$

where $\Delta\phi = 2\pi N \pm \gamma$. $\qquad (5.8)$

Towards spatial infinity, (5.8) simplifies to $T^{(n=0)} = \Delta\phi - 2\ln 2$, which should be compared with the "null geodesic time" given in (3.23) (with $H = 1$, as it corresponds to null geodesics). In Sec. V D we compare the singularities of the approximation (4.34) with the singularities of the exact solution (4.30) at spatial infinity. Note that the singularity times $T^{(n=0)}$ are periodic, with period 2π. Clearly, the periodic times $T^{(n=0)}$, for any $\rho = \rho' \in (-1, +1)$, are not quite equal to the null geodesic times. Nevertheless, the latter approaches the former, i.e. Eq. (3.22), as $N \to \infty$. These last properties are not surprising: $n = 0$ corresponds to the least-damped modes, which are the dominating ones

in the QNM Green function at late times. Therefore, one would expect that the singularity times, at late times, of the $n = 0$ Green function correspond to those null geodesics that come in from ρ', orbit very near the two-sphere at $\rho = 0$ (the unstable photon orbit) a very large number of times ($N \to \infty$), and then come back out to ρ. Since it takes a null geodesic a coordinate time of 2π (recall that all two-spheres in Nariai have radius $a = 1$) to orbit around the two-sphere at $\rho = 0$, this time of 2π should be (at least at late times) precisely the time difference between singularities for the $n = 0$ QNM Green function.

To investigate the form of the Green function we now introduce two methods for converting a sum over l into an integral in the complex l plane. One method—the Watson transformation—is used to investigate the Green function away from the null cone, and the other method—the Poisson sum—is used near the null cone.

B. Watson transform and Poisson sum

In Sec. IV B, the distant past Green function was expressed via a sum over l of the form

$$I \equiv \mathrm{Re} \sum_{l=0}^{+\infty} \mathcal{F}\left(l + \frac{1}{2}\right) P_l(\cos\gamma). \qquad (5.9)$$

Here, $\mathcal{F}(l + \frac{1}{2})$ may be immediately read off from (4.30), (4.33), and (4.34). The so-called *Watson transform* [84] and *Poisson sum formula* [85,86] [see Eq. (C5)] provide two closely related ways of transforming a sum over l into an integral in the complex l plane. The two methods provide complementary advantages in understanding the sum over l.

A key element of the Watson transform is that, when extending the Legendre polynomial to noninteger l, the function with the appropriate behavior is $P_l(-\cos\gamma)$. This is obscured by the fact that $P_l(-\cos\gamma) = (-1)^l P_l(\cos\gamma)$ when l is an integer. Our first step is then to rewrite the sum (5.9) as

$$I = \mathrm{Re} \sum_{l=0}^{+\infty} e^{i(2N+1)\pi l} \mathcal{F}\left(l + \frac{1}{2}\right) P_l(-\cos\gamma), \qquad (5.10)$$

where we have also introduced an integer N for later convenience. Using the Watson transform, we may now express the sum (5.9) as a contour integral

$$I = \mathrm{Re} \frac{(-1)^N}{2i} \int_{\mathcal{C}_1} e^{i2N\pi\nu} \mathcal{F}(\nu) P_{\nu-1/2}(-\cos\gamma) \frac{d\nu}{\cos(\pi\nu)}, \qquad (5.11)$$

where $\nu = l + 1/2$. The contour $\mathcal{C}_1$ starts just below the real axis at ∞, encloses the points $\nu = \frac{1}{2}, 1 + \frac{1}{2}, 2 + \frac{1}{2}, \ldots$ which are poles of the integrand, and returns to just above the real axis at ∞. The contour $\mathcal{C}_1$ is shown in Fig. 7. If the integrand is exponentially convergent in both quadrants I and IV, the contour may be deformed in the complex-l plane onto a contour $\mathcal{C}_2$ parallel to the imaginary axis (see Fig. 7).

Note that there are no poles present inside quadrants I and IV in this case.

To study the asymptotic behavior of the Green function near singularities, it is convenient to use the alternative representation of the sum obtained by writing

$$\frac{1}{\cos(\pi\nu)} = \begin{cases} 2i\sum_{l=0}^{\infty} e^{i\pi(2l+1)(\nu-1/2)} & \text{Im}(\nu) > 0 \\ -2i\sum_{l=0}^{\infty} e^{-i\pi(2l+1)(\nu-1/2)} = -2i\sum_{l=-\infty}^{-1} e^{i\pi(2l+1)(\nu-1/2)} & \text{Im}(\nu) < 0. \end{cases} \quad (5.12)$$

Inserting representation (5.12) into (5.11) leads to the Poisson sum formula

$$I = \sum_{s=-\infty}^{+\infty} (-1)^s \, \text{Re} \int_0^{\infty} d\nu e^{2\pi i s\nu} \mathcal{F}(\nu) P_{\nu-1/2}(\cos\gamma). \quad (5.13)$$

The Poisson sum formula is applied in Sec. V D to study the form of the singularities.

C. Watson transform: Computing the series

Let us now show how the Watson transform may be applied to extract well-defined values from series over l, even if these are divergent. We will illustrate the approach by considering the nth-overtone QNM contribution to the Green function, Eq. (4.33), for which case

$$\mathcal{F}(x, x'; \nu) = \frac{1}{n!} \left[\frac{4e^{-T}}{(1+\rho)(1+\rho')} \right]^{n+1/2} 2\nu e^{i\lambda[T-\ln(2/(1+\rho))-\ln(2/(1+\rho'))]} \frac{\Gamma(-n+2i\lambda)}{[\Gamma(-n+1/2+i\lambda)]^2}$$

$$\times {}_2F_1\left(-n-2i\lambda, -n, -n+\frac{1}{2}+i\lambda; (1-\rho)/2\right) {}_2F_1\left(-n-2i\lambda, -n, -n+\frac{1}{2}+i\lambda; (1-\rho')/2\right), \quad (5.14)$$

where λ was defined in (4.5). We will choose the integer N so that this contour may be deformed into the complex plane (as shown in Fig. 7) to a contour on which the integral converges more rapidly. First, we note that the Legendre function may be written as the sum of waves propagating clockwise and counterclockwise, $P_{\nu-1/2}(\cos\gamma) = \mathcal{Q}_{\nu-1/2}^{(+)}(\cos\gamma) + \mathcal{Q}_{\nu-1/2}^{(-)}(\cos\gamma)$, where

$$\mathcal{Q}_{\mu}^{(\pm)}(z) = \frac{1}{2}\left[P_\mu(z) \pm \frac{2i}{\pi} Q_\mu(z) \right] \quad (5.15)$$

and here $Q_\mu(z)$ is a Legendre function of the second kind.

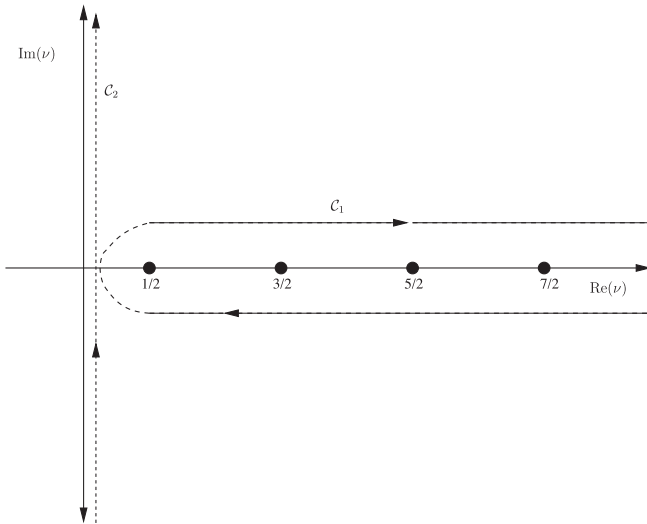FIG. 7. The Watson transform. The plot shows the contour $\mathcal{C}_1$ that defines the Watson transform in Eq. (5.11). Provided the integrand is convergent in both quadrants I and IV, the contour may be deformed onto $\mathcal{C}_2$.

The functions $\mathcal{Q}_{\nu-1/2}^{(\pm)}$ have exponential asymptotics in the limit $\nu\gamma \gg 1$,

$$\mathcal{Q}_{\nu-1/2}^{(\pm)}(\cos\gamma) \sim \left(\frac{1}{2\pi\nu\sin\gamma}\right)^{1/2} e^{\pm i\pi/4} e^{\mp i\nu\gamma}. \quad (5.16)$$

If the integrand is convergent in both the upper and lower complex-ν planes, the integration contour may be rotated to run, for example, along a line $\text{Re}(\nu) = c$ with c a constant between 0 and $\frac{1}{2}$. We are free to choose N to ensure convergence; for example, for the "fundamental mode" series ($n = 0$) we choose N to be

$$-N = \begin{cases} [(T+\log((\rho+1)(\rho'+1))+\gamma)/(2\pi)] & \text{for } \mathcal{Q}^{(+)} \\ [(T+\log((\rho+1)(\rho'+1))+2\pi-\gamma)/(2\pi)] & \text{for } \mathcal{Q}^{(-)} \end{cases} \quad (5.17)$$

where here $[x]$ denotes the greatest integer less than or equal to x.

We performed the integrals along $\text{Re}(\nu) = \frac{1}{4}$ and found rapid convergence of the integrals except near the critical times defining the jumps in N given by Eq. (5.17), when the integrands fall to 0 increasingly slowly. An alternative method for extracting meaningful values from divergent series is described in Sec. VII D.

D. The Poisson sum formula: Singularities and asymptotics

In this section we study the singularity structure of the Green function by applying the Poisson sum formula (5.13). The first step is to group the terms together so that

$$I = \sum_{N=0}^{\infty} I_N \quad \text{where} \quad I_N \equiv \text{Re} \int_0^{+\infty} d\nu \mathcal{F}(\nu) R_N(\nu, \gamma) \quad (5.18)$$

and

$$R_N = \begin{cases} (-1)^{N/2}[\mathcal{Q}_{\nu-1/2}^{(-)}(\cos\gamma)e^{iN\pi\nu} + \mathcal{Q}_{\nu-1/2}^{(+)}(\cos\gamma)e^{-iN\pi\nu}] & N \text{ even} \\ (-1)^{(N+1)/2}[\mathcal{Q}_{\nu-1/2}^{(+)}(\cos\gamma)e^{i(N+1)\pi\nu} + \mathcal{Q}_{\nu-1/2}^{(-)}(\cos\gamma)e^{-i(N+1)\pi\nu}] & N \text{ odd.} \end{cases} \tag{5.19}$$

$\mathcal{Q}_{\nu-1/2}^{(\pm)}$ were defined in Eq. (5.15). We can now use the exponential approximations for $\mathcal{Q}_{\nu-1/2}^{(\pm)}$ given in (5.16) to establish

$$R_N \sim \frac{1}{(2\pi\nu\sin\gamma)^{1/2}} \begin{cases} (-1)^{N/2}[e^{-i\pi/4}e^{i\nu(N\pi+\gamma)} + \text{c.c.}] & N \text{ even} \\ (-1)^{(N+1)/2}[e^{i\pi/4}e^{i\nu((N+1)\pi-\gamma)} + \text{c.c.}] & N \text{ odd.} \end{cases} \tag{5.20}$$

It should be borne in mind that the exponential approximations (5.16) are valid in the limit $\gamma\nu \gg 1$. Hence the approximations are not suitable in the limit $\gamma \to 0$. Below, we use alternative asymptotics (5.28) to investigate this case.

1. Fundamental mode $n = 0$

Let us apply the method to the fundamental mode QNM series (4.34). In this case we have

$$\mathcal{F}(\nu) = \left(\frac{4e^{-T}}{\pi(1+\rho)(1+\rho')}\right)^{1/2} \frac{\nu\Gamma(i\lambda)}{\Gamma(1/2+i\lambda)} e^{i\lambda\chi} \tag{5.21}$$

where T was defined in (4.23), λ was defined in (4.5), and

$$\chi = T + \ln[(1+\rho)(1+\rho')]. \tag{5.22}$$

Taking the asymptotic limit $\nu \to \infty$ we find

$$\mathcal{F}(\nu) \sim \left(\frac{4\nu e^{-T}}{i\pi(1+\rho)(1+\rho')}\right)^{1/2} e^{i\nu\chi}, \qquad \nu \to \infty. \tag{5.23}$$

Now let us combine this with the "exponential approximations" (5.20) for R_N,

$$\mathcal{F}(\nu)R_N(\nu,\gamma) \sim \left(\frac{2e^{-T}}{\pi^2\sin\gamma(1+\rho)(1+\rho')}\right)^{1/2} \begin{cases} (-1)^{N/2}[-ie^{i\nu(\chi+N\pi+\gamma)} + e^{i\nu(\chi-N\pi-\gamma)}] & N \text{ even} \\ (-1)^{(N+1)/2}[e^{i\nu(\chi+(N+1)\pi-\gamma)} - ie^{i\nu(\chi-(N+1)\pi+\gamma)}] & N \text{ odd,} \end{cases} \tag{5.24}$$

for $\nu \to \infty$. It is clear that the integral in (5.18) will be singular if the phase factor in either term in (5.24) is zero. In other words, each wave R_N gives rise to two singularities, occurring at particular singularity times. We are only interested in the singularities for $T > 0$; hence we may neglect the former terms in (5.24). Now let us note that

$$\lim_{\epsilon\to 0^+} \int_0^\infty e^{i\nu(\zeta+i\epsilon)}d\nu = \lim_{\epsilon\to 0^+} \left(\frac{i}{\zeta+i\epsilon}\right) = i/\zeta + \pi\delta(\zeta). \tag{5.25}$$

Upon substituting (5.24) into (5.18) and performing the integral [adding a small ϵ in (5.25) is equivalent to imposing a smooth high-frequency cutoff upon the integral], we find

$$I_N^{(n=0)} \sim \left(\frac{2e^{-T}}{\sin\gamma(1+\rho)(1+\rho')}\right)^{1/2} \begin{cases} (-1)^{N/2}\delta(t-t'-t_N^{(n=0)}) & N \text{ even} \\ \frac{(-1)^{(N+1)/2}}{\pi(t-t'-t_N^{(n=0)})} & N \text{ odd,} \end{cases} \tag{5.26}$$

where $I_N^{(n=0)}$ is I_N in (5.18) with $\mathcal{F}(\nu)$ given by (5.21), and

$$t_N^{(n=0)} = \rho_* + \rho_*' - \ln((1+\rho)(1+\rho')) + \begin{cases} N\pi + \gamma & N \text{ even} \\ (N+1)\pi - \gamma & N \text{ odd.} \end{cases} \tag{5.27}$$

These times $t_N^{(n=0)}$ are equivalent to the "periodic" times identified in Sec. V A [Eq. (5.8)] and, for $\rho = \rho' = \rho_1$ and $N \to \infty$, in Sec. III C [Eq. (3.22)].

Let us consider the implications of Eq. (5.26) carefully. Let us fix the spatial coordinates ρ, ρ', and γ and consider variations in $t - t'$ only. Each term I_N corresponds to a particular singularity in the mode-sum expression (4.34) for the $(n = 0)$-Green function. The Nth singularity occurs at $t - t' = t_N^{(n=0)}$. For times close to $t_N^{(n=0)}$, we expect the term I_N to give the dominant contribution to the $(n = 0)$ Green function. Equation (5.26) suggests that the $(n = 0)$ Green function has a repeating fourfold singularity structure. The "shape" of the singularity alternates between a delta distribution [$\pm \delta(t - t' - t_N^{(n=0)})$, N even] and a

singularity with antisymmetric "wings" [$\pm 1/(t - t' - t_N^{(n=0)})$, N odd].

The Nth wave may be associated with the Nth orbiting null geodesic shown in Fig. 2. Note that "even N" and "odd N" geodesics pass in opposite senses around $\rho = 0$ (see, for example, Fig. 2). Now, N has a clear geometrical interpretation: it is the number of *caustics* through which the corresponding geodesic has passed. Caustics are points where neighboring geodesics are focused, and in a spherically symmetric spacetime caustics occur whenever a geodesic passes through angles $\Delta\phi = \pi$, 2π, 3π, etc. Equation (5.26) implies that the singularity structure of the Green function changes each time the wave front passes through a caustic [87].

More accurate approximations to the singularity structure may be found by using the uniform asymptotics established by Olver [88] [as an improvement on the "exponential asymptotics" (5.16)],

$$Q^{(\pm)}_{\nu-1/2}(\cos\gamma) \sim \frac{1}{2}\left(\frac{\gamma}{\sin\gamma}\right)^{1/2} H_0^{(\mp)}(\nu\gamma), \tag{5.28}$$

where $H_0^{(\pm)}(\cdot) = J_0(\cdot) \pm iY_0(\cdot)$ are Hankel functions of the first (+) and second (−) kinds. This approximation (5.28) is valid in the large-ν limit for angles in the range $0 \le \gamma < \pi$. With these asymptotics, we replace (5.20) with

$$R_N \sim \frac{1}{2}\left(\frac{\gamma}{\sin\gamma}\right)^{1/2}\begin{cases}(-1)^{N/2}[H_0^{(+)}(\nu\gamma)e^{iN\pi\nu} + H_0^{(-)}(\nu\gamma)e^{-iN\pi\nu}] & N \text{ even} \\ (-1)^{(N+1)/2}[H_0^{(-)}(\nu\gamma)e^{i(N+1)\pi\nu} + H_0^{(+)}(\nu\gamma)e^{-i(N+1)\pi\nu}] & N \text{ odd.}\end{cases} \tag{5.29}$$

In Appendix B we derive the following asymptotics for the fundamental mode ($n = 0$) Green function,

$$I_1^{(n=0)} \sim \begin{cases}\frac{2\mathcal{A}(\gamma)}{\sqrt{\pi}[(2\pi-\gamma)-\chi][(2\pi+\gamma)-\chi]^{1/2}}E(2\gamma/[(2\pi+\gamma)-\chi]) & \chi < 2\pi - \gamma \\ \frac{-\mathcal{A}(\gamma)\sqrt{\pi}}{2[\chi-(2\pi-\gamma)]^{3/2}}\,_2F_1(3/2, 1/2; 2; \frac{\chi-2\pi-\gamma}{\chi-2\pi+\gamma}) & \chi > 2\pi - \gamma,\end{cases} \tag{5.30}$$

$$I_2^{(n=0)} \sim \begin{cases}-\sqrt{\frac{2\pi}{\gamma}}\mathcal{A}(\gamma)\delta(\chi - (2\pi + \gamma)) & \chi \le 2\pi + \gamma \\ \frac{\mathcal{A}(\gamma)\sqrt{\pi}}{2[\chi-(2\pi-\gamma)]^{3/2}}\,_2F_1(3/2, 1/2; 2; \frac{\chi-2\pi-\gamma}{\chi-2\pi+\gamma}) & \chi > 2\pi + \gamma,\end{cases} \tag{5.31}$$

where E is the complete elliptic integral of the second kind, χ was defined in (5.22), and

$$\mathcal{A}(\gamma) = \left(\frac{\gamma}{\sin\gamma}\right)^{1/2}\left(\frac{e^{-T}}{\pi(1 + \rho)(1 + \rho')}\right)^{1/2}. \tag{5.32}$$

The asymptotics (5.30) and (5.31) provide insight into the singularity structure near the caustic at $\Delta\phi = 2\pi$. Figure 8 shows the asymptotics (5.30) and (5.31) at $\rho = \rho' \to +1$ for two cases: (i) $\gamma = \pi/20$ (left plot) and

(ii) $\gamma = 0$ (right plot). In the left plot, the $I_1^{(n=0)}$ integral has a (nearly) antisymmetric form. The $I_2^{(n=0)}$ integral is a delta function with a tail. However, the tail is exactly canceled by the $I_1^{(n=0)}$ integral in the regime $\chi > 2\pi + \gamma$. The cancellation creates a step discontinuity in the Green function at $\chi = 2\pi + \gamma$. The form of the divergence shown in the right plot ($\gamma = 0$) may be understood by substituting $\gamma = 0$ into (5.30) to obtain
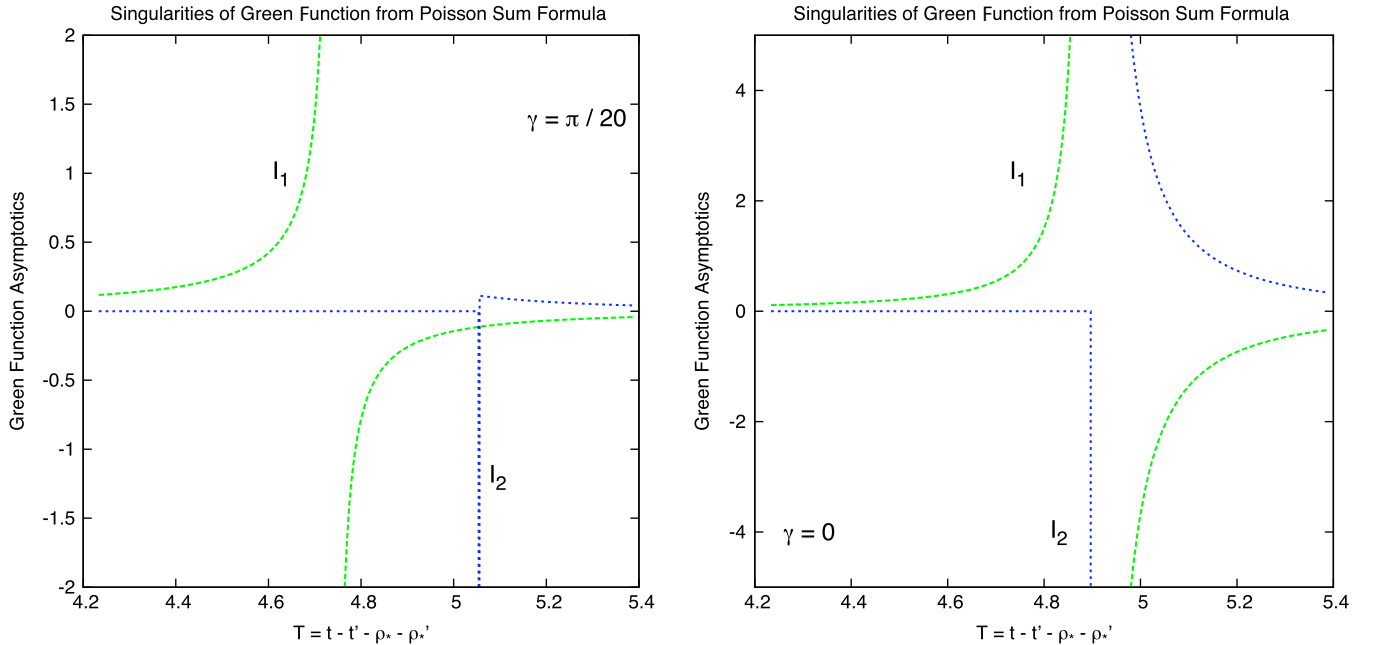

FIG. 8 (color online). Singularities of the fundamental mode Green function (4.34) near the caustic at 2π and $\rho = \rho' \to +1$. These plots show the I_1 (dashed line) and I_2 (dotted line) contributions to the Poisson sum, given explicitly by (5.30) and (5.31). The left plot shows an angular separation $\gamma = \pi/20$ and the right plot shows angular coincidence $\gamma = 0$. Note that, for $T > 2\pi + \gamma - 2\ln 2$, the I_1 and I_2 integrals are equal and opposite and will exactly cancel out (see text).

$$I_1^{(n=0)}(\gamma = 0) \sim \left(\frac{e^{-T}}{(1 + \rho)(1 + \rho')}\right)^{1/2}(2\pi - \chi)^{-3/2}.$$
$$(5.33)$$

2. Near spatial infinity, ρ, $\rho' \to +1$

It is straightforward to repeat the steps in the above analysis for the closed-form Green function (4.30), valid for ρ, $\rho' \to +1$. We reach a result of the same form as (5.26), but with modified singularity times,

$$t_N^{(\rho \sim 1)} \sim \rho_* + \rho_*'$$
$$+ \begin{cases} \ln(\sinh^2([N\pi + \gamma]/2)) & N \text{ even} \\ \ln(\sinh^2([(N + 1)\pi - \gamma]/2)) & N \text{ odd,} \end{cases}$$
$$(5.34)$$

corresponding to the geodesic times (3.23). For instance, with the exponential asymptotics (5.20) applied to (4.30), we obtain

$$I_N^{(\rho \sim 1)} \sim \left(\frac{e^{-T}}{2 \sin\gamma\sqrt{1 + e^{-T}}}\right)^{1/2}$$
$$\times \begin{cases} (-1)^{N/2}\delta(t - t' - t_N^{(\rho \sim 1)}) & N \text{ even} \\ \frac{(-1)^{(N+1)/2}}{\pi(t - t' - t_N^{(\rho \sim 1)})} & N \text{ odd.} \end{cases}$$
$$(5.35)$$

In Sec. VIII the asymptotic expressions derived here are compared against numerical results from the mode sums.

We believe that the fourfold cycle in the singularity structure of the Green function which we have just unearthed using tricks we picked up from seismology [86] is characteristic of the $\mathbb{S}^2$ topology (different types of cycles arising in different cases). This cycle may thus also appear in the more astrophysically interesting case of the Schwarzschild spacetime. Since this cycle does not seem to be widely known in the field of general relativity (with the notable exception of [87]), in Appendix C we apply the large-l asymptotic analysis of this section to the simplest case with $\mathbb{S}^2$ topology: the spacetime of $T \times \mathbb{S}^2$, where the same cycle blossoms in a clear manner.

E. Hadamard approximation and the Van Vleck determinant

In this section, we rederive the singularity structure found in (5.26) and (5.35) using a "geometrical" argument based on the Hadamard form of the Green function. In Sec. IV C we used the Hadamard parametrix of the Green function to find the quasilocal contribution to the self-force. Strictly speaking, the Hadamard parametrix of Eq. (4.35) is only valid when x and x' are within a normal neighborhood [42] (see footnote [1]). Nevertheless, it is plausible (particularly in light of the previous sections) that the Green function near the singularities may be adequately described by a Hadamard-like form, but with contributions from *all appropriate orbiting geodesics*

(rather than just the unique timelike geodesic joining x and x').

We first introduce the Feynman propagator $G_F(x, x')$ (see, e.g., [11,89]) which satisfies the inhomogeneous scalar wave equation (2.3). The Hadamard form, which in principle is only valid for points x' within the normal neighborhood of x, for the Feynman propagator in 4-D is [11,90]

$$G_F(x, x') = \frac{i}{2\pi}\left[\frac{U(x, x')}{\sigma + i\epsilon} + V(x, x')\ln(\sigma + i\epsilon) + W(x, x')\right],$$
$$(5.36)$$

where $U(x, x')$, $V(x, x')$ (already introduced in Sec. IV C), and $W(x, x')$ are bitensors which are regular at coincidence ($x \to x'$), and $\sigma(x, x')$ is Synge's world function: half the square of the geodesic distance *along a specific geodesic* joining x and x'. Note the *Feynman prescription* "$\sigma \to \sigma + i\epsilon$" in (5.36), where ϵ is an infinitesimally small positive value, which is necessary so that the Feynman propagator has the appropriate analytical properties; this implies that Eq. (5.37) below is then satisfied.

The retarded Green function is readily obtained from the Feynman propagator by

$$G_{\text{ret}}(x, x') = 2\theta_-(x, x')\,\text{Re}(G_F(x, x')),\qquad(5.37)$$

which yields (4.35) inside the normal neighborhood, since $U(x, x')$, $V(x, x')$, and $W(x, x')$ are real-valued there. We posit that the "direct" part of the Green function remains in Hadamard form,

$$G_{\text{ret}}^{\text{dir.}}(x, x') = \lim_{\epsilon \to 0^+} \frac{1}{\pi}\,\text{Re}\left[i\frac{U(x, x')}{\sigma + i\epsilon}\right]$$
$$= \text{Re}\left[U(x, x')\left(\delta(\sigma) + \frac{i}{\pi\sigma}\right)\right],\qquad(5.38)$$

even *outside* the normal neighborhood [note that outside the normal neighborhood we still use the term direct part to refer to the contribution from the $U(x, x')$ term, even though its support may not be restricted on the null cone anymore]. It is plausible that the Green function near the Nth singularity (see previous section) is dominated by the direct Green function (5.38) calculated along geodesics near the Nth orbiting null geodesic. To test this assertion, we will calculate the structure and magnitude of the singularities and compare with (5.35).

In four-dimensional spacetimes, the symmetric bitensor $U(x, x')$ is given by

$$U(x, x') = \Delta^{1/2}(x, x'),\qquad(5.39)$$

where $\Delta(x, x')$ is the Van Vleck determinant [91–93]. The Van Vleck determinant can be found by integrating a system of transport equations along the appropriate geodesic joining x and x'. The first of these [16],

$$\lambda\frac{d\ln\Delta}{d\lambda} = 4 - \sigma^\alpha{}_\alpha,\qquad(5.40)$$

is a transport equation for the Van Vleck determinant itself, with the initial condition $\Delta(\lambda = 0) = 1$. Here, λ is an affine parameter along the geodesic joining x and x', and $\sigma^\alpha{}_\beta = \nabla_\beta \nabla^\alpha \sigma$ is the second covariant derivative (taken with respect to spacetime point x) of Synge's world function, which in turn is found from the coupled system of transport equations [58,94]

$$\lambda \frac{d\sigma^\alpha{}_\beta}{d\lambda} = \sigma^\alpha{}_\beta - \sigma^\alpha{}_\mu \sigma^\mu{}_\beta + \lambda u^\mu (\Gamma^\nu{}_{\beta\mu} \sigma^\alpha{}_\nu - \Gamma^\alpha{}_{\nu\mu} \sigma^\nu{}_\beta)$$
$$- \lambda^2 R^\alpha{}_{\mu\beta\nu} u^\mu u^\nu \tag{5.41}$$

and the boundary condition $\sigma^\alpha{}_\beta(\lambda = 0) = \delta^\alpha_\beta$.

In principle, transport equations (5.40) and (5.41) may be integrated numerically to determine the Van Vleck determinant along any given geodesic on any given spacetime. This is the approach that we might take on, for example, in Schwarzschild. A numerical approach is not necessary for the Nariai spacetime, however. This spacetime is the Cartesian product of a two-sphere with a 2-D de Sitter spacetime. On a product spacetime $\mathcal{M} = \mathcal{M}_1 \times \mathcal{M}_2$ we may make the following decomposition:

$$\sigma = \sigma_1 + \sigma_2, \qquad \Delta = \Delta_1 \Delta_2, \tag{5.42}$$

where σ_i and Δ_i ($i = 1, 2$) are, respectively, Synge's world function and the Van Vleck determinant on the manifold $\mathcal{M}_i$. It will be shown in a forthcoming work [95] that the Van Vleck determinant on the Nariai spacetime when the two points x and x' are within the normal neighborhood is simply

$$\Delta(x, x') = \left(\frac{\gamma}{\sin\gamma}\right)\left(\frac{\eta}{\sinh\eta}\right) \tag{5.43}$$

where, here, γ is the geodesic distance traversed on the two-sphere and η is the geodesic distance traversed in the two-dimensional de Sitter subspace. Hence the Van Vleck determinant is singular at the angle $\gamma = \pi$.

This may be seen another way. Using the spherical symmetry, let us assume, without loss of generality, that the motion is in the plane $\phi = $ const, from which it follows that the equation for $\sigma^\phi{}_\phi$ in (5.41) decouples from the remainder; it is

$$\theta \frac{d\sigma^\phi{}_\phi}{d\theta} + \theta^2 - \sigma^\phi{}_\phi(1 - \sigma^\phi{}_\phi) = 0. \tag{5.44}$$

Here we have rescaled the affine parameter λ to be equal to the angle θ subtended by the geodesic. Note that here we let θ take values greater than π. It is straightforward to show that the solution of Eq. (5.44) is $\sigma^\phi{}_\phi = \theta \cot\theta$. Hence $\sigma^\phi{}_\phi$ is singular at the angles $\theta = \pi, 2\pi, 3\pi$, etc. In other words, the Van Vleck determinant is singular at the antipodal points, where neighboring geodesics are focused: the *caustics*. The Van Vleck determinant may be separated in the following manner: $\Delta = \Delta_\phi \Delta_{t\rho}$, where

$$\theta \frac{d\ln\Delta_\phi}{d\theta} = 1 - \sigma^\phi{}_\phi, \tag{5.45}$$

$$\theta \frac{d\ln\Delta_{t\rho}}{d\theta} = 2 - \sigma^t{}_t - \sigma^\rho{}_\rho. \tag{5.46}$$

Equation (5.45) yields

$$\ln\Delta_\phi = \ln\left(\frac{\theta}{\theta_0}\right) - \int_{\theta_0}^\theta d\theta' \cot\theta' \tag{5.47}$$

which can be integrated analytically by following a Landau contour in the complex θ' plane around the (simple) poles of the integrand (located at $\theta' = k\pi, k \in \mathbb{Z}$), which are the caustic points. Following the Feynman prescription $\sigma \to \sigma + i\epsilon$, we choose the Landau contour so that the poles lie *below* the contour. We then obtain (setting $\theta_0 = 0$, without loss of generality)

$$\Delta_\phi = \left|\frac{\theta}{\sin\theta}\right| e^{-iN\pi}. \tag{5.48}$$

Here, N is the number of caustic points the geodesic has passed through. The phase factor, obtained by continuing the contour of integration past the singularities at $\theta = \pi$, 2π, etc., is crucial. Inserting the phase factor $e^{-iN\pi/2}$ in (5.38) leads to exactly the fourfold singularity structure predicted by the large-l asymptotics of the mode sum (5.35). That is,

$$G_N^{\text{dir}} \sim \left(\frac{\eta}{\sinh\eta}\right)^{1/2}\left(\frac{\theta}{\sin\theta}\right)^{1/2}\begin{cases}(-1)^{N/2}\delta(\sigma) & N \text{ even} \\ \frac{(-1)^{(N-1)/2}}{\pi\sigma} & N \text{ odd.}\end{cases}$$
$$\tag{5.49}$$

The accumulation of a phase of "$-i$" on passing through a caustic, and the alternating singularity structure which results, is well known to researchers in other fields involving wave propagation—for example, in acoustics [96], seismology [86], symplectic geometry [97], and quantum mechanics [98], the integer N is known as the Maslov index [99,100].

We would expect to find an analogous effect in, for example, the Schwarzschild spacetime. The fourfold structure has been noted before by at least one researcher [87]. Nevertheless, the effect of caustics on wave propagation in four-dimensional spacetimes does not seem to have received much attention in the gravitational literature (see [101,102] for exceptions).

To compare the singularities in the mode-sum expression (5.35) with the singularities in the Hadamard form (5.49), let us consider the odd-N singularities of $1/\sigma$ form. We will rearrange (5.35) into an analogous form by expanding σ to first order in $t - t_N^{(\rho\sim1)}$, where $t_N^{(\rho\sim1)}$ is the Nth singularity time for orbiting geodesics starting and finishing at $\rho \to 1$. For the orbiting geodesics described in Sec. III C we have $\sigma = -\frac{1}{2}(H^2 - 1)\theta^2$. At $\rho \to 1$, expanding to first order and using (3.23) yields

$$\sigma \sim -(H\theta)\tanh(H\theta/2)(t - t_N^{(\rho\sim1)}). \tag{5.50}$$

The mode-sum expression (5.35) may then be rewritten in analogous form to the N-odd expression in (5.49),

$$G_{\rm ret}^{\rm QNM} \sim (-1)^{(N-1)/2} \frac{|\Delta_{\rm (QNM)}|^{1/2}}{\pi\sigma}$$

where $|\Delta_{\rm (QNM)}|^{1/2} = \left(\frac{H\eta \sinh(\eta/2)}{2\cosh^3(\eta/2)}\right)^{1/2} \left|\frac{\theta}{\sin\theta}\right|^{1/2}.$

$$(5.51)$$

Here $\eta = H\theta$, where H is the constant of motion introduced in Sec. III C. We find very good agreement between (5.43) and (5.51) in the $\theta \gtrsim \pi$ regime. The disagreement at small angles is not unexpected, as the QNM sum is invalid at early times (or equivalently, for orbiting geodesics which have passed through small angles θ).

VI. SUMMARY

After a series of equations and results, for the benefit of the reader we will now take a moment to recap and (literally) rewrite the main equations obtained thus far. We recall that $\beta = -1/2 + i\lambda$, $\lambda = \sqrt{(l+1/2)^2 + 4\xi - 1/2}$, $\rho_* = \tanh^{-1}\rho$; that we tend to use $T = t - t' - \rho_* - \rho_*'$ as the independent "time" variable; and that the unbounded orbital angle is given by $\Delta\phi = N\pi + \gamma$ for N even and by $\Delta\phi = (N + 1)\pi - \gamma$ for N odd, where N is the number of caustics the null geodesic has gone through.

The main equations for the "retarded" Green function we have obtained so far are as follows:

(i) QNM retarded Green function (valid $\forall x, x'$ where $T > 0$), Eq. (4.33):

$$G_{\rm ret}^{\rm QNM}(x, x') = 2{\rm Re}\sum_{l=0}^{\infty}(2l+1)P_l(\cos\gamma)e^{i\lambda[T-\ln(2/(1+\rho))-\ln(2/(1+\rho'))]}\sum_{n=0}^{\infty}\mathcal{B}_{ln}\left[\frac{4e^{-T}}{(1+\rho)(1+\rho')}\right]^{n+1/2}\mathcal{S}_{ln}(\rho)\mathcal{S}_{ln}(\rho'),$$

$$(6.1)$$

where $\mathcal{B}_{ln}$ are the excitation factors (4.26) and $\mathcal{S}_{ln}(\rho)$ is the finite series (4.32) essentially based on the radial functions evaluated at the QNM frequencies.

(ii) QNM retarded Green function (after summing over all overtone numbers n) at $\rho_*, \rho_*' \to +\infty$ (and $T > 0$), Eq. (4.30):

$$G_{\rm ret}^{\rm QNM}(T, \gamma) \sim \frac{e^{-T/2}}{\sqrt{\pi}}{\rm Re}\sum_{l=0}^{+\infty}\frac{(l+1/2)\Gamma(i\lambda)}{\Gamma(1/2+i\lambda)}P_l(\cos\gamma)e^{i\lambda(T+2\ln2)}{}_2F_1(-\beta, -\beta; -2\beta; -e^{-T}), \quad \rho_*, \rho_*' \to +\infty, \quad (6.2)$$

with singularities at times given by Eq. (5.7) [also Eq. (3.23) with $H = 1$ and Eq. (5.34)], $T^{(\rho\sim1)} = \ln[\sinh^2(\Delta\phi/2)]$. The corresponding singularity structure is given by Eq. (5.35):

$$\mathcal{I}_N^{(\rho\sim1)} \sim \left(\frac{e^{-T}}{2\sin\gamma\sqrt{1+e^{-T}}}\right)^{1/2}\begin{cases}(-1)^{N/2}\delta(t - t' - t_N^{(\rho\sim1)}) & N \text{ even} \\ \frac{(-1)^{(N+1)/2}}{\pi(t-t'-t_N^{(\rho\sim1)})} & N \text{ odd,}\end{cases}$$

$$(6.3)$$

where $\mathcal{I}_N^{(\rho\sim1)}$ is the contribution $\mathcal{I}_N$ to the retarded Green function associated with the Nth orbiting null geodesic in the case where the points are located at spatial infinity.

(iii) Contribution of the fundamental mode $n = 0$ to the QNM retarded Green function (valid $\forall x, x'$ where $T > 0$), Eq. (4.34):

$$G_{\rm ret}^{(n=0)}(x, x') = \left(\frac{e^{-T}}{\pi(1+\rho)(1+\rho')}\right)^{1/2}{\rm Re}\sum_{l=0}^{+\infty}\frac{(2l+1)P_l(\cos\gamma)\Gamma(i\lambda)}{\Gamma(1/2+i\lambda)}e^{i\lambda[T+\ln(1+\rho)(1+\rho')]}, \quad (6.4)$$

with singularities at times given by Eq. (5.8) [also Eq. (5.27)], $T^{(n=0)} = \Delta\phi - \ln[(1 + \rho)(1 + \rho')]$, which coincide with $T^{(\rho\sim1)}$ [and with Eq. (3.23) with $H = 1$] for $\rho, \rho' \to 1$ and $N \to +\infty$. The corresponding singularity structure is given by Eq. (5.26):

$$\mathcal{I}_N^{(n=0)} \sim \left(\frac{2e^{-T}}{\sin\gamma(1+\rho)(1+\rho')}\right)^{1/2}$$
$$\times \begin{cases}(-1)^{N/2}\delta(t - t' - t_N^{(n=0)}) & N \text{ even} \\ \frac{(-1)^{(N+1)/2}}{\pi(t-t'-t_N^{(n=0)})} & N \text{ odd}\end{cases}$$

$$(6.5)$$

[for more accurate asymptotics, which include the tail in the singularity, see Eqs. (5.30) and (5.31)], where $\mathcal{I}_N^{(n=0)}$ is $\mathcal{I}_N$ for $n = 0$ only.

(iv) The extension beyond the normal neighborhood of the direct part in the Hadamard form of the retarded Green function has a contribution from the Nth orbiting null geodesic given by (5.49):

$$G_N^{\rm dir} \sim \left(\frac{\eta}{\sinh\eta}\right)^{1/2}\left(\frac{\theta}{\sin\theta}\right)^{1/2}$$
$$\times \begin{cases}(-1)^{N/2}\delta(\sigma) & N \text{ even} \\ \frac{(-1)^{(N-1)/2}}{\pi\sigma} & N \text{ odd,}\end{cases}$$

$$(6.6)$$

which, for $\rho \to 1$ and $\theta \gtrsim \pi$, agrees well with

$I_N^{(\rho \sim 1)}$ with $\eta = H\theta$ (where $H > 1$ for timelike geodesics, $H = 1$ for null geodesics, and $H < 1$ for spacelike geodesics).

VII. SELF-FORCE ON THE STATIC PARTICLE

In this section we turn our attention to a simple case: the self-force acting on a static scalar particle in the Nariai spacetime. By ''static'' we mean a particle with constant spatial coordinates. It is not necessarily at rest, since its worldline may not be a geodesic, and it may require an external force to keep it static. In Sec. VII A we review previous calculations for the static self-force on a range of spacetimes, and in Sec. VII B we explore one such analytic method for computing the static self-force in Nariai spacetime. This method, based on the massive-field approach of Rosenthal [40,41], provides an independent check on the matched-expansion approach. In Sec. VII C we describe how the method of matched expansions may be applied to the static case. To compute the self-force, we require robust numerical methods for evaluating the quasinormal mode sums such as (6.1); two such methods are outlined in Sec. VII D. The results of all methods are validated and compared in Sec. VIII.

A. The static particle

A static particle—a particle with constant spatial coordinates—has been the focus of several scalar self-force calculations, in particular, for the Schwarzschild spacetime [37,40,48,103–106]. Although a static particle may not be a particularly physical case, it is frequently chosen because it involves relatively straightforward calculations and has an exact solution for the Schwarzschild spacetime. It therefore provides a good testing ground for new approaches to the calculation of the self-force.

Smith and Will [103] calculated the self-force on a static *electric* charge in the Schwarzschild background and found it to be nonzero. In [104], Wiseman considered the analogous case of a static *scalar* charge in the case of *minimal coupling* (i.e., $\xi = 0$) in Schwarzschild spacetime. Using isotropic coordinates, he managed to sum the Hadamard series for the Green function in the static case (i.e., the ''Helmholtz''-like equation in Schwarzschild spacetime with zero frequency, $\omega = 0$) and thus obtain in closed form the field created by the static charge in the scalar and also electrostatic (already found in [107,108] using a different method) cases. He then found the self-force to be zero in the scalar, minimally coupled case.

In [106], the calculation of the self-force on a static scalar charge in Schwarzschild spacetime is extended to the case of *nonminimal coupling* ($\xi \neq 0$) and is found to be zero as well. The fact that the value of the scalar self-force in Schwarzschild spacetime is the same (zero) independently of the value of the coupling constant is in agreement

with the *Quinn-Wald axioms* [14,15]: their method relies only on the field equations, and these are independent of the coupling constant in a Ricci-flat spacetime such as Schwarzschild spacetime. The calculation (without using the Quinn-Wald axioms) is by no means trivial, however, since the effect of the coupling constant might be felt through the stress-energy tensor (in fact, [106] corrected a previous result in [109], where the self-force had been incorrectly found to be nonzero). Rosenthal [40] has also considered the case of a static particle in Schwarzschild spacetime and used it as an example application of the *massive-field approach* [41] to self-force calculations.

On the other hand, using the conformal invariance of Maxwell's equations, Hobbs [110] showed that, in a *conformally flat* spacetime, the tail contribution (2.2) to the self-force on an *electric* charge (on any motion, static or not) is zero. The only possible contribution to the self-force might then come from the local Ricci terms, which are zero in cases of physical interest such as in a de Sitter universe.

One would expect the tail contribution to the *scalar* self-force to also be zero for a charge undergoing any motion in a conformally flat 4-D spacetime with conformal coupling (i.e., $\xi = 1/6$). In a recent article [65], it was further argued using Hobbs' result that the self-force should be zero for a static charge (where the time independence effectively reduces the problem to a 3-D spatial one), in a spacetime such that its 3-D spatial section is conformally flat and with conformal coupling in 3-D (i.e., $\xi = 1/8$). Indeed, they showed that the scalar self-force on a massless static particle in a *wormhole spacetime* (with a nonzero Ricci scalar and where the 3-D spatial section is conformally flat) is equal to zero at $\xi = 1/8$ and it actually changes sign at this 3-D conformal value. (Note that in this case the local contribution to the self-force is exactly zero, so there may only be a tail contribution—if any.) It is not completely clear to us, however, that the argument that the tail contribution to the self-force is zero due to the conformality of the physical system carries through intact from a 4-D spacetime to its 3-D spatial section. Note that, from the Hadamard form in 3-D [43,111], the corresponding Green function (the so-called ''scalarstatic'' or ''electrostatic'' Green function) never (regardless of whether there is conformality or not) possesses a tail part $V(x, x')$, and the self-force is calculated from this static Green function, not via Eqs. (1.3), (1.4), (2.1), and (2.2), but rather via, e.g., Eq. (7.2) below.

The Nariai spacetime, not being Ricci-flat and being conformal to a wormhole spacetime (and so with a conformally flat 3-D spatial section), suggests a very interesting playground for calculating the self-force: What role does the coupling constant ξ play? Do particular values such as $\xi = 1/6$ (4-D conformal coupling) and $\xi = 1/8$ (3-D conformal coupling, so a particular value in the case of a static charge) yield ''particular'' values (namely, zero) for the self-force? Are the Quinn-Wald axioms satisfied?

B. Static Green function approach

The conventional approach to calculating the self-force on a static particle due to Wiseman [104] uses the scalar-static Green function. Following Copson [107], Wiseman was able to obtain this Green function by summing the Hadamard series. Only by performing the full sum was he able to verify that his Green function satisfied the appropriate boundary conditions. Linet [112] has classified all spacetimes in which the scalarstatic equation is solvable by the Copson ansatz and, unfortunately, the Nariai metric does not fall into any of the classes given. Therefore, instead we work with the mode form for the static Green function. This corresponds to the integrand at $\omega = 0$ of Eq. (4.18) (with integral measure $\frac{d\omega}{2\pi}$),

$$
\begin{aligned}
G_{\text{static}}(\rho, \Omega; \rho', \Omega') = \sum_{l=0}^{\infty} (2l+1) P_l(\cos\gamma) \\
\times \frac{\pi P_{-1/2+i\lambda}(-\rho_<) P_{-1/2+i\lambda}(\rho_>)}{2\cosh(\pi\lambda)}
\end{aligned}
\tag{7.1}
$$

where, as before, $\lambda = \sqrt{(l+\frac{1}{2})^2 + d}$. This equation, having only one infinite series, is amenable to numerical computation.

To regularize the self-force we follow the method of Rosenthal [40], who used a massive-field approach to calculate the static self-force in Schwarzschild. Following his prescription, we calculate the derivative of the scalar field and of a massive scalar field. In the limit of the field mass going to infinity, we obtain the derivative of the radiative field which is regular. This method can be carried through to Nariai spacetime, where it yields the expression

$$
\begin{aligned}
ma^\rho = q^2(1-\rho^2)^{3/2} \lim_{\rho'\to\rho^-} \Big[\partial_\rho G_{\text{static}}(\rho, \Omega; \rho', \Omega) \\
+ \frac{1}{(\rho - \rho')^2} - \frac{(\xi R - \frac{2}{3})}{2(1-\rho^2)} \Big],
\end{aligned}
\tag{7.2}
$$

where $R = 4$. Note that the massive-field approach was developed in [40] for the case $\xi = 0$, but it can be seen that it equally applies to $\xi \neq 0$ too. The limiting process $\rho' \to \rho^-$ does not affect the term with $1/(1-\rho^2)$ in (7.2). We will therefore omit it from the following calculation and we will trivially subtract it from the self-force in the calculations we carry out later in Sec. VIII D. The singular (as $\rho' \to \rho^-$) subtraction term may be expressed in a convenient form using the identity [113,114]

$$
\begin{aligned}
\int_0^{+\infty} d\lambda \lambda \tanh(\pi\lambda) \frac{\pi P_{-1/2+i\lambda}(-\rho_<) P_{-1/2+i\lambda}(\rho_>)}{\cosh(\pi\lambda)} \\
= \frac{1}{\rho_> - \rho_<}.
\end{aligned}
\tag{7.3}
$$

Subtracting (7.3) from (7.1), we can express the regularized Green function as a sum of two well-defined and easily calculated sums/integrals,

$$
G_{\text{static}}(\rho, \Omega; \rho', \Omega) - \frac{1}{\rho_> - \rho_<} = I(\rho, \rho') + \mathcal{J}(\rho, \rho')
\tag{7.4}
$$

where

$$
\begin{aligned}
I(\rho, \rho') = \int_0^{+\infty} d\lambda \lambda (1 - \tanh(\pi\lambda)) \\
\times \frac{\pi P_{-1/2+i\lambda}(-\rho_<) P_{-1/2+i\lambda}(\rho_>)}{\cosh(\pi\lambda)}
\end{aligned}
\tag{7.5}
$$

and

$$
\begin{aligned}
\mathcal{J}(\rho, \rho') = \sum_{l=0}^{+\infty} \left(l + \frac{1}{2}\right) \frac{\pi P_{-1/2+i\lambda}(-\rho_<) P_{-1/2+i\lambda}(\rho_>)}{\cosh(\pi\lambda)} \\
- \int_0^{+\infty} d\lambda \lambda \frac{\pi P_{-1/2+i\lambda}(-\rho_<) P_{-1/2+i\lambda}(\rho_>)}{\cosh(\pi\lambda)}.
\end{aligned}
\tag{7.6}
$$

The first term in $\mathcal{J}(\rho, \rho')$ may either be calculated directly as a sum or by using the Watson-Sommerfeld transform to write

$$
\sum_{l=0}^{+\infty} g\left(l + \frac{1}{2}\right) = \text{Re}\left[\frac{1}{i} \int_\gamma dz \tan(\pi z) g(z)\right],
\tag{7.7}
$$

where γ runs from 0 to ∞ just above the real axis, and for us

$$
g(z) = z \frac{\pi P_{-1/2+i\sqrt{z^2+d}}(-\rho_<) P_{-1/2+i\sqrt{z^2+d}}(\rho_>)}{\cosh(\pi\sqrt{z^2 + d})}.
\tag{7.8}
$$

Writing

$$
\tan(\pi z) = i - \frac{2i}{1 + e^{-2\pi i z}},
\tag{7.9}
$$

the contribution to (7.7) from the first term in (7.9) yields

$$
\int_0^\infty dx g(x) = \int_{\sqrt{d}}^\infty d\lambda \lambda \frac{\pi P_{-1/2+i\lambda}(-\rho_<) P_{-1/2+i\lambda}(\rho_>)}{\cosh(\pi\lambda)}.
\tag{7.10}
$$

The contribution to (7.7) from the second term in (7.9) can be best evaluated by rotating the original contour to a contour γ', running from 0 to $i\infty$ just to the right of the imaginary axis. This is permitted since the Legendre functions are analytic functions of their parameter and the contribution from the arc at infinity vanishes for our choice of $g(z)$. From the form of $g(z)$ it is clear that it possesses poles along the contour γ' but these give a purely imaginary contribution to the integral. We conclude that

$$\mathcal{J}(\rho, \rho') = -\int_0^{\sqrt{d}} t\,dt \tanh(\pi\sqrt{d - t^2}) \frac{\pi P_{-1/2+it}(-\rho_<)P_{-1/2+it}(\rho_>)}{\cosh(\pi t)}$$

$$+ \mathcal{P}\int_0^{+\infty} \frac{2\pi t\,dt}{(1 + e^{2\pi\sqrt{d+t^2}})\cos(\pi t)} P_{-1/2-t}(-\rho_<)P_{-1/2-t}(\rho_>) \tag{7.11}$$

where $\mathcal{P}$ denotes the principal value. These integrals and that defining $\mathcal{I}(\rho, \rho')$ and their derivatives with respect to ρ are very rapidly convergent and easily calculated.

C. Matched expansions for the static particle

In Sec. II, we outlined the method of matched expansions. In this subsection, we show how to apply the method to a specific case: the computation of the self-force on a static particle in the Nariai spacetime.

The four-velocity of the static particle is simply

$$u^\rho = u^\theta = u^\phi = 0, \qquad u^t = (1 - \rho^2)^{-1/2} \tag{7.12}$$

and hence $d\tau' = (1 - \rho^2)^{1/2}dt'$. We find from Eqs. (1.4), (4.5), and (2.1) that $ma^t = ma^\theta = ma^\phi = 0$ and

$$ma^\rho = q^2\Big(\frac{1}{3}\dot{a}^\rho + \lim_{\epsilon\to 0^+}\int_{-\infty}^{\tau-\epsilon} g^{\rho\rho}\partial_\rho G_{\text{ret}}(z(\tau), z(\tau'))d\tau'\Big), \tag{7.13}$$

$$\frac{dm}{d\tau} = -q^2\Big(\frac{1}{12}(1 - 6\xi)R + (1 - \rho^2)^{-1/2}$$

$$\times \lim_{\epsilon\to 0^+}\int_{-\infty}^{\tau-\epsilon} \partial_t G_{\text{ret}}(z(\tau), z(\tau'))d\tau'\Big). \tag{7.14}$$

We note that in the tail integral of the mass loss equation (7.14), the time derivative ∂_t may be replaced with $-\partial_{t'}$ since the retarded Green function is a function of $(t - t')$. Hence we obtain a total integral,

$$(1 - \rho^2)^{-1/2}\lim_{\epsilon\to 0^+}\int_{-\infty}^{\tau-\epsilon}\partial_t G_{\text{ret}}(z(\tau), z(\tau'))d\tau'$$

$$= -\lim_{\epsilon\to 0^+}\int_{-\infty}^{t-\epsilon}\partial_{t'}G_{\text{ret}}(z(\tau), z(\tau'))dt'$$

$$= -\lim_{\epsilon\to 0^+}[G_{\text{ret}}(x, x')]_{t'\to-\infty}^{t'=t-\epsilon}. \tag{7.15}$$

The total integral depends only on the values of the Green function at the present time and in the infinite past ($t' \to -\infty$). The QNM sum expressions for the Green function [e.g. Eq. (6.2)] are zero in the infinite past, as the quasinormal modes decay exponentially. The value of the Green function at coincidence ($t' \to t$) is found from the coinci-

dence limit of the function $-V(x, x')$ in the Hadamard form (4.35). It is $\frac{1}{12}(1 - 6\xi)R$, which exactly cancels the local contribution in the mass loss equation (7.14). It is no surprise to find that this cancellation occurs—the local terms were originally derived from the coincidence limit of the Green function. In fact, because $\frac{d\Phi_R}{d\tau} = 0$ due to time-translation invariance, we can see directly from the original equation (1.5) that the mass loss is zero in the static case.

Now let us consider the radial acceleration (7.13). The acceleration keeping the particle in a static position is constant ($\dot{a}^\rho = 0$). The remaining tail integral may be split into two parts,

$$ma^\rho = q^2(1 - \rho^2)^{3/2}\Big(-\lim_{\epsilon\to 0^+}\int_{t-\Delta t}^{t-\epsilon}\partial_\rho V(z(t), z(t'))dt'$$

$$+ \int_{-\infty}^{t-\Delta t}\partial_\rho G_{\text{ret}}(z(t), z(t'))dt'\Big), \tag{7.16}$$

where Δt is a free parameter corresponding to $\Delta\tau$ introduced in (2.4) that determines the matching time in the matched-expansions method. For the first part of (7.16), we use the quasilocal calculation of $V(x, x')$ from Sec. IV C. As $V(x, x')$ is given as a power series in $(\rho - \rho')$ and $(t - t')$, the derivatives and integrals can be done termwise and are straightforward. The quasilocal integral contribution is therefore simply

$$\lim_{\epsilon\to 0}\int_{t-\Delta t}^{t-\epsilon}\partial_\rho V(z(t), z(t'))dt'$$

$$= \frac{1}{2}\sum_{k=0}^{+\infty}\frac{1}{(2k + 1)}\partial_\rho v_{k0}(\Delta t)^{2k+1}. \tag{7.17}$$

The second part of (7.16) can be computed using the QNM sum (6.1). To illustrate the approach, let us rewrite (6.1) as

$$G_{\text{ret}}^{\text{QNM}}(\rho, t; \rho', t; \gamma)$$

$$= \text{Re}\sum_{l,n}\mathcal{G}_{ln}(\rho', \gamma)e^{-i\omega_{ln}(t-t'-\rho_*-\rho_*')}\tilde{u}_{ln}(\rho). \tag{7.18}$$

Applying the derivative with respect to ρ and taking the integral with respect to t' leads to

$$\int_{-\infty}^{t-\Delta t}\partial_\rho G_{\text{ret}}(z(t), z(t'))dt' = \Big(\frac{d\rho}{d\rho_*}\Big)^{-1}\int_{-\infty}^{t-\Delta t}\partial_{t'}G_{\text{ret}}^{\text{QNM}}dt' + \text{Re}\sum_{l,n}\int_{-\infty}^{t-\Delta t}\mathcal{G}_{ln}e^{-i\omega_{ln}(t-t'-\rho_*-\rho_*')}\frac{d\tilde{u}_{ln}}{d\rho}dt'$$

$$= (1 - \rho^2)^{-1}[G_{\text{ret}}]^{t'=t-\Delta t} + \sum_{l,n}\frac{\mathcal{G}_{ln}}{i\omega_{ln}}e^{-i\omega_{ln}(\Delta t-\rho_*-\rho_*')}\frac{d\tilde{u}_{ln}}{d\rho}. \tag{7.19}$$

It is straightforward to find the derivative of the radial wave function from the definition (4.31). In Sec. VII D we outline two methods for numerically computing mode sums such as (7.19).

The self-force computed via (7.16), (7.17), and (7.19) should be independent of the choice of the matching time (we verify this in Sec. VIII D). This invariance provides a useful test of the validity of our matched expansions. Additionally, through varying $\Delta\tau$ we may estimate the numerical error in the self-force result.

D. Numerical methods for computing mode sums

The static-self-force calculation requires the numerical calculation of mode sums like (7.19). We used two methods for robust numerical calculations: (1) "smoothed sum" and (2) Watson transform (described previously in Sec. V C). We see in Sec. VIII that the results of the two methods are consistent.

The smoothed sum method is straightforward to describe and implement. Let us suppose that we wish to extract a numerical value from an infinite series

$$\sum_{l=0}^{+\infty} a_l \tag{7.20}$$

such that $\lim_{l\to\infty} a_l \neq 0$, and so the series is divergent. Let us now suppose that the divergence is "sufficiently weak" that $\lim_{l\to\infty} e^{-k(l+1)^2}|a_{l+1}|/(e^{-kl^2}|a_l|) < 1$ for all $k > 0$. Then we may instead compute the finite sum

$$S(l_{\text{cut}}) = \sum_{l=0}^{l_\infty} a_l e^{-l^2/2l_{\text{cut}}^2} \tag{7.21}$$

where l_∞ is large enough to suppress any high-l oscillations in the result (typically $l_\infty > 4l_{\text{cut}}$). We find that (7.21) is a good approximation to (7.20) provided we are not within $\delta t \sim 1/l_{\text{cut}}$ of a singularity of the Green function. Increasing the cutoff l_{cut} therefore improves the resolution of the singularities. The introduction of such a cutoff is—although of different magnitude—in the same spirit as the Feynman prescription of Sec. V E.

VIII. RESULTS

We now present a selection of results from our numerical calculations. In Sec. VIII A the distant past Green function is examined. We plot the Green function as a function of coordinate time $t - t'$ for fixed spatial points. A fourfold singularity structure is observed. In Sec. VIII B we test the asymptotic approximations of the singular structure, derived in Secs. V D and V E [Eqs. (6.3) and (6.6)]. We show that the fundamental mode ($n = 0$) series (6.4) is a good approximation of the exact result (6.2), if a time-offset correction is applied. In Sec. VIII C the quasilocal and distant past expansions for the Green function are compared and matched. We show that the two methods for
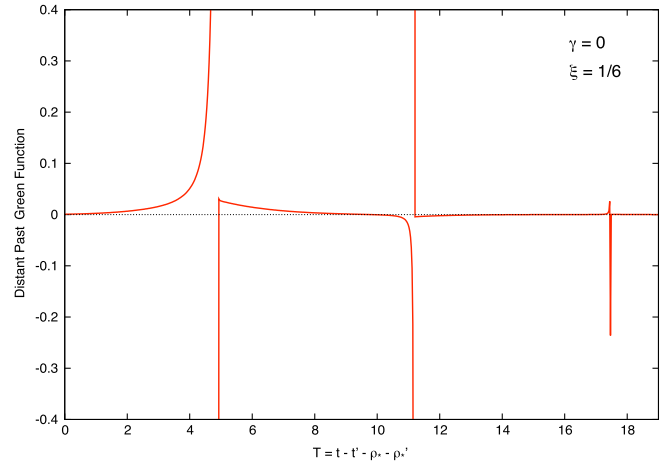

FIG. 9 (color online). Distant past Green function for spatially coincident points near infinity ($\rho = \rho' \to 1$, $\gamma = 0$). The Green function was calculated from mode sum (6.2) numerically using the smoothed sum method (7.21) with $l_{\text{cut}} = 200$ and curvature coupling factor $\xi = 1/6$.

finding the Green function are in excellent agreement for a range of matching times $\Delta\tau$. In Sec. VIII D we consider the special case of the static particle. We present the Green function, the radiative field,[2] and the self-force in turn. The radial self-force acting on the static particle is computed via the matched-expansion method (described in Secs. II and VII C), plotted as a function of coordinate ρ, and compared with the result derived in Sec. VII B.

A. The Green function near infinity from quasinormal mode sums

Let us begin by looking at the Green function for fixed points near spatial infinity, $\rho = \rho' \to 1$ (i.e. $\rho_* = \rho_*' \to +\infty$). The Green function may be computed numerically by applying either the Watson transform (Sec. V C) or the smoothed sum method (Sec. VII D) to the QNM sum (6.2).

Figure 9 shows the Green function for fixed spatially coincident points near infinity ($\rho = \rho' \to 1$, $\gamma = 0$) and $\xi = 1/6$. The Green function has been calculated from series (6.2) using the smoothed sum method. It is plotted as a function of QNM time, $T = t - t' - (\rho_* + \rho_*')$. We see that singularities occur at the times (3.23) predicted by the geodesic analysis of Sec. III C. In this case, $T_C = \ln[\sinh^2(N\pi)] \approx 4.893, 11.180, 17.463$, etc. At times prior to the first singularity at $T \approx 4.893$, the Green function shows a smooth power-law rise. At the singularity itself, there is a feature resembling a delta distribution, with a negative sign. Immediately after the singularity the Green

---

[2]In this section what is referred to as the "radiative field" is more precisely the "tail field," found from the integral of the retarded Green function along the past worldline (excluding coincidence). The self-force derived from the tail field is equivalent to that derived from the radiative field.
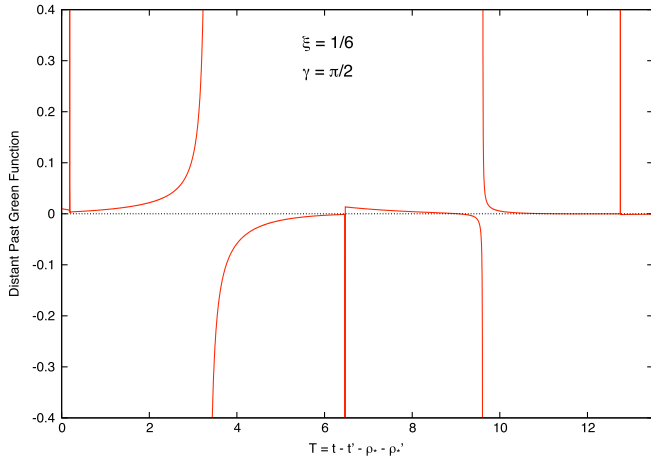
FIG. 10 (color online). Distant past Green function near spatial infinity ($\rho = \rho' \to 1$) for points separated by the angle $\gamma = \pi/2$ and $\xi = 1/6$. The Green function was calculated from the fundamental mode approximation (6.4) numerically using the smoothed sum method with $l_{cut} = 1000$. Note the fourfold singularity structure (see text).

function falls close to zero (although a small tail does appear). This behavior is even more marked in the case $\xi = 1/8$ (not shown). A similar pattern is found close to the second singularity at $T \approx 11.180$, but here the Green function takes the opposite sign, and its amplitude is smaller.

Figure 10 shows the Green function for points near infinity ($\rho = \rho' \to 1$) separated by an angle of $\gamma = \pi/2$

and $\xi = 1/6$. The Green function shown here is computed from the fundamental mode approximation (6.4), again using the smoothed sum method. In this case, the singularities occur at periodic times (3.24), given by $T = \Delta\phi - 2\ln 2 \approx 0.1845$, 3.326, 6.468, etc., where $\Delta\phi = \pi/2, 3\pi/2, 5\pi/2, \ldots$. As discussed, there is a one-to-one correspondence between singularities and orbiting null geodesics, and the fourfold singularity pattern predicted in Sec. V D [(6.6)] and Sec. V E [(6.3)] is clearly visible. Every "even" singularity takes the form of a delta distribution. Numerically, the delta distribution is manifest as a Gaussian-like spike whose width (height) decreases (increases) as l_{cut} is increased. By contrast (for $\gamma \neq 0, \pi$), every "odd" singularity diverges as $1/(T - T_c)$; it has antisymmetric wings on either side. The singularity amplitude diminishes as T increases.

B. Asymptotics and singular structure

The analyses of Secs. V D and V E yielded approximations for the singularity structure of the Green function. In particular, Eq. (6.3) gives an estimate for the amplitude of the odd singularities as $\rho, \rho' \to 1$. We tested our numerical computations against these predictions. Figure 11 shows the Green function near the singularity associated with the null geodesic passing through an angle $\Delta\phi = 3\pi/2$. The left plot compares the numerically determined Green function (6.4) with the asymptotic prediction (6.3). The right plot shows the same data on a log-log plot. The asymptotic
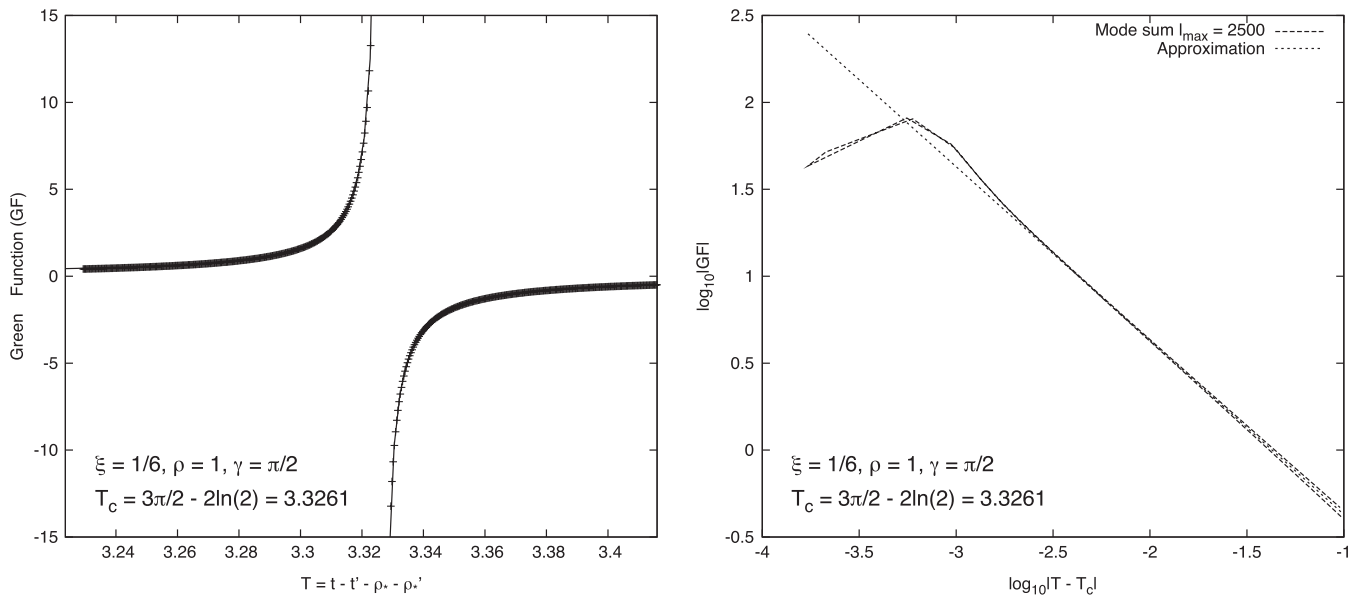

FIG. 11. Green function near the singularity arising from a null geodesic passing through an angle $\Delta\phi = 3\pi/2$ and with $\rho = \rho' \to 1$. The fundamental mode ($n = 0$) Green function (6.4) (with $l_{cut} = 2500$) is compared with approximations (6.3) and (6.6) from considering high-l asymptotics. The approximations give $G_{ret} \sim -0.042\,68/(T - T_c)$ and $G_{ret} \sim -0.043\,44/(T - T_c)$, respectively. The left panel shows the Green function in the vicinity of the (periodic) singularity at $T_c = 3\pi/2 - 2\ln 2 \approx 3.3261$. The right panel shows the same data on a log-log scale, and compares the mode sum (dashed line) with the approximation (dotted line). The discrepancy close to the singularity may be improved by increasing l_{cut}.
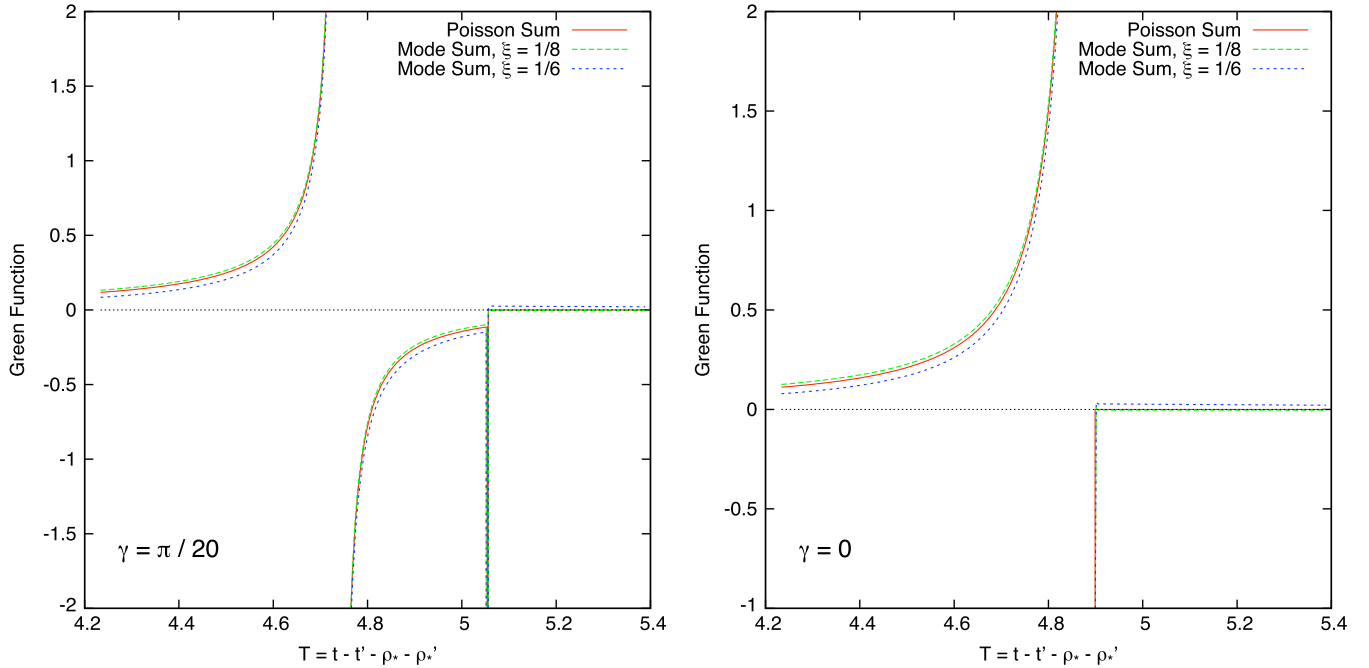
FIG. 12 (color online). Singularities of the fundamental mode Green function (6.4) compared with asymptotics from the Poisson sum (5.30) and (5.31). The left plot shows a small angular separation $\gamma = \pi/20$, and the right plot shows coincidence $\gamma = 0$, for ρ, $\rho' \to 1$.

prediction (6.3) is a straight line with gradient -1, and it is clear that the numerical data are in excellent agreement.

Improved asymptotic expressions for the singular structure of the fundamental mode Green function were given in (5.30) and (5.31). These asymptotics are valid all the way up to $\gamma = 0$. Figure 12 compares the asymptotic expressions (5.30) and (5.31) (solid line) with numerical computations (broken lines) from the mode sum (6.4). It is clear that the asymptotics (5.30) and (5.31) are in excellent agreement with the numerically determined Green function. The closest agreement is found near the singular times, but the asymptotics provide a remarkably good fit over a range of t.

In Fig. 13, the fundamental mode ($n = 0$) approximation (6.4) is compared with the exact QNM Green function (6.2) near spatial infinity. Away from singularities, the former is found to be a good approximation to the latter. However, close to singularities this is not the case. The singularities of the fundamental mode approximation (6.4) occur at slightly different times to the singularities of the exact solution (6.2), as discussed in Sec. VA. For the fundamental mode series (6.4), the singularity times T^N_{reg} given in Eq. (5.8) are periodic. For the exact solution (6.2) near spatial infinity, the singularity times T^N_{exact} are precisely the "null geodesic times" given in Eq. (3.23). Remarkably, if we apply a *singularity time offset* to the fundamental mode approximation ($T \to T + \Delta T$ where $\Delta T = T^N_{\mathrm{exact}} - T^N_{\mathrm{reg}}$), we find that the fundamental mode Green function is an almost perfect match to the exact Green function. This is clearly shown in the lower plot of Fig. 13. Comparing the series (6.2) and (6.4) we see that, in
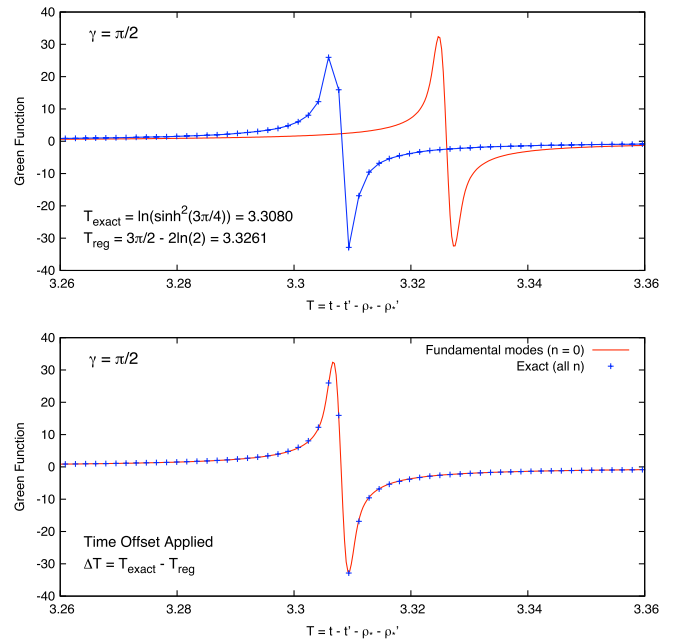

FIG. 13 (color online). Singularities of fundamental mode approximation. The top plot shows the Green function near spatial infinity ($\rho = \rho' \to 1$, $\rho_* = \rho'_* \to \infty$), for an angular separation $\gamma = \pi/2$. It compares the exact solution (6.2) [plain solid (red) line] and the approximation from the fundamental modes [crossed (blue) line], as a function of time $T = t - t' - \rho_* - \rho'_*$. The singularities occur at two distinct times, marked T_{exact} and T_{reg}, respectively. If a time offset is applied to the fundamental mode approximation (see text), then we find the singularities look remarkably similar (lower plot).
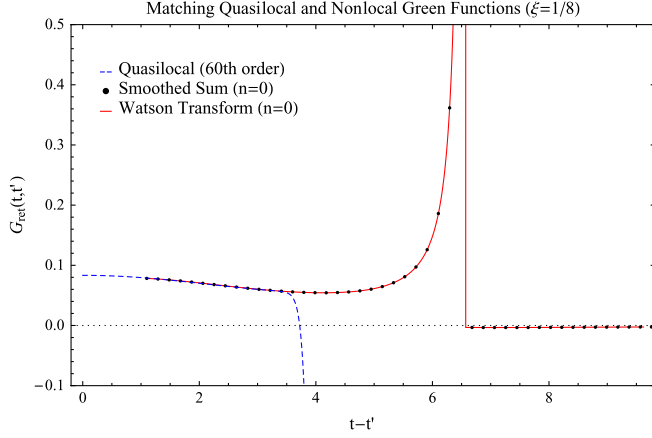
FIG. 14 (color online). Matching of the quasilocal and distant past Green functions for $\xi = 1/8$ and for a static particle at $\rho = \rho' = 0.5$. Here, the Green functions are plotted as functions of coordinate time, $t - t'$ (*not* QNM time, as in most other plots). The (black) dots and solid (red) line show the results of the smoothed sum and Watson transform methods applied to compute the $n = 0$ QNM sum (6.4) (see text). The dashed (blue) line shows the quasilocal series expansion taken to order $(t - t')^{60}$. The distant past Green function cannot be computed for early times $t - t' < \rho_* + \rho'_* = 2\tanh^{-1}(1/2) = 1.099$, whereas the quasilocal series diverges at large $t - t' \gtrsim 3.46$. In the intermediate regime, we find excellent agreement (see also Figs. 15 and 16). Note that the quasilocal Green function tends to $\frac{1}{12} \times (1 - 6\xi)R = \frac{1}{12}$ in the limit $t' \to t$.

both cases, the magnitude of the terms in the series increases as $(l + 1/2)^{1/2}$ in the large-l limit [see Eqs. (5.3) and (5.23)]. This observation raises the possibility that the $n = 0$ modes may give the essential features of the full solution; if true, this would certainly aid the analysis of the

Schwarzschild case, where it is probably not feasible to perform a sum over n analytically.

C. Matched expansions: Quasilocal and distant past

Let us now turn our attention to the match between quasilocal and distant past Green functions. The quasilocal expansion (4.36) is valid within the convergence radius of the series, $t - t' < t_{QL}$, while the QNM n series is convergent at "late" times, $t - t' > \rho_* + \rho'_*$. Hence, a matched-expansion method will only be practical if the quasilocal and distant past Green functions overlap in an intermediate regime $\rho_* + \rho'_* < t - t' < t_{QL}$. It is expected that the convergence radius of the quasilocal series, t_{QL}, will lie within the normal neighborhood, t_{NN}, of spacetime point x. The size of the normal neighborhood is limited by the earliest time at which spacetime points x and x' may be connected by more than one nonspacelike geodesic. Typically this will happen when a null geodesic has orbited once, taking a time $t_{NN} > \rho_* + \rho'_*$, so we can be optimistic that an intermediate regime will exist. To test this idea, we computed the quasilocal Green function using (4.36), and the distant past Green function (6.1) [or its approximation (6.4) for $n = 0$] for a range of situations.

Figure 14 shows the $n = 0$ retarded Green function (6.4) as a function of coordinate time $t - t'$ for a static particle at $\rho = \rho' = 0.5$. At early times, the quasilocal Green function is well defined, but the distant past Green function is not. Conversely, at late times the quasilocal series is not convergent. At intermediate times $1.099 < \Delta t \lesssim 3.45$, we find an excellent match. Figure 14 also shows that the results of the two numerical methods for evaluating QNM sums are equivalent. That is, the Green function found from the Watson transform (Sec. V C, solid (red)
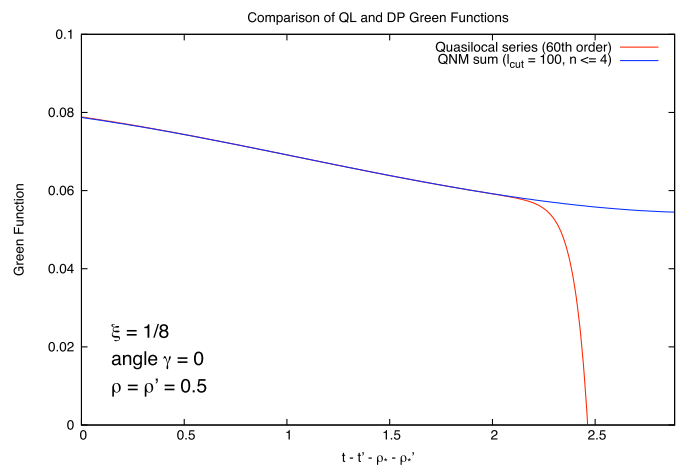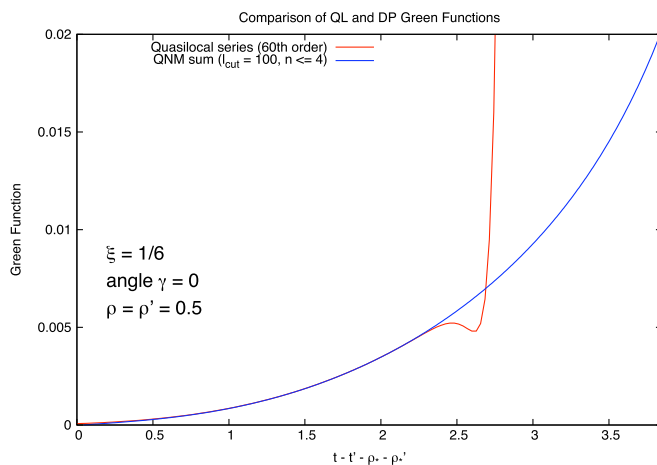

FIG. 15 (color online). Matching of the quasilocal and distant past Green functions. The left plot shows curvature coupling $\xi = 1/6$ and the right plot shows $\xi = 1/8$, for a static particle at $\rho = \rho' = 0.5$. Note the time scale on the horizontal axis, $T = t - t' - \rho_* - \rho'_*$. The distant past Green function [(blue) lines reaching up to the last value for T] cannot be computed for $T < 0$, whereas the quasilocal series [(red) lines *not* reaching up to the last value for T] clearly diverges at large T. In the intermediate regime, we find excellent agreement.
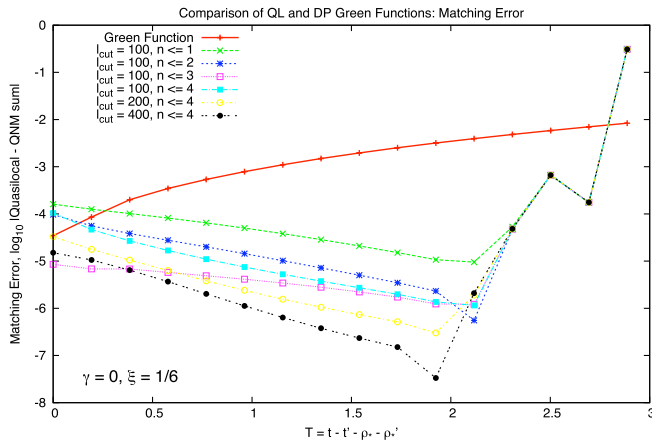
FIG. 16 (color online). Error in matching the quasilocal and distant past Green functions. This plot shows the difference between the quasilocal and distant past Green functions in the matching regime. The magnitude of the Green function as a function of time $T = t - t' - \rho_* - \rho'_*$ is shown as a solid red line. The broken lines show the "matching error": the difference between the quasilocal and QNM sum Green functions, for various l_{cut} in (7.21) (see Sec. VII D) and n_{max}. Note the logarithmic scale on the vertical axis. It is clear that the matching error is reduced by increasing n_{max} and l_{cut}, and that the best agreement is found close to the radius of convergence of the quasilocal series (at $T \sim 1.9$). The plot shows that a matching accuracy of above one part in 10^4 is achievable.

line) coincides with the Green function calculated by the method of smoothed sums (Sec. VII D, black dots).

Let us now examine the matching procedure in more detail. Figure 15 shows the match between the distant past and quasilocal Green functions, computed from (4.36) and (6.1), in the case $\rho = \rho' = 0.5$. The double sum in (6.1) has been calculated by applying the smoothed sum method (7.21) to the l sum and by summing over n up to the value $n_{\text{max}} = 4$. In Fig. 15, the left plot shows the case for conformal coupling $\xi = 1/6$ and the right plot shows the case for $\xi = 1/8$. Note that the Green function tends to the constant value $\frac{1}{12}(1 - 6\xi)R$ in the limit $\Delta t \to 0^+$. In both cases, we find that the fit between quasilocal and distant past Green functions is good up to nearly the radius of convergence of the quasilocal series.

Figure 16 quantifies the accuracy of the match between quasilocal and distant past Green functions. Here, we have used the smoothed sum method (Sec. VII D) to compute the distant past Green function from (6.1). To apply this method, we must choose appropriate upper limits for l (angular momentum) and n (overtone number). We have experimented with various cutoffs l_{cut} and n_{max}. As expected, better accuracy is obtained by increasing l_{cut} and n_{max}, although the run time for the code increases commensurately. With care, a relative accuracy of one part in 10^4 to 10^5 is possible. This accuracy is sufficient for confidence in the self-force values computed via matched expansions, presented in Sec. VIII D.

D. The self-force on a static particle

In this section, we present a selection of results for a specific case: a static particle at fixed spatial coordinates. Our goal is to compute the self-force as a function of ρ, to demonstrate the first practical application of the Poisson-Wiseman-Anderson method of matched expansions [36,37].

The radiative field may be found by integrating the Green function with respect to τ', where $d\tau' = (1 - \rho^2)^{1/2}dt'$. Integrating a mode sum like (6.4) with respect to t' is straightforward; we simply multiply each term in the sum by a factor $1/(i\omega_{ln})$. Hence it is straightforward to compute a *partial field* defined by

$$\Phi_{\text{partial}}(\Delta t) = q(1 - \rho^2)^{1/2} \int_{-\infty}^{t - \Delta t} G_{\text{ret}}(t - t', \rho = \rho', \gamma = 0)dt'.$$

(8.1)

This may be interpreted as "the field generated by the segment of the static-particle worldline lying between $t' \to -\infty$ and $t' = t - \Delta t$." In the limit $\Delta t \to 0$, the partial field Φ_{partial} will coincide with the radiative field Φ_R. An example of this calculation is shown in Fig. 17. Here, $q^{-1}\Phi_{\text{partial}}$ is plotted as a function of $T = \Delta t - \rho_* - \rho'_*$ for a static particle near spatial infinity, $\rho \to 1$. We have used the $n = 0$ QNM Green function (6.4) together with the method of smoothed sums (Sec. VII D), with $l_{\text{cut}} = 200$. The "partial field" Φ_{partial} shares singular points with G_{ret}. Figure 17 shows that a significant amount of the total radiative field arises from the segment of the worldline *after* the first singularity. The Green function tends to zero
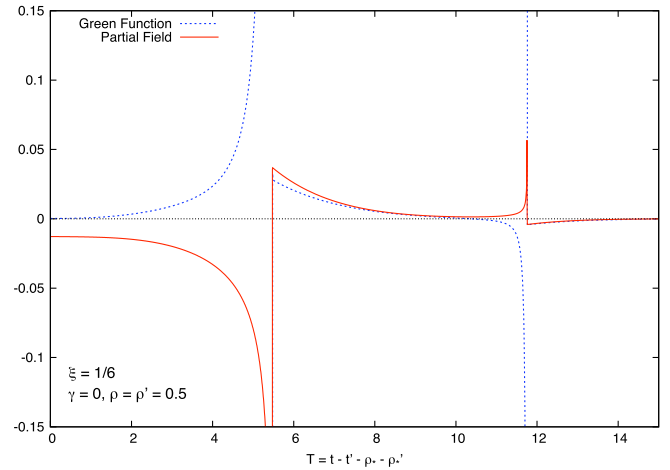

FIG. 17 (color online). Partial field generated by a static particle at $\rho = 0.5$. The dotted (blue) line shows the $n = 0$ QNM Green function (6.4). The solid (red) line shows the partial field $q^{-1}\Phi_{\text{partial}}$ defined in Eq. (8.1). This may be interpreted as the portion of the radiative field generated by the segment of the static-particle worldline between $t' \to -\infty$ and $t' = t - \Delta t$. Here $\Delta t = T + \rho_* + \rho'_*$, where T is the time coordinate shown on the horizontal axis.
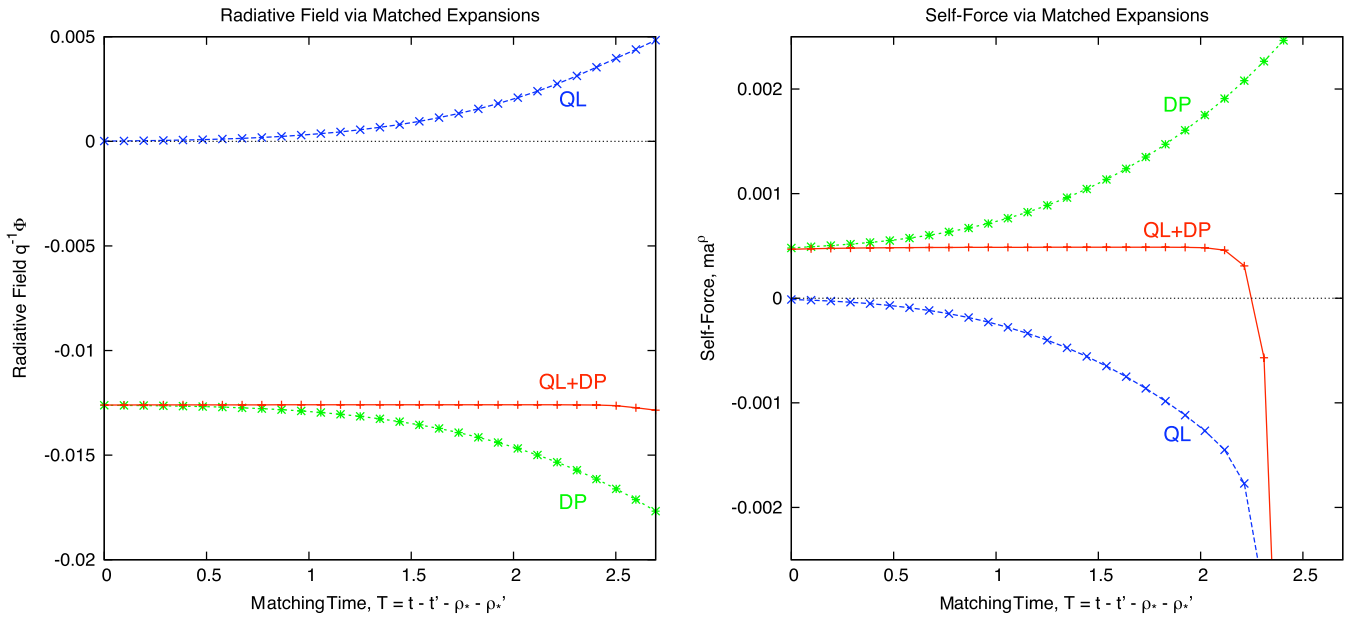
FIG. 18 (color online).   Illustration of the matching calculation of the self-force for $\xi = 1/6$ on a static particle at $\rho = \rho' = 0.5$. The (blue) dashed line shows the quasilocal contribution, integrated from $\tau - \Delta\tau = (1 - \rho^2)^{1/2}[T + \rho_* + \rho_*']$ to (almost) coincidence. The (green) dotted line shows the distant past contribution, integrated from $-\infty$ to $\tau - \Delta\tau$. The (red) solid line shows the total. In the matching region $1 \lesssim T \lesssim 2$ the total approaches a constant, which corresponds to the value of the radiative field (left plot) and radial self-force (right plot).

in the limit $\Delta t \to 0$ (for $\xi = 1/6$). On the other hand, the partial field tends to a constant nonzero value in this limit. The constant value is the radiative field $q^{-1}\Phi_R$.

An accurate value for the total radiative field is found by using the quasilocal Green function to extend Φ_{partial} to (almost) coincidence, $\Delta t \to 0^+$. The method is illustrated in Fig. 18 (left plot). The dashed line shows the quasilocal contribution to the radiative field, and the dotted line shows the distant past contribution to the radiative field, as a function of matching time. The former is the result of

integrating from the matching point $\tau - \Delta\tau$ to (almost) coincidence, and the latter from integrating from $-\infty$ to the matching point. Here, $\Delta\tau$ varies linearly with the x-axis scale T (see caption). The right plot illustrates the same calculation for the radial self-force. Here, the dotted line representing the contribution from the distant past is found from the sum (7.19) using the smoothed sum method (7.21) with $l_{\text{cut}} = 400$ for the l sum and summing over n up to the value $n_{\max} = 4$.
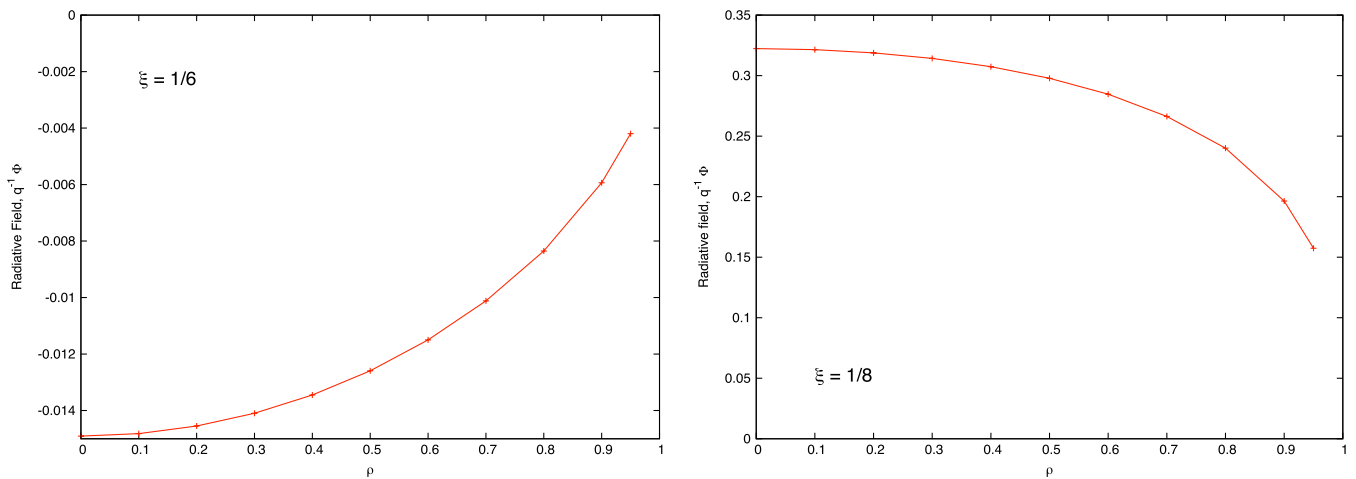

FIG. 19 (color online).   The radiative field generated by the static particle. The plot shows the radiative field for the static particle at $\rho = \rho'$. For the case $\xi = 1/6$ (left plot) the field is negative, whereas for the case $\xi = 1/8$ it is positive (right plot). Note the differing scales on the vertical axis.
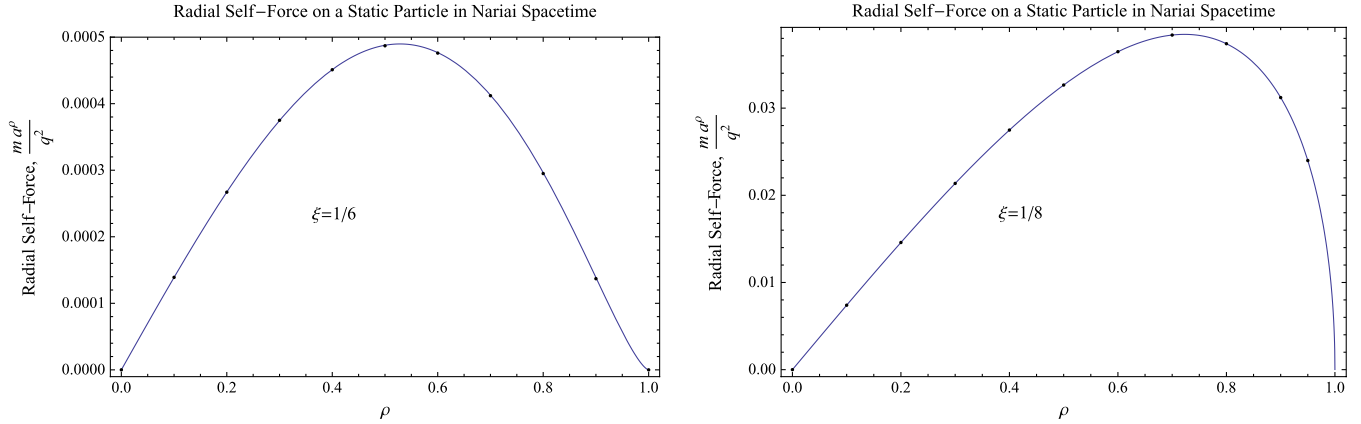
FIG. 20 (color online).   The radial self-force on the static particle. The radial component of the self-force, $q^{-2}ma^\rho$, is plotted as a function of the ρ of the static particle. The self-force was calculated by two methods: matched expansion [(black) dots] and massive-field regularization [(blue) curve]. The left plot shows the curvature coupling $\xi = 1/6$ whereas the right plot shows $\xi = 1/8$. Note the difference in scales for the two cases.

Figure 19 shows the total radiative field Φ_R generated by a static particle in the Nariai spacetime. The field is plotted as a function of ρ, for two cases: $\xi = 1/6$ and $\xi = 1/8$. In the former case, the field is negative. In the latter case, the field is positive, and about 2 orders of magnitude greater in amplitude. In both cases, the amplitude of the field is maximal at $\rho = 0$ and tends to zero as $\rho \to 1$ as $\Phi_R \sim (1 - \rho^2)^{1/2}$.

Figure 20 shows the radial self-force ma^ρ acting on a static particle. The results of the matched-expansion are shown as points, and the results of the "massive-field regularization method" (described in Sec. VII B) are shown as the solid line. The latter method provides an independent check on the accuracy of the former. We find agreement to approximately six decimal places between the two approaches. We find the self-force at $\rho = 0$ to be zero, as expected from the symmetry of the static region of the Nariai spacetime. The self-force also tends to zero as $\rho \to 1$. Between these limits, the self-force rises to a single peak, the magnitude and location of which depend on the curvature coupling ξ. We find that the peak of the self-force is approximately 4.9×10^{-4} for $\xi = 1/6$ and approximately 3.8×10^{-2} for $\xi = 1/8$. Note that the argument (see Sec. VII A) in [65] that the scalar self-force with $\xi = 1/8$ should be zero for a static particle in a spacetime (such as Nariai) possessing a conformally flat 3-D spatial section does not seem to hold here.

IX. DISCUSSION AND CONCLUSIONS

In this paper we have presented the first practical demonstration of a self-force calculation using the method of matched expansions. The matched-expansions method was first proposed over a decade ago by Poisson and Wiseman [36]. We have shown that the quasilocal expansion in coordinate separation [44,47–49], valid only in the normal neighborhood, may be accurately matched onto a mode-

sum expansion, valid in the distant past. Through matching the quasilocal and distant past expansions, the full retarded Green function may be reconstructed. With full knowledge of the Green function, one may accurately compute the tail contribution to the self-force. In this work, we employed the matching method to numerically compute the self-force acting on a static particle, and showed that the resulting self-force is in excellent agreement with the result from an alternative method (Sec. VII B), to approximately one part in 10^6.

The key new ingredient in our formulation is the so-called quasinormal mode-sum expansion for the distant past Green function. Following Leaver's approach [50], the integral over frequency in the mode-sum expansion of the Green function (4.1) may be performed by deforming the contour of integration in the complex frequency plane. Poles of the Green function arise at (complex) quasinormal mode frequencies in the lower half-plane. The sum over the residues of the poles gives the quasinormal mode sum—a key contribution to the Green function (see below).

The QNM sum is only valid at late times, $t - t' \gtrsim t_c$, where t_c is approximately the time it takes for a geodesic to reflect from the peak of the potential barrier. We have demonstrated that there is a sufficient regime of overlap in $t - t'$ in which both the quasilocal and QNM sum expansions are valid for the method to be applied successfully.

The QNM spectra of black holes have received much attention in the last three decades. In some studies [53,54,115], approximations to QNM frequencies are found by replacing the effective potential $V_l^{(S)}$ (3.5) with the so-called Pöschl-Teller potential (3.7). The advantage of this replacement is that the QNMs and radial solutions of the Pöschl-Teller potential are known in closed form. In this paper, we have taken the idea a step further. We have shown that the Pöschl-Teller potential arises naturally if we

consider the radial equation resulting from waves on an alternative spacetime: the product spacetime $dS_2 \times \mathbb{S}^2$, first introduced by Nariai [38,39] in 1950. This is an Einstein spacetime of constant scalar curvature.

The symmetry of Nariai spacetime undoubtedly makes calculations easier. For example, geodesic motion may be separated into motion on the two submanifolds, dS_2 and $\mathbb{S}^2$; the Van Vleck determinant may be written in closed form (5.43); and the decay rate of the quasinormal modes is independent of l. We view the Nariai spacetime as an excellent *testing ground* for our methods. Nevertheless, we should not forget the overall goal of the Poisson-Wiseman-Anderson proposal [36,37]: accurate matched-expansions calculations on physical black hole spacetimes. Below, we review some of the insights provided by our "experiment" with the Nariai spacetime which will help any future calculations.

At late times $t - t' > \rho_* + \rho_*'$ it has previously been established [68] that the quasinormal modes provide a *complete basis* on the Nariai spacetime. Here, we demonstrated that, at late times, the QNM sum (4.22) fully describes the retarded Green function. This is *not* expected to be the case on the Schwarzschild spacetime [50]. In the latter case, there arises a branch point at $\omega = 0$ and a branch cut in the frequency integral which gives a power-law tail contribution [51] to the Green function (Fig. 6). The branch point is notably absent for the Nariai spacetime, making the analysis simpler. In this paper we have thoroughly investigated the effect of the quasinormal modes. The contribution of the branch-cut integral to the self-force remains to be quantified. We hope to pursue this calculation in a forthcoming work.

This study has provided a number of insights into the properties of the Green function, which are of relevance to any future investigation of the Schwarzschild spacetime. Namely,

(i) The Green function $G_{\mathrm{ret}}(x, x')$ is singular whenever x and x' are connected by a null geodesic. The nature of the singularity depends on the number of caustics that the wave front has passed through. After an even number of caustics, the singularity is a delta distribution, with support only on the light cone. After an odd number of caustics, the Green function diverges as $1/\pi\sigma$, where σ is the Synge world function. A fourfold repeating pattern occurs, i.e. $\delta(\sigma)$, $1/\pi\sigma$, $-\delta(\sigma)$, $-1/\pi\sigma$, $\delta(\sigma)$, etc.

(ii) The fourfold singular structure can be shown to arise from a Hadamard-like ansatz (5.38) valid even outside the normal neighborhood, if we allow $U(x, x')$ to pick up a phase of $-i$ upon passing through a caustic. The accumulation of phase may be deduced by analytically continuing the integral for the Van Vleck determinant through the singularities (due to caustics).

(iii) The Hadamard parametrix for the Green function (4.35) is only strictly valid if x and x' are in a normal neighborhood [42] (see footnote [1]). The extension beyond the normal neighborhood does not seem to be known. However, this work and some previous studies [116] would tentatively suggest that, if x and x' are connected by a countable number of distinct geodesics, then the Green function may be found from the sum of their Hadamard contributions.

(iv) The effect of caustics on wave propagation has been well studied in a number of other fields, such as optics [117], acoustics [96], seismology [86], symplectic geometry [97], and quantum mechanics [98]. It may be that mathematical results developed in other fields may be usefully applied to wave propagation in gravitational physics.

(v) The "shape" of the fundamental mode ($n = 0$) Green function is remarkably similar to that of the whole (with sum over all n) QNM Green function after a time offset has been applied (see Fig. 13). This offers a potentially very practical way of evaluating the whole QNM Green function from only the $n = 0$ overtone. If this were also true in other spacetimes of more astrophysical interest such as Schwarzschild, such a method would be particularly valuable given the difficulty in calculating the sum over n up to large values in these spacetimes.

A further observation made in this work is confirmation that the tail self-force cannot be calculated from the quasilocal contribution alone. For instance, Fig. 17 would appear to show that a significant part of the radiative field is generated by the segment of the worldline which lies *outside* of the normal neighborhood (i.e. beyond the first caustic). Unlike in flat space, the radiated field generated by an accelerated particle may propagate once, twice, etc. around the black hole before later reintersecting the worldline of the particle (see Fig. 2). Radiation from near these orbits will give an important contribution to the self-force which cannot be neglected.

Let us conclude by examining the prospects for a practical matched expansions calculation on the Schwarzschild spacetime. Happily, the quasilocal expansion is now in excellent shape, as described in [48]; the challenge remains the distant past expansion. We have already mentioned that a quasinormal mode sum will not be sufficient; it must be augmented by a branch-cut integral. We have reason to be optimistic that this is a tractable calculation [51]. Perhaps more difficult will be the accurate numerical computation of QNM frequencies and radial functions. A further difficulty will be in integrating the mode sum over the worldline; for accuracy we wish to avoid numerical integration if possible. For the static particle, it was straightforward to integrate each term in the mode sum analytically (Sec. VII C) with respect to time. For other trajectories (e.g. circular orbits) this may present more of a challenge. Finally, we note that a range of established results is available on Schwarzschild spacetime. For the static par-

ticle the self-force is zero [104,106,118]; for radial trajectories and circular and eccentric orbits, accurate numerical results are available [26,29,105,119]. This will surely help the validation of the matched-expansions method. We hope to undertake such a study in the near future.

APPENDIX A: LARGE-λ ASYMPTOTICS OF $_2F_1(\frac{1}{2} - i\lambda, \frac{1}{2} - i\lambda; 1 - 2i\lambda; -e^{-T})$

To determine the singularity structure of the Green function in Sec. VA we required the large-λ asymptotic behavior of $_2F_1(-\beta, -\beta; -2\beta; z)$ where $\beta = -\frac{1}{2} + i\lambda$, $z = -e^{-T}$. The required asymptotics may be found by applying the WKB method [120] to the hypergeometric differential equation

$$z(1 - z)\frac{d^2u}{dz^2} - [2\beta(1 - z) + z]\frac{du}{dz} - \beta^2 u = 0 \quad \text{(A1)}$$

which has solutions $u(z) = {}_2F_1(-\beta, -\beta; -2\beta; z)$. Inserting the WKB ansatz

$$u(z) \sim e^{\lambda S_0(z) + S_1(z) + \lambda^{-1}S_2(z) + \dots} \quad \text{(A2)}$$

immediately yields a quadratic equation for S_0',

$$z(1 - z)(S_0')^2 - 2i(1 - z)S_0' + 1 = 0. \quad \text{(A3)}$$

In our case, $z = -e^{-T}$, we require the root which is finite at $z = 0$. We impose $S_0(0) = 0$ to get

$$S_0' = \frac{i}{z}(1 - (1 - z)^{-1/2})$$

$$\Rightarrow S_0(z) = \ln\left(\frac{(-z)}{4}\frac{[\sqrt{1 - z} + 1]}{[\sqrt{1 - z} - 1]}\right)$$

$$= -T - 2\ln 2 + \ln\left(\frac{\sqrt{1 + e^{-T}} + 1}{\sqrt{1 + e^{-T}} - 1}\right). \quad \text{(A4)}$$

At next order, we obtain the equation

$$2[i(1 - z) - z(1 - z)S_0']S_1' = z(1 - z)S_0'' + (1 - 2z)S_0'$$
$$+ i. \quad \text{(A5)}$$

It is straightforward to show that this reduces to

$$S_1' = (4(1 - z))^{-1} \Rightarrow S_1 = -\frac{1}{4}\ln(1 + e^{-T}). \quad \text{(A6)}$$

Inserting (A4) and (A6) into (A2) leads to the quoted result, Eq. (5.2). Of course, the asymptotic approximation may be further refined by taking the WKB method to higher orders.

APPENDIX B: POISSON SUM ASYMPTOTICS

In this appendix we derive asymptotic approximations for the singular structure of the Green function using the Poisson sum formula (5.18). Our starting point is expression (5.29) for the "$n = 0$" fundamental modes, in which the Legendre polynomials $P_l(\cos\gamma)$ have been replaced by angular waves $\mathcal{Q}_{\nu-1/2}^{(\pm)}(\cos\gamma)$ which are, in turn, approximated by Hankel functions $H_0^{(\mp)}(\nu\gamma)$ using (5.28).

Let us consider the $\mathcal{I}_1$ and $\mathcal{I}_2$ integrals arising from substituting (5.29) into (5.18). These integrals are singular at $\chi = 2\pi - \gamma$ and $\chi = 2\pi + \gamma$, respectively. First, let us consider $\mathcal{I}_1$ (5.18) which can be written

$$\mathcal{I}_1 \approx -\mathcal{A}(\gamma)\text{Re}\int_0^\infty d\nu(-i\nu)^{1/2}e^{i(\chi - 2\pi)\nu}H_0^{(+)}(\nu\gamma) \quad \text{(B1)}$$

with $\mathcal{A}(\gamma)$ as defined in Eq. (5.32).

For $\chi > 2\pi - \gamma$, the integral may be computed by rotating the contour onto the *positive* imaginary axis ($\nu = iz$) to obtain

$$\mathcal{I}_1 \approx -\frac{2\mathcal{A}(\gamma)}{\pi}\int dz z^{1/2}e^{-(\chi - 2\pi)z}K_0(\gamma z)$$

$$\approx -\frac{\mathcal{A}(\gamma)\sqrt{\pi}}{2[\chi - (2\pi - \gamma)]^{3/2}}{}_2F_1\left(3/2, 1/2; 2; \frac{\chi - 2\pi - \gamma}{\chi - 2\pi + \gamma}\right). \quad \text{(B2)}$$

Here we have applied the identity $H_0^{(+)}(ix) = 2K_0(x)/(i\pi)$, where K_0 is the modified Bessel function of the second kind, and the integral is found from Eq. 621(3) of Ref. [66].

For $\chi < 2\pi - \gamma$, the integral may be computed by rotating the contour onto the *negative* imaginary axis ($\nu = -iz$). First, we make the replacement $H_0^{(+)}(\nu\gamma) = 2J_0(\nu\gamma) - H_0^{(-)}(\nu\gamma)$ and note $H_0^{(-)}(-ix) = 2K_0(x)/(-i\pi)$ to obtain

$$\mathcal{I}_1 \approx \frac{2\mathcal{A}(\gamma)}{\pi}\text{Re}\int dz z^{1/2}e^{-(2\pi - \chi)z}[\pi I_0(\gamma z) + iK_0(\gamma z)]. \quad \text{(B3)}$$

Here I_0 is a modified Bessel function of the first kind. Since we are taking the real part, the K_0 term is eliminated, and we obtain

$$\mathcal{I}_1 \approx \frac{2\mathcal{A}(\gamma)}{\sqrt{\pi}}(2\pi - \gamma - \chi)^{-1}(2\pi + \gamma - \chi)^{-1/2}$$

$$\times E\left(\frac{2\gamma}{2\pi + \gamma - \chi}\right) \quad \text{(B4)}$$

where E is the elliptic integral of the second kind defined in, for example, Eq. 111(3) of Ref. [66].

The I_2 integral may be calculated in a similar manner. For $\chi < 2\pi + \gamma$, we rotate the contour onto the negative imaginary axis,

$$
\begin{aligned}
I_2 &\approx -\mathcal{A}(\gamma)\,\mathrm{Re}\int_0^\infty d\nu(-i\nu)^{1/2}H_0^{(-)}(\nu\gamma)e^{i(\chi-2\pi)\nu} \\
&\approx \frac{2\mathcal{A}(\gamma)}{\pi}\,\mathrm{Re}\,i\int_0^\infty dz\,z^{1/2}e^{-(2\pi-\chi)z}K_0(\gamma z) = 0.
\end{aligned}
$$

(B5)

For $\chi > 2\pi + \gamma$, we rotate the contour onto the positive imaginary axis after taking the complex conjugate

$$
\begin{aligned}
I_2 &\approx -\mathcal{A}(\gamma)\,\mathrm{Re}\int_0^\infty d\nu(i\nu)^{1/2}H_0^{(+)}(\nu\gamma)e^{i(\chi-2\pi)\nu} \\
&\approx \frac{2\mathcal{A}(\gamma)}{\pi}\,\mathrm{Re}\int_0^\infty dz\,z^{1/2}e^{-(\chi-\pi)z}(i\pi I_0(\gamma z)+K_0(\gamma z)).
\end{aligned}
$$

(B6)

The imaginary term does not contribute and hence I_2 is equal and opposite to I_1 defined by Eq. (B2) when $\chi > 2\pi + \gamma$.

APPENDIX C: GREEN FUNCTION ON $T \times \mathbb{S}^2$

To the best of our knowledge, the fourfold singularity structure for the Green function of Sec. V has not been shown before in the literature (with the exception of [87]) within the theory of general relativity. We therefore wish to illustrate its derivation and manifestation in the simplest of spacetimes including $\mathbb{S}^2$ topology:

$$ds^2 = -dt^2 + d\Omega_2^2, \qquad (C1)$$

where Synge's world function is simply given by $\sigma = \frac{1}{2} \times (-\Delta t^2 + \Delta\phi^2)$, in the case of a conformally coupled ($\xi = 1/8$) scalar field. Let $x = (t, \theta, \phi)$ denote any point in this spacetime. In this appendix, $\Delta \equiv t - t'$ is the time interval between any two spacetime points x and x' (rather than the free parameter determining the matching time in the main body of the paper).

We introduce the Wightman function $G_+(x, x')$ (it satisfies the homogeneous scalar wave equation—see, e.g., [89]), from which the retarded Green function $G_{\mathrm{ret}}(x, x')$ is easily obtained:

$$
\begin{aligned}
G_+(x, x') &= \sum_{l=0}^{+\infty}\sum_{m=-l}^{+l}\Phi_{lm}(x)\Phi_{lm}^*(x') \\
&= \frac{1}{4\pi}\sum_{l=0}^{+\infty}e^{-i(l+1/2)\Delta t}P_l(\cos\gamma),
\end{aligned}
$$

(C2)

$$G_{\mathrm{ret}}(x, x') = -2\theta(\Delta t)\,\mathrm{Im}(G_+(x, x')), \qquad (C3)$$

where $\Delta t \equiv t - t'$, $\Phi_{lm}(x) = e^{-i(l+1/2)t}Y_{lm}(\theta, \phi)/\sqrt{(2l+1)}$ are the Fourier-decomposed scalar-field modes on (C1)

normalized with respect to the scalar product

$$
\begin{aligned}
&(\Phi_{lm}, \Phi_{l'm'}) \\
&= -i\int_\Sigma dV n^\mu[\Phi_{lm}(x)\partial_\mu\Phi_{l'm'}^*(x) - \Phi_{l'm'}^*(x)\partial_\mu\Phi_{lm}(x)] \\
&= \delta_{ll'}\delta_{mm'},
\end{aligned}
$$

(C4)

where Σ is a Cauchy hypersurface with future-directed unit normal vector n^μ and volume element dV.

We now apply exactly the same tricks as in Sec. V D in order to derive the fourfold singularity structure in the Green function from the large-l asymptotics of the field modes. We use the *Poisson sum formula* [85,86]

$$\sum_{l=0}^{+\infty}g(l+1/2) = \sum_{s=-\infty}^{+\infty}(-1)^s\int_0^{+\infty}d\nu g(\nu)e^{2\pi is\nu} \quad (C5)$$

to rewrite the mode sum in (C2) as

$$
\begin{aligned}
4\pi G_+(x, x') &= \sum_{s=-\infty}^{+\infty}(-1)^s\int_0^{+\infty}d\nu e^{-i\nu\Delta t}P_{\nu-1/2}(\cos\gamma)e^{2\pi is\nu} \\
&= \sum_{N=1}^{+\infty}G_+^N,
\end{aligned}
$$

(C6)

$$G_+^N(x, x') \equiv \int_0^{+\infty}d\nu R_N(\cos\gamma)e^{-i\nu\Delta t}. \qquad (C7)$$

The Legendre functions $P_\mu(\cos\gamma)$ and $Q_\mu(\cos\gamma)$, as well as $R_N(\cos\gamma)$, are standing waves. This is in contrast to $Q_\mu^{(\pm)}(\cos\gamma)$, which are traveling waves.

We can now use large-order uniform asymptotics (see [88,121]) for the Legendre functions:

$$P_{\nu-1/2}(\cos\gamma) \sim \left(\frac{\gamma}{\sin\gamma}\right)^{1/2}J_0(\nu\gamma), \qquad |\nu| \to \infty,$$

"valid in a closed uniform interval containing $\gamma = 0$,"

(C8)

$$Q_{\nu-1/2}(\cos\gamma) \sim -\frac{\pi}{2}\left(\frac{\gamma}{\sin\gamma}\right)^{1/2}Y_0(\nu\gamma), \qquad |\nu| \to \infty,$$

"valid with respect to $\gamma \in (0, \pi/2]$," (C9)

$$\mathcal{Q}_{\nu-1/2}^{(\pm)}(\cos\gamma) \sim \frac{1}{2}\left(\frac{\gamma}{\sin\gamma}\right)^{1/2}H_0^{(\mp)}(\nu\gamma), \qquad |\nu| \to \infty,$$

(C10)

to leading order.

The contribution to the Wightman function from the $N = 1$ orbit wave is immediately obtained by using the large-order asymptotics of the Legendre function $P_\nu(\cos\gamma)$ only, which are "valid in a closed uniform interval containing $\gamma = 0$"—this is what we will mean by a result being valid "near" $\gamma = 0$. Similarly, we can obtain a result valid near $\gamma = \pi$ by using in (C2) the symmetry

$P_l(\cos\gamma) = (-1)^l P_l(\cos(\pi - \gamma))$ for $l \in \mathbb{N}$. We then obtain for $N = 1$

$$4\pi G_+^{N=1}(x, x') \sim \sqrt{\frac{\gamma}{\sin\gamma}} \frac{1}{\sqrt{\gamma^2 - \Delta t^2}}, \qquad \text{near } \gamma = 0,$$

$$(C11)$$

$$4\pi G_+^{N=1}(x, x') \sim \sqrt{\frac{\pi - \gamma}{\sin(\pi - \gamma)}} \frac{-i}{\sqrt{(\pi - \gamma)^2 - (\Delta t - \pi)^2}}$$

$$= \sqrt{\frac{\pi - \gamma}{\sin(\pi - \gamma)}} \frac{-i}{\sqrt{-(\Delta t - \gamma)[\Delta t - (2\pi - \gamma)]}},$$

$$\text{near } \gamma = \pi, \qquad (C12)$$

where, for convergence, a small imaginary part was given to Δt and/or γ, in agreement with the Feynman prescription $\sigma \rightarrow \sigma + i\epsilon$. The result for $G_+^{N=1}(x, x')$ valid near $\gamma = 0$ is singular at $\Delta t = \pm\gamma$, corresponding to $\sigma = 0$ before a caustic has been crossed. It is in accord with the Hadamard form in 3-D [111] and the Van Vleck determinant (5.48), before a caustic has been crossed (and so without the phase

factor). The result for $G_+^{N=1}(x, x')$ valid near $\gamma = \pi$ is singular at $\Delta t = \gamma$, corresponding to the case where it has not gone through any caustics, and at $\Delta t = 2\pi - \gamma$, corresponding to the case where it has gone through one caustic; it has thus picked up a factor $-i$, as expected. Note that these zeros inside the squared root in the denominator are simple zeros along the null geodesic, except at the caustic point itself, where the two zeros coincide and so it becomes a double zero.

Similarly to $N = 1$, we can use (C6) and the asymptotics (C10) together with [66]

$$I_\pm(T, \gamma) \equiv \int_0^\infty d\nu e^{-i\nu(T - i\epsilon)} H_0^{(\pm)}(\nu\gamma)$$

$$= \frac{1}{\sqrt{\gamma^2 - (T - i\epsilon)^2}} \left[1 \mp \frac{2i}{\pi} \ln(iX + \sqrt{1 - X^2}) \right],$$

$$T \in \mathbb{R}, \qquad \epsilon > |\text{Im}\gamma|, \qquad (C13)$$

where $X \equiv (T - i\epsilon)/\gamma$ (again, a small imaginary part needs to be given for convergence, in accordance with the Feynman prescription), in order to obtain for $N > 1$

$$4\pi G_+^N(x, x') \sim \sqrt{\frac{\Xi}{\sin\Xi}} \frac{(-1)^{N/2}}{2} \begin{cases} [I_+(\Delta t + N\pi, \Xi) + I_-(\Delta t - N\pi, \Xi)] & \text{near } \gamma = 0 \\ -i[I_+(\Delta t + (N - 1)\pi, \Xi) + I_-(\Delta t - (N + 1)\pi, \Xi)] & \text{near } \gamma = \pi, \end{cases} \qquad (C14)$$

for N even, where $\Xi = \gamma$ near $\gamma = 0$ and $\Xi = \pi - \gamma$ near $\gamma = \pi$. For N odd, merely (1) swap $I_\pm \rightarrow I_\mp$ and (2) replace N by $N - 1$ if near $\gamma = 0$ or N by $N + 1$ if near $\gamma = \pi$ in (C14). We can rewrite the equation as $\gamma^2 - (\Delta t \pm N\pi - i\epsilon)^2 = -[(\Delta t - i\epsilon) - (\mp N\pi - \gamma)][(\Delta t - i\epsilon) - (\gamma \mp N\pi)]$. Note, however, that $I_\pm(T, \gamma)$ is regular at $X = \mp 1$.

We then have that the singular behavior goes as

$$4\pi G_+(x, x') \sim \frac{1}{2} \sqrt{\frac{\Xi}{\sin\Xi}} \begin{cases} +I_+(\Delta t, \gamma) & 0 < \Delta t < \pi & \gamma \sim 0 \\ -iI_+(\Delta t - \pi, \pi - \gamma) & \pi < \Delta t < 2\pi & \gamma \sim \pi \\ -I_+(\Delta t - 2\pi, \gamma) & 2\pi < \Delta t < 3\pi & \gamma \sim 0 \\ +iI_+(\Delta t - 3\pi, \pi - \gamma) & 3\pi < \Delta t < 4\pi & \gamma \sim \pi. \end{cases} \qquad (C15)$$

The fourfold singularity structure arises clearly: a phase of $\pi/2$ is picked up every time the null geodesic joining x and x' goes through a caustic ($\gamma = 0$ or π).

The expression for $G_+(x, x')$ is simplified by noting that, near $\gamma = 0$,

$$4\pi[G_+^N(x, x') + G_+^{N+1}(x, x')]$$

$$\sim i^N \sqrt{\frac{\gamma}{\sin\gamma}} \left[\frac{1}{\sqrt{\gamma^2 - (\Delta t - N\pi - i\epsilon)^2}} + \frac{1}{\sqrt{\gamma^2 - (\Delta t + N\pi - i\epsilon)^2}} \right], \qquad N \text{ even,}$$

$$i^N \sqrt{\frac{\pi - \gamma}{\sin(\pi - \gamma)}} \left[\frac{1}{\sqrt{(\pi - \gamma)^2 - (\Delta t - N\pi - i\epsilon)^2}} + \frac{1}{\sqrt{(\pi - \gamma)^2 - (\Delta t + N\pi - i\epsilon)^2}} \right], \qquad N \text{ odd,} \qquad (C16)$$

and similarly near $\gamma = \pi$. The Poisson sum formula has yielded a sum over geodesic paths, labeled by the index N, and the large-order asymptotics for the Legendre functions have yielded the correct singularity structure near the null geodesics, allowing for the correct phase change at each caustic.

[1] http://www.ligo.caltech.edu.
[2] http://www.virgo.infn.it.
[3] http://geo600.aei.mpg.de.
[4] http://lisa.nasa.gov.

[5] T. E. Bell, Nature (London) **452**, 18 (2008).
[6] M. Vallisneri, Classical Quantum Gravity **26**, 094024 (2009).
[7] S. A. Hughes, S. Drasco, E. E. Flanagan, and J. Franklin, Phys. Rev. Lett. **94**, 221101 (2005).
[8] J. A. Gonzalez, U. Sperhake, and B. Bruegman, arXiv:0811.3952.
[9] S. Detweiler and B. F. Whiting, Phys. Rev. D **67**, 024025 (2003).
[10] P. A. M. Dirac, Proc. R. Soc. A **167**, 148 (1938).
[11] B. S. DeWitt and R. W. Brehme, Ann. Phys. (Paris) **9**, 220 (1960).
[12] J. M. Hobbs, Ann. Phys. (N.Y.) **47**, 141 (1968).
[13] Y. Mino, M. Sasaki, and T. Tanaka, Phys. Rev. D **55**, 3457 (1997).
[14] T. C. Quinn and R. M. Wald, Phys. Rev. D **56**, 3381 (1997).
[15] T. C. Quinn, Phys. Rev. D **62**, 064029 (2000).
[16] E. Poisson, Living Rev. Relativity **7**, 6 (2004).
[17] S. Detweiler, Classical Quantum Gravity **22**, S681 (2005).
[18] C. R. Galley, B. L. Hu, and S.-Y. Lin, Phys. Rev. D **74**, 024017 (2006).
[19] A. I. Harte, Classical Quantum Gravity **25**, 235020 (2008).
[20] S. E. Gralla and R. M. Wald, Classical Quantum Gravity **25**, 205009 (2008).
[21] T. Futamase, P. A. Hogan, and Y. Itoh, Phys. Rev. D **78**, 104014 (2008).
[22] E. E. Flanagan and T. Hinderer, Phys. Rev. D **78**, 064028 (2008).
[23] L. Barack and A. Ori, Phys. Rev. D **61**, 061502 (2000).
[24] L. Barack, Phys. Rev. D **64**, 084021 (2001).
[25] L. Barack, Y. Mino, H. Nakano, A. Ori, and M. Sasaki, Phys. Rev. Lett. **88**, 091101 (2002).
[26] L. Barack and N. Sago, Phys. Rev. D **75**, 064021 (2007).
[27] S. Detweiler, E. Messaritaki, and B. F. Whiting, Phys. Rev. D **67**, 104016 (2003).
[28] I. Vega and S. Detweiler, Phys. Rev. D **77**, 084008 (2008).
[29] R. Haas, Phys. Rev. D **75**, 124011 (2007).
[30] L. Barack, D. A. Golbourn, and N. Sago, Phys. Rev. D **76**, 124036 (2007).
[31] L. Barack, A. Ori, and N. Sago, Phys. Rev. D **78**, 084021 (2008).
[32] N. Sago, L. Barack, and S. Detweiler, Phys. Rev. D **78**, 124024 (2008).
[33] L. Blanchet, L. P. Grishchuk, and G. Schaefer, in *Proceedings of the 11th Marcel Grossman Meeting on General Relativity*, edited by H. Kleinert and R. T. Jantzen (World Scientific, Singapore, 2009), p. 2475.
[34] T. Damour and A. Nagar, Phys. Rev. D **79**, 081503 (2009).
[35] S. Detweiler, Phys. Rev. D **77**, 124026 (2008).
[36] E. Poisson and A. G. Wiseman, Suggestion at the 1st Capra Ranch Meeting on Radiation Reaction, 1998.
[37] W. G. Anderson and A. G. Wiseman, Classical Quantum Gravity **22**, S783 (2005).
[38] H. Nariai, Sci. Rep. Res. Inst. Tohoku Univ., Ser. A **34**, 160 (1950).
[39] H. Nariai, Sci. Rep. Res. Inst. Tohoku Univ., Ser. A **35**, 62 (1951).
[40] E. Rosenthal, Phys. Rev. D **70**, 124016 (2004).
[41] E. Rosenthal, Phys. Rev. D **69**, 064035 (2004).
[42] F. G. Friedlander, *The Wave Equation on a Curved Space-time* (Cambridge University Press, Cambridge, England, 1975), ISBN 978-0521205672.
[43] J. Hadamard, *Lectures on Cauchy's Problem in Linear Partial Differential Equations* (Dover Publications, New York, 1923), ISBN 978-0486495491.
[44] P. R. Anderson and B. L. Hu, Phys. Rev. D **69**, 064039 (2004).
[45] P. R. Anderson and B. L. Hu, Phys. Rev. D **75**, 129901(E) (2007).
[46] P. R. Anderson and B. L. Hu, Phys. Rev. D **77**, 089901(E) (2008).
[47] W. G. Anderson, E. E. Flanagan, and A. C. Ottewill, Phys. Rev. D **71**, 024036 (2005).
[48] A. C. Ottewill and B. Wardell, Phys. Rev. D **77**, 104002 (2008).
[49] A. C. Ottewill and B. Wardell, Phys. Rev. D **79**, 024031 (2009).
[50] E. W. Leaver, Phys. Rev. D **34**, 384 (1986).
[51] N. Andersson, Phys. Rev. D **55**, 468 (1997).
[52] G. Pöschl and E. Teller, Z. Phys. **83**, 143 (1933).
[53] V. Ferrari and B. Mashhoon, Phys. Rev. D **30**, 295 (1984).
[54] E. Berti and V. Cardoso, Phys. Rev. D **74**, 104020 (2006).
[55] V. Cardoso and J. P. S. Lemos, Phys. Rev. D **67**, 084020 (2003).
[56] S. Zerbini and L. Vanzo, Phys. Rev. D **70**, 044030 (2004).
[57] M. Ortaggio, Phys. Rev. D **65**, 084046 (2002).
[58] S. W. Hawking and G. F. R. Ellis, *The Large-Scale Structure of Spacetime* (Cambridge University Press, Cambridge, England, 1973).
[59] G. Gibbons and S. Hawking, Phys. Rev. D **15**, 2738 (1977).
[60] P. Ginsparg and M. J. Perry, Nucl. Phys. **B222**, 245 (1983).
[61] O. J. C. Dias and J. P. S. Lemos, Phys. Rev. D **68**, 104010 (2003).
[62] V. Cardoso, O. J. C. Dias, and J. P. S. Lemos, Phys. Rev. D **70**, 024002 (2004).
[63] R. Bousso and S. Hawking, Phys. Rev. D **52**, 5659 (1995).
[64] R. Bousso and S. Hawking, Phys. Rev. D **54**, 6312 (1996).
[65] V. B. Bezerra and N. R. Khusnutdinov, Phys. Rev. D **79**, 064012 (2009).
[66] I. Gradshteyn and I. Ryzhik, *Table of Integrals, Series, and Products* (Academic Press, New York, 2007).
[67] J. B. Hartle and D. C. Wilkins, Commun. Math. Phys. **38**, 47 (1974).
[68] H. R. Beyer, Commun. Math. Phys. **204**, 397 (1999).
[69] E. W. Leaver, Proc. R. Soc. A **402**, 285 (1985).
[70] H.-P. Nollert, Classical Quantum Gravity **16**, R159 (1999).
[71] K. D. Kokkotas and B. G. Schmidt, Living Rev. Relativity **2**, 2 (1999).
[72] V. Cardoso, A. S. Miranda, E. Berti, H. Witek, and V. T. Zanchin, Phys. Rev. D **79**, 064016 (2009).
[73] S. Iyer, Phys. Rev. D **35**, 3632 (1987).
[74] R. A. Konoplya, Phys. Rev. D **68**, 024018 (2003).
[75] J. L. Synge, *Relativity: The General Theory* (North-Holland, Amsterdam, 1960), ISBN 978-0720400663.
[76] B. S. DeWitt, *Dynamical Theory of Groups and Fields* (Gordon and Breach, New York, 1965).
[77] M. Casals, S. R. Dolan, A. C. Ottewill, and B. Wardell, following Article, Phys. Rev. D **79**, 124044 (2009).
[78] K. W. Howard, Phys. Rev. D **30**, 2532 (1984).
[79] E. Winstanley and P. M. Young, Phys. Rev. D **77**, 024008

(2008).

[80] J. Duistermaat and L. Hörmander, Acta Math. **128**, 183 (1972).

[81] L. Hörmander, *The Analysis of Linear Partial Differential Operators IV* (Springer, Berlin, Heidelberg, New York, 1985).

[82] B. Kay, M. Radzikowski, and R. Wald, Commun. Math. Phys. **183**, 533 (1997).

[83] Y. Décanini, A. Folacci, and B. Jensen, Phys. Rev. D **67**, 124017 (2003).

[84] G. Watson, Proc. R. Soc. A **95**, 83 (1918).

[85] P. Morse and H. Feshbach, *Methods of Theoretical Physics* (McGraw-Hill, New York, 1953).

[86] K. Aki and P. G. Richards, *Quantitative Seismology* (University Science Books, Sausalito, California, 2002).

[87] A. Ori, 2008. The fourfold structure of the singular part of the Green function beyond the caustics was found by Ori some time ago. He also conducted measurements in an analog acoustic system, which seem to verify his theoretical prediction. Private communication (2008) and report (2009) available at http://physics.technion.ac.il/~amos/acoustic.pdf.

[88] F. W. J. Olver, *Asymptotics and Special Functions* (Academic Press, New York, 1974).

[89] N. Birrell and P. Davies, *Quantum Fields in Curved Space* (Cambridge University Press, Cambridge, England, 1984).

[90] Y. Décanini and A. Folacci, Phys. Rev. D **78**, 044025 (2008).

[91] J. H. Van Vleck, Proc. Natl. Acad. Sci. U.S.A. **14**, 178 (1928).

[92] C. Morette, Phys. Rev. **81**, 848 (1951).

[93] M. Visser, Phys. Rev. D **47**, 2395 (1993).

[94] I. Avramidi, *Heat Kernel and Quantum Gravity* (Springer, Berlin, 2000).

[95] M. Casals, S. R. Dolan, B. Nolan, A. C. Ottewill, and B. Wardell (unpublished).

[96] Y. A. Kravtsov, Sov. Phys. Acoust. **14**, 1 (1968).

[97] V. I. Arnold, *Singularities of Caustics and Wave Fronts* (Kluwer Academic Publishers, Dordrecht, 1990).

[98] M. Berry and K. Mount, Rep. Prog. Phys. **35**, 315 (1972).

[99] V. Maslov, Theory of Perturbations and Asymptotic Methods [in Russian] (Izdat. Moskov. Gos. Univ., Moscow, 1965 [French translation (Dunod, Paris, 1972]).

[100] V. Maslov, "The WKB Method in the Multidimensional Case;" Appendix II of J. Heading, *Introduction to the Phase Integral Method (WKB Method)* (Wiley, New York, 1962), p. 177 [Russian translation: (Izd-vo Mir., Moscow, 1965)].

[101] H. Friedrich and J. M. Stewart, Proc. R. Soc. A **385**, 345 (1983).

[102] J. Ehlers and E. T. Newman, J. Math. Phys. (N.Y.) **41**, 3344 (2000).

[103] A. Smith and C. Will, Phys. Rev. D **22**, 1276 (1980).

[104] A. G. Wiseman, Phys. Rev. D **61**, 084014 (2000).

[105] P. R. Anderson, A. Eftekharzadeh, and B. L. Hu, Phys. Rev. D **73**, 064023 (2006).

[106] D. Cho, A. Tsokaros, and A. G. Wiseman, Classical Quantum Gravity **24**, 1035 (2007).

[107] E. Copson, Proc. R. Soc. A **118**, 184 (1928).

[108] B. Linet, J. Phys. A **9**, 1081 (1976).

[109] A. Zel'nikov and V. Frolov, Zh. Eksp. Teor. Fiz. **82**, 321 (1982) [Sov. Phys. JETP **55**, 191 (1982)].

[110] J. Hobbs, Ann. Phys. (N.Y.) **47**, 141 (1968).

[111] Y. Décanini and A. Folacci, Phys. Rev. D **73**, 044027 (2006).

[112] B. Linet, Gen. Relativ. Gravit. **37**, 2145 (2005).

[113] A. Erdelyi, W. Magnus, F. Oberhettinger, and F. Tricomi, *Higher Transcendental Functions Vol. 1* (McGraw-Hill, New York, 1953).

[114] P. Candelas and B. Jensen, Phys. Rev. D **33**, 1596 (1986).

[115] I. G. Moss and J. P. Norman, Classical Quantum Gravity **19**, 2323 (2002).

[116] M. R. Brown, P. G. Grove, and A. C. Ottewill, Lett. Nuovo Cimento Soc. Ital. Fis. **32**, 78 (1981).

[117] O. N. Stavroudis, *Optics of Rays, Wavefronts and Caustics* (Academic Press, New York, 1972).

[118] L. M. Burko, Classical Quantum Gravity **17**, 227 (2000).

[119] L. M. Burko, Phys. Rev. Lett. **84**, 4529 (2000).

[120] C. M. Bender and S. A. Orszag, *Advanced Mathematical Methods for Scientists and Engineers* (Springer, New York, 1999).

[121] D. Jones, Mathematical Methods in the Applied Sciences **24**, 369 (2001).